BIOMOLECULAR ENGINEERING OF SIRNA THERAPEUTICS

By

Amanda Portis Malefyt

A DISSERTATION

Submitted to
Michigan State University
in partial fulfillment of the requirements
for the degree of

Chemical Engineering – Doctor of Philosophy

2013

ABSTRACT

BIOMOLECULAR ENGINEERING OF SIRNA THERAPEUTICS

By

Amanda Portis Malefyt

RNA interference (RNAi) has unlimited potential for therapeutic applications in regulating disease-associated proteins. The versatility of RNAi allows for treating a wide variety of targets with high specificity, making it an ideal complement to small molecule drugs. Despite on-going clinical trials utilizing short interfering RNA (siRNA) therapeutics for eye diseases, cancer, kidney disorders, and antiviral defenses, none have yet been approved for clinical use. Also, in the majority of these trials, delivery is accomplished through topical administration, localized injections, or systemic delivery to the liver or kidneys (natural filtering organs). Difficulties in development can be partly attributed to complications in optimizing delivery and maximizing function, while minimizing cytotoxicity and immunogenicity. To meet these challenges, this research aims to improve siRNA therapeutics through (1) optimization of the siRNA molecules and (2) development of more efficient vehicles for delivery of active siRNAs into cells.

When utilizing the RNAi pathway, merely selecting siRNA sequences complementary to the messenger RNA (mRNA) target does not guarantee target silencing. Factors such as 5' end stability are critical for ensuring incorporation of the correct strand into the RNA induced silencing complex (RISC). Two methods for determining this asymmetry, the relative likelihood of incorporating one strand compared to the other, are the terminal end sequence and relative terminal thermodynamic stability. To address the first aim, we developed an algorithm for predicting highly active siRNA sequences based on only these two parameters. The algorithm

successfully predicts weakly and highly active sequences for two test proteins, enhanced green fluorescent protein (EGFP) and protein kinase R (PKR). Going forward, we plan to characterize these and additional mechanistic factors that are valuable in predicting siRNA function.

For clinical applications, the primary roadblock in siRNA therapeutic development is delivery. Using cationic polymers to deliver siRNAs has the potential to address this issue but is limited by low delivery efficiencies. It is still not clear what properties are needed to ensure the formation of active polymer-siRNA complexes. To address part of the second aim, we sought to determine key characteristics of effective delivery vehicles by analyzing differences between siRNAs delivered using novel polymeric nanoparticles (NPs) and those delivered by linear polyethyleneimine (LPEI) and Lipofectamine 2000 (LF2K), two known effective delivery vehicles. Our results showed that for LF2K and LPEI, large quantities of siRNA were delivered rapidly, presumably overwhelming the basal levels of mRNA to initiate silencing. In contrast, our novel polymeric NPs showed delivery of siRNAs but at initial concentrations too low to achieve silencing. Nonetheless, the exceptionally low cytotoxicity of our NPs, and their ability for easy modification, makes them good candidates for further study and optimization.

Finally, in addition to delivery to cells, delivery efficiency is hindered by our lack of knowledge on how siRNA-vehicle complexes traffic across the plasma membrane and into the cytoplasm. To address this challenge, we have developed novel dextran functionalized silica solid-core NPs with the ability to effectively deliver siRNA to human lung cancer (H1299) cells expressing EGFP. Through modifications to the particle size and amine content, we were able to relate the chemical and physical characteristics of the particles to changes in cellular uptake, endocytotic trafficking, and ultimately silencing efficiency. Taken together, this research provides new information to guide the continued development of effective siRNA therapeutics.

ACKNOWLEDGEMENTS

Thank you to everyone who contributed to the work described in this document as well as those who supported me through its completion. These acknowledgements of thanks and gratitude include, but are not limited to, the following people:

Thank you to my advisors, Professors Pat Walton and Christina Chan, who supported and guided me throughout my years at Michigan State. Their mentoring and advice in both research and teaching was greatly appreciated. Despite their confusion and reluctance to send me off to a teaching school, they respected my future career goals and aimed to help me achieve them.

Thank you to my committee members, Professors Mark Worden and Greg Baker. Their recommendations and critique were vital to the advancement of this research. I'll always remember my first visit to MSU when I sat down with Dr. Worden for the first time only to find out he had already "Googled" me. He was constantly a friendly face in the hall and not only interested in the progress of my research but in my running hobby as well. My collaboration with Greg Baker deserves a special thanks and remembrance. Without his help, I would not be where I am today. He was a valuable asset to this project as well as an influential mentor and will be truly missed.

In addition to all of the doctorate professionals, I would like to express my gratitude to my lab mates, undergrads, and long-time collaborator. Their help and advice played a valuable role in this research and their friendly attitude at work made the environment more enjoyable. The roles of Liz, Sean, and Stephen, were priceless. Thanks to Liz for sticking with me from the very beginning and to Stephen and Sean for doing everything I asked, even playing on my softball

team. Thank you, Gina, for sharing your nanoparticles, organic chemistry expertise, frustrations, and friendship.

Last but not least, thank you to my family, both new and old. To my parents: for their support from the beginning in their quest to say I graduated from a “real” university. To my sister and brother: who tag-teamed keeping me company in East Lansing. To my husband: for choosing to marry me, despite all the stress and anxiety I vented. To my in-laws, who always made the effort to ask about my research. Thank you all for your continuous love and support.

~ Thanks.

TABLE OF CONTENTS

LIST OF TABLES

LIST OF FIGURES

LIST OF ABBREVIATIONS

AAV	adeno-associated viruses
AD	adenoviruses
AFM	atomic force microscopy
Ago2	argonaute 2
aiRNA	asymmetric interfering RNAs
APTES	3-(triethoxysilyl)-propyl amine
AS	antisense strand
BPEI	branched PEI
C3PO	component 3 promoter of RISC
CME	clathrin-mediated endocytosis
DEX	dextran
dgRNA	double-guide siRNA
DLS	dynamic light scattering
DNA	deoxyribonucleic acid
DOTAP	N-[1-(2,3-Dioleoyloxy)propyl]-N,N,N-trimethylammonium methyl-sulfate
DOTMA	N-[1-(2,3-dioleyloxy)propyl]-N,N,N-trimethylammonium chloride
dsDNA	double stranded DNA
EGFP	enhanced green fluorescent protein
H1299	human lung carcinoma
HepG2	hepatocellular carcinoma
LDL	low density lipoprotein

LF2K	lipofectamine 2000
liRNA	long interfering RNA
LPEI	linear PEI
miRNA	microRNA
mRNA	messenger RNA
nn	nearest neighbor
NP	nanoparticle
OAS1	2’-5’-oligoadenylate synthetase
PACT	protein activator of PKR
PAH	poly(anhydrides)
PAMAM	poly(amidoamine)
PBAE	poly(β-amino esters)
pDNA	plasmid DNA
PEI	poly(ethylenimine)
PEG	poly(ethylene glycol)
PEO	ply(ethylene oxide)
PKR	dsRNA-dependent protein kinase R
PLGA	poly(lactic-co-glycolic acid)
PLL	poly-L-lysine
PPGL (PG)	poly(propargyl glycolide)
PVA	poly(vinyl alcohol)
RISC	RNA induced silencing complex
RLC	RISC loading complex

RNA	ribonucleic acid
RNAi	RNA interference
sd	standard deviation
SEM	scanning electron microscopy
shRNA	short hairpin RNA
siRNA	short interfering RNA
sisiRNA	small internally-segmented interfering RNA
SS	sense strand
TEM	transmission electron microscopy
TEOS	tetraethoxysilane
TLR	toll-like receptor
TRBP	TAR RNA binding protein

CHAPTER 1: INTRODUCTION

Note: This chapter has been modified from work published in (Malefyt et al. 2012a) and (Malefyt et al. 2012b)

1.1 Significance

One of the National Academy of Engineering's grand challenges for the 21st century is the engineering of better medicines with the goal of developing personalized treatments that can be tailored to fit the needs of an individual patient. As a result, therapies which have the potential to take into account sequence-specific differences within the genetic makeup of healthy and unhealthy cells and individuals are becoming more desirable. The use of short interfering RNA (siRNA) through the RNA interference (RNAi) pathway to regulate specific disease-associated proteins is a powerful resource toward addressing this challenge. Since its discovery in 1998 (Fire et al. 1998), clinical trials have been initiated for siRNA therapeutics targeting eye diseases, cancer, kidney disorders, and antiviral defenses (Davidson and McCray 2011). However, none of these clinical trials have yet to evolve into approved treatments. Difficulties in designing effective therapies stem partly from incomplete knowledge in the mechanistic pathway of siRNAs as they traverse intracellularly as well as difficulties in efficient extracellular delivery. Therefore, the identification of key design variables (1) within the siRNA molecule to promote efficient incorporation into the RNAi pathway and (2) delivery vehicle development are valuable areas of continued research. This work highlights the identification of important design features within each of these two categories as well as the development and characterization of a novel, solid-core, silica, dextran delivery vehicle for active siRNA delivery.

1.2 Background

RNA interference (RNAi) is a naturally occurring pathway within human cells that can be induced both endogenous and exogenously (Carthew and Sontheimer 2009). For therapeutic applications, the external pathway is most relevant (Figure 1-1). In this pathway, double stranded, short, interfering ribonucleic acids (siRNAs), are internalized by cells, typically through the aid of some type of delivery vehicle and trafficked to the cytoplasm. They are then loaded into a complex of proteins, which form the RNA induced silencing complex (RISC) (MacRae et al. 2007; Maniataki and Mourelatos 2005). A single stranded siRNA and Argonaute2 (Ago2) have been shown to be the minimal components required for active silencing *in vitro* (Rivas et al. 2005). Additional proteins and protein complexes, such as Dicer and TAR RNA Binding Protein (TRBP), are known to be central to the pathway, but their functional roles are not fully defined (Hammond et al. 2000; Liu et al. 2004; Chendrimada et al. 2005; Haase et al. 2005; Lee et al. 2006; Wang et al. 2009).

Creating an active RISC involves the loading of one siRNA strand, the guide strand, into Ago2. The other strand, the passenger strand, is nicked by Ago2 and discarded (Tomari et al. 2004; Matranga et al. 2005; Leuschner et al. 2006). The active RISC cleaves the target messenger RNA (mRNA) at the center region of the mRNA that is complementary to the siRNA strand (Hammond et al. 2000; Rivas et al. 2005; Elbashir et al. 2001b; Leuschner et al. 2006). Once cleaved, the mRNA is targeted for destruction and the protein it encodes for is no longer produced. This allows for sequence-specific targeting of mRNAs for the reduction of selected proteins. While either siRNA strand can be loaded into the active RISC, to ensure correct targeting, the strand selected as the guide strand must be the strand that is complementary to the

target mRNA. This targeted sequence should also be unique to the intended target. When the incorrect strand is loaded into RISC, or the correct strand is complementary to multiple target mRNAs, damaging "off-target" effects can occur (Jackson and Linsley 2010).

1.3 siRNA design

The unique structure of siRNAs, ~19 base paired duplexes with 2 nucleotide overhangs on each 3' end, is a result of the endonucleolytic processing of longer dsRNAs by Dicer (Zamore et al. 2000), although exogenously introduced siRNAs of similar length can also be taken up by Dicer (Elbashir et al. 2001a; Lima et al. 2009). The presence of a 5' phosphate is required for the siRNA to be recognized by the RNAi pathway proteins (Nykänen et al. 2001), but synthetically introduced siRNAs are rapidly phosphorylated upon entry to cells by the protein Clp1 (Weitzer and Martinez 2007). Thus, exogenous siRNAs synthesized with the canonical siRNA structure are active as silencers (Lima et al. 2009; Sakurai et al. 2011).

Canonical siRNA characteristics can be further manipulated through changes in the length of either siRNA strand or by the addition of chemical modifications to the phosphate backbone, ribose sugar or aromatic base. With the large number of potential modifications that can be made, it is difficult to know which to use to generate the desired effect. To further complicate design, chemical modifications used in tandem require subsequent structural optimization (Dande et al. 2006). Two common chemical modifications, 2' methylation of the sugar and phosphothioate backbone modifications, have been used to improve nuclease stability (Guo et al. 2010a; Watts et al. 2008). Various structural designs have been found to enhance siRNA activity, promote guide strand selection, as well as mitigate unintended effects. Some examples include asymmetric interfering RNAs (aiRNAs), small internally-segmented interfering RNA (sisiRNA)

double-guide siRNA (dgRNA), and long interfering RNA (liRNA) (Chang et al. 2011; Hossbach et al. 2006; Watts et al. 2008; Sun et al. 2008). The future of siRNA designs will likely include at least some modifications to the native siRNA design; what is still not clear is how best to select the optimal set of modifications for clinical applications.

The silencing activity of siRNA synthesized to target a specific mRNA varies depending on the chosen sequence. Analyses of large data sets have been used to shed light on features characteristic of active and inactive siRNAs (Reynolds et al. 2004; Ui-Tei et al. 2004; Huesken et al. 2005; Shabalina et al. 2006). These datasets helped distinguish the impact of positional base preferences, overall hybridization stability, and local hybridization stability. Designing siRNAs with knowledge of these interactions can be used to minimize the recognition of siRNAs by cellular immune responses, ensure proper strand selection, and maximize RISC turnover and stability.

The preferential selection of one strand of siRNA over the other to become the guide strand is termed “asymmetry”. For successful RNAi, it is important that the antisense strand, complementary to the chosen mRNA target, is selected as the guide strand. The exact mechanisms for determining asymmetry are still under debate, however TRBP, Dicer, and Ago2 have all been shown to directionally bind siRNAs based upon differences localized to the termini of the siRNA (Gredell et al. 2010; Noland et al. 2011; Frank et al. 2010; Matranga et al. 2005). In humans, asymmetry sensing and the formation of an active RISC is less defined than the *Drosophila* model, although the pathway is known to be different in some ways (Sakurai et al. 2011). Methods used to predict asymmetry in relation to silencing activity may depend upon on the nucleotides at the 5'-termini (Gredell et al. 2010; Frank et al. 2010), hybridization stability of

the termini (Schwarz et al. 2003; Lu and Mathews 2008), or both (Gredell et al. 2010; Walton et al. 2010). With increasing studies reporting more active siRNAs and miRNAs contain A or U base pairs at the 5' position of the guide strand (Reynolds et al. 2004; Gredell et al. 2010; Seitz et al. 2011), believed to be a result of Ago2 binding specificity (Frank et al. 2010), future asymmetry predictions for RNAi should also take into account both hybridization stability as well as nucleotide preferences at the 5' termini.

The secondary structure of the mRNA target is also influential in determining silencing effectiveness (Vickers et al. 2003; Brown et al. 2005; Ameres et al. 2007). A variety of methods have been employed for predicting the efficiency of silencing from secondary structure (Kiryu et al. 2011; Lu and Mathews 2008; Overhoff et al. 2005; Schubert et al. 2005; Shao et al. 2007). Regions of low secondary structure have been shown to be better targets. Specifically, mRNAs with minimal secondary structure at the 3' and 5' ends of the siRNA target region silence more efficiently when compared to other structures (Ameres et al. 2007; Brown et al. 2005; Gredell et al. 2008; Kiryu et al. 2011). The prediction and experimental characterization methods for target mRNA structures still contain areas of variability and will have to be improved to include additional effects due to mRNA tertiary structures.

In addition to off-targeting of the incorrect gene, the use of siRNA can also have other detrimental effects such as interference with endogenous RNAi or cytoplasmic and immune responses. There are many similarities between the endogenous miRNA and exogenous siRNA pathways, including shared machinery (Carthew and Sontheimer 2009), such that excess siRNAs interfere with naturally occurring miRNA function (Grimm et al. 2006). For *in vivo* use, siRNAs can be recognized by the human innate immune system through surface, cytoplasmic, or

immune cell receptors (Samuel-Abraham and Leonard 2010; Sioud 2007; Jackson and Linsley 2010). Outside the RNAi pathway, multiple cytoplasmic proteins recognize RNAs such as 2'-5'-oligoadenylate synthetase (OAS1) and Protein Kinase R (PKR) (Samuel-Abraham and Leonard 2010; Sioud 2007). Recognition by these proteins has been shown to trigger cellular immune responses. However, siRNAs do not initiate most cytoplasmic immune responses since OAS1 and PKR tend to prefer longer base pair sequences. Recognition by immune cell toll-like receptors (TLRs), either extracellular or within endosomes, can cause severe inflammatory responses, with some sequence specificity (Jackson and Linsley 2010; Samuel-Abraham and Leonard 2010). Chemical modifications, such as methylation, have been shown to reduce immune stimulation by TLRs although the exact mechanism is still unclear (Jackson and Linsley 2010). Similarly to viral vectors, minimization of these non-specific effects can be achieved through reduced concentrations, however often at the risk of decreasing efficacy. Extracellular immunogenicity can sometimes be mitigated through the use of an appropriate delivery vehicle, but must be carefully designed to avoid compromising silencing activity.

1.4 Delivery vehicle design

The direct administration of siRNAs has shown some success when delivered topically or through localized injection (Whitehead et al. 2009). However, this requires direct and sometimes intrusive access to the areas of interest. When delivered systemically, naked siRNAs have minimal *in vivo* success due to degradation by serum nucleases and early filtration through the renal system (Soutschek et al. 2004; van de Water et al. 2006). Additionally, naked siRNAs cannot be targeted directly to the tissues/cells of interest. As a result, it is preferred to utilize some type of carrier to protect the siRNA cargo and aid in its delivery to the cells of interest.

Delivery approaches are generally divided between biological (viral or bacterial) (Seow and Wood 2009) and non-viral methods. With respect to RNAi, viral vectors are primarily useful for chronic therapies requiring long-term expression of short hairpin RNAs (shRNAs). Bacterial vectors are less common, but nonetheless still an area of continuing investigation (Xiang et al. 2006). Non-viral delivery vehicles, which can deliver either siRNAs or shRNAs for transient therapies, are further categorized according to the chemical or physical properties into several different groups such as lipids, polymers, or solid-core particles. These carriers typically range in size from 50-200nm and are sometimes termed nanoparticles (NPs). Each of these approaches has shown success in cell culture and in some *in vivo* studies (Shim and Kwon 2010). Nonetheless, refinement of currently available vehicles is necessary for development of highly effective, non-cytotoxic, tissue-specific, systemic delivery vehicles.

Viral-based delivery can be achieved using adenoviruses (ADs), adeno-associated viruses (AAVs), or retroviruses such as lentiviruses (Ghosh et al. 2006; Coura and Nardi 2007; Cockrell and Kafri 2007). RNAi-based strategies initiated by viral infection rely on transduction of DNA encoding shRNAs, which are then processed and enter the RNAi pathway (Grimm et al. 2006). High shRNA-expression can result in competition between endogenous miRNAs and viral shRNAs utilizing the same RNAi pathway, saturating the shared nuclear exporter, exportin-5 (Grimm et al. 2006). As a result, normal miRNA functionality is impeded, leading to cell dysregulation and death. Viral delivery systems are highly efficient in delivering their therapeutic cargo but do so with the concomitant risk of immunogenicity (Kaiser 2007; Hartman et al. 2008), though this is not solely a shortcoming of viral delivery systems (Robbins et al. 2009). Even if innate immune recognition is avoided, adaptive immunity can lead to decreased viral vector efficiency over time (Ghosh et al. 2006). Additionally, all viral vectors, however

modified, run the risk of uncontrolled insertional mutagenesis with active viruses or untargeted cells (Cockrell and Kafri 2007). Negative cell responses can be mitigated by using smaller doses of viral vectors or using weaker promoters for shRNA expression but must be balanced against lower efficacy. These risk factors aid in the motivation for the development of biologically safe, synthetic vectors.

Among lipid-based approaches, the majority of delivery vehicles are based on cationic lipids. The use of cationic lipids allows for complex formation with anionic nucleic acids. The resulting complexes, sometimes referred to as lipoplexes, protect siRNAs from serum degradation during transport to cells of interest (Buyens et al. 2008). The first reported cationic transfection lipid was N-[1-(2,3-dioleyloxy)propyl]-N,N,N-trimethylammonium chloride (DOTMA) (Malone et al. 1989). DOTMA was subsequently modified to create a second transfection reagent, N-[1-(2,3-Dioleoyloxy)propyl]-N,N,N-trimethylammonium methyl-sulfate (DOTAP) (Ren et al. 2000). Their common structure consists of a quaternary amine head group and a glycerol-based backbone linked to two long hydrocarbon chains. A variety of cationic lipids are now available commercially, with their principal application being siRNA delivery in cell culture.

For improved delivery specificity, targeting ligands have been conjugated to the lipids (e.g., such as transferrin to mediate uptake via the transferrin receptor) (Cardoso et al. 2007). High-throughput screening approaches have been used to identify the important characteristics of successful lipid-based delivery agents (Akinc et al. 2008). Based on this study, lipid-based reagents should include amide linkages, two or more alkyl tails of 8-12 carbon length, as well as the presence of secondary amines, though the incorporation of these characteristics does not ensure successful siRNA delivery. Interestingly, it has been reported that combinations of ineffective lipid-based reagents can yield more active reagents through synergistic effects

(Whitehead et al. 2011). To date, lipid development has not overcome the significant cytotoxicity that has limited their use *in vivo* (Zhang et al. 2007).

Endogenous liposome-like structures termed exosomes have gained attention recently as potential siRNA delivery vehicles (Thery 2011). Exosomes are small membrane vesicles, averaging 100 nm in diameter, that are released from most cell types. Originating from endocytotic vesicles, their existence has been known for over 25 years, however their ability to carry RNA molecules, including miRNAs, between cells is a relatively recently discovered phenomenon (Valadi et al. 2007). Exosomes have been shown to cross the blood-brain barrier, another advantage for *in vivo* application. Moreover, exogenous exosomes can be generated containing targeting peptides for targeted delivery applications (Alvarez-Erviti et al. 2011).

Polymeric vehicles have been used for the delivery of both plasmids and siRNAs. As with lipid-based vehicles, polymers used for nucleic acid delivery are typically cationic, allowing for self-assembly of the polymer-nucleic acid complexes, sometimes termed polyplexes. Linear and branched polyethylenimine (LPEI, BPEI) have been routinely used, despite their significant cytotoxicity (Burke and Pun 2008). Current polymer systems lack the efficacy of lipid-based systems. Modifications of single polymer systems have been explored, such as adding poly(ethylene glycol) (PEG)(Mao et al. 2006) or ethyl acrylate (Zintchenko et al. 2008), and have been found to increase *in vivo* delivery efficiency by increasing circulation time and decreasing toxicity.

Other polymer systems that have been used for nucleic acid delivery include poly (β-amino esters) (PBAE) (Lynn and Langer 2000), poly(amidoamine) (PAMAM) dendrimers (Tang et al. 1996), and chitosan (Katas and Alpar 2006; Liu et al. 2007). In order to combine positive attributes from varied synthetic polymers, combinations of polymers to create di- or tri-block

polymers have also been tested as successful methods of improving nucleic acid delivery in cell culture. These include polyvinyl alcohol/poly(D,L-lactide-co-glycolide) (PVA-b-PLGA) (Nguyen et al. 2008), poly(ethylene oxide) (PEO)/poly(ε-caprolactone) (PEO-b-PCL)(Xiong et al. 2009), or methacrylate block polymers (York et al. 2009). While cationic polymer systems rely on the electrostatic attraction of the siRNA for complex formation, covalent attachment of the siRNA to the polymer by disulfide bonds has also shown some success (Rozema et al. 2007). It is believed that the presence of disulfide bonds, which are reduced through cellular levels of glutathione and thioredoxin, can also aid in the intracellular release of the complex. The numerous and varied functional groups that are available on polymers allow for extensive modifications to tune the properties of the polymers for siRNA delivery applications. Rules for such modifications are just beginning to emerge (Portis et al. 2010; Siegwart et al. 2011).

A third type of delivery vehicle currently under development uses solid core particles such as iron, gold, or silica (Hom et al. 2010; Rosi et al. 2006; Veiseh et al. 2011). One advantage of these NPs is tighter control of the size and structure of complexes formed. Also, solid-core particles have the potential to provide enhanced imaging and diagnostic signals for *in vivo* applications.

Iron NPs can be coated with other compounds to improve delivery efficiency. Commercially available iron NPs (ex. SilenceMag, OZ Biosciences) rely on a mixture of solid core iron particles with lipids to create a combination delivery reagent. Other iron NPs utilize cationic polymer coatings or polymer peptides to help bind siRNAs and improve delivery efficiency (Veiseh et al. 2011). Delivery of iron NPs can be controlled with a magnetic field, termed magnetofection (Lee et al. 2011). This can enhance delivery to the cells of interest and increase transfection rates.

siRNAs have been conjugated to gold NPs via disulfide bonds (Rosi et al. 2006). This improves their nuclease stability over free siRNAs (Patel 2011). In addition, combinations between delivery systems such as using a gold NP modified with PEG and/or PBAE polymers (Lee et al. 2009; Lee et al. 2008) or PEI and Polyanhydrides (PAH) in a layer-by layer approach (Guo et al. 2010b). Gold NPs modified with folate for receptor targeting and near-IR photoactivity have shown selective *in vivo* activity in tumors (Lu et al. 2010) indicating the ability for receptor-mediated targeting.

Increasingly, silica NPs are being studied for siRNA delivery. Similar to other solid-core NPs, silica particle size can be finely tuned, and particles can be easily modified with the addition of polymers such as PEI (Hom et al. 2010). Furthermore, the porous nature of silica particles allows for co-delivery of siRNAs with other small molecule drugs such as doxorubicin for cancer treatment (Meng et al. 2010). However, solid-core particles create additional barriers to *in vivo* applications since their size and insolubility also plays a role in their ability to traverse the circulation. It has been shown that sedimentation of solid core gold NPs in two-dimensional cell culture has a direct effect on cellular uptake (Cho et al. 2011).

1.5 Internalization Mechanisms

Requirements for extracellular transport of siRNA and plasmid DNA (pDNA) delivery are relatively similar; both needing protection from degradation and the ability to target and enter the cells of interest. Conversely, there are several notable differences between the intracellular trafficking necessary for these nucleic acids, the most evident being siRNA activity occurs in the cytoplasm while pDNA expression requires nuclear delivery. Additionally, a large number of siRNAs are required within a single cell for protein reduction while delivery of a single plasmid

molecule is sufficient for successful protein expression. Given these differences, it is likely that the internalization processes that result in strong target silencing by siRNAs are unique from those that lead to strong pDNA expression. However, to date, few studies have been performed that investigate routes of internalization for siRNAs.

Phagocytosis, macropinocytosis, and endocytosis/pinocytosis are the three major mechanisms of uptake for extracellular molecules. Endocytosis can be further sub-classified into clathrin-dependent, caveolae-dependent, or clathrin- and caveolae-independent methods (Figure 1-2) (Khalil et al. 2006; Dausend et al. 2008; Conner and Schmid 2003). The vesicles that form in each of these processes have different intracellular destinations and fates, in many cases precluding all access to the cytoplasm. As such, depending on the drug being delivered, the preferred uptake pathway will vary.

Phagocytosis is an actin-dependent pathway most commonly used by white blood cells such as macrophages, monocytes, and neutrophils for initiating the adaptive immune response (Conner and Schmid 2003). Phagocytosis has been utilized for targeting and delivery of magnetic nanoparticles to macrophages (Kamat et al. 2010). Macrophages can internalize larger particles, on the order of 5-10 μm, with increased internalization of ellipsoid- over spherical-shaped particles (Champion and Mitragotri 2006). Despite this ability, it is not a general mechanism by which one can expect to deliver drugs to cells outside of these specific types.

Another mechanism for internalizing particles is through macropinocytocis, the encapsulation of extracellular fluid in vesicles with diameters in excess of 150-5000 nm (Conner and Schmid 2003). Unlike most forms of endocytosis, macropinocytosis results from the cell membrane reaching out and enveloping extracellular contents. The pathway is actin driven,

characterized by outward-directed actin polymerization (surface ruffing) (Medina-Kauwe et al. 2005). Unlike clathrin or caveolar mediated endocytosis, macropinocytosis does not rely on special protein coatings or concentrated receptors on the membrane surface, although it may depend on the presence of cholesterol (Kerr and Teasdale 2009). Macropinocytotic vesicles do not transition into acidic lysosomes or merge with other endocytotic pathways; (Hewlett et al. 1994) rather, some contents leak into the cytosol prior to the vesicle recycling back to the cell surface (Khalil et al. 2006). Macropinosome trafficking has also been shown to vary by cell type (Kerr and Teasdale 2009).

Clathrin-mediated endocytosis (CME) is the most common and universal endocytotic pathway among cells (Medina-Kauwe et al. 2005; Wang et al. 1993; Conner and Schmid 2003). CME is characterized by the presence of clathrin protein pits which form a polygonal lattice structure around a portion of the cell membrane, pinching it off to form an internalized vesicle (Kaksonen et al. 2006; Wang et al. 1993; Conner and Schmid 2003). Particles taken up by CME can range in size from 100-150nm in diameter. The process is energy and dynamin dependent, however there are conflicting reports on the role of actin in this process (Khalil et al. 2006; Macia et al. 2006; Kaksonen et al. 2006). It is likely that while actin may not be required for formation of clathrin vesicles, it is necessary for further trafficking of clathrin endosomes within the cell (Kirkham and Parton 2005). Although CME is not the only form of receptor-mediated endocytosis, receptors for transferrin and low density lipoprotein (LDL) also concentrate within these organelles (Conner and Schmid 2003). Clathrin-coated endosomes transition into late endosomes and acidified lysosomes, a process which often occurs closer to the nucleus (Huotari and Helenius 2011), a possible benefit for pDNA delivery vehicles.

The second type of protein coated endocytosis is caveolae-mediated endocytosis. These vesicles are 50-60nm in diameter, contain hydrophobic domains high in cholesterol and glycosphingolipids, called lipid-rafts, and typically have a flask-shaped formation (Kirkham and Parton 2005) but can also have flat or tubular structures (Khalil et al. 2006). Activation of this pathway is both dynamin and actin dependent (Kirkham and Parton 2005). Caveolae are most abundant in epithelial and adipocyte cells (Conner and Schmid 2003) but not always present in others, such as HepG2 cells (Fujimoto et al. 2000). Folate (Pelkmans and Helenius 2002) and insulin receptors (Gustavsson et al. 1999) are among those that localize on the cell membrane within caveolar regions. Trafficking of caveolae typically follows a non-acidic route (Khalil et al. 2006; Conner and Schmid 2003), with vesicles processed toward the golgi or endoplasmic reticulum organelles (Hewlett et al. 1994; Damm et al. 2005; Pelkmans and Helenius 2002). However, caveolar vesicles have been shown to occasionally undergo acidification (Huotari and Helenius 2011).

The final uptake pathway identified within cells involves the formation of lipid rafts but does not require clathrin or caveolin proteins. These clathrin- and caveolin- independent pathways form cholesterol-rich structures 40-50nm in size and may be both dynamin and actin independent (Damm et al. 2005; Kirkham and Parton 2005; Conner and Schmid 2003). While less well-understood than the classical pathways, it is believed these independent vesicles have the ability to merge with other pathways during endosome maturation (Conner and Schmid 2003).

Historically, the proton sponge hypothesis has been used to explain the release of nucleic acid delivery vehicles from endosomal vesicles into the cytoplasm (Akinc et al. 2005; Cho et al. 2003; Sonawane et al. 2003). According to this theory, amine containing vehicles, most

specifically polymers containing many amines, are internalized through some type of endocytotic pathway. As the endosome acidifies, the buffering capacity of the amines draws in an excess of protons followed by an excess of chloride ions. Osmotic swelling then causes the endosome to burst, releasing the contents into the cytoplasm of the cell (Akinc et al. 2005; Cho et al. 2003; Sonawane et al. 2003). Other delivery vehicles are reported to utilize fusogenic peptides to create more potent and active endosomal escape (Kwon et al. 2008). For this mechanism to hold, these vehicles would need to rely heavily on clathrin-mediated endocytosis. Discerning the exact internal cellular trafficking of delivery vehicles is critical for achieving active silencing and is emerging as an important area of study. Designing vehicles to target specific endocytic pathways as well as understanding how these pathways affect their ultimate destinations are essential to overcoming some of the hurdles in the efficiency of current delivery vehicles.

Currently, there are relatively few published studies on mechanisms of uptake for nucleic acid delivery complexes. The results of these studies support the idea that preferred uptake pathways vary depending on complex composition, surface charge, and particle size, in addition to cell type (Table 1-1). In many cases, the pathway most prominent in particle uptake is not necessarily the pathway which permits nucleic acid activity (Lu et al. 2009; Gabrielson and Pack 2009; McLendon et al. 2010; van der Aa et al. 2007). It has also been reported that for lipid delivery vehicles, pDNA and siRNA activity may result, independent of any endocytotic events. This suggests that cytoplasmic access of active lipid-containing complexes occurs through direct fusion with or transport across the lipid bilayer membrane, resulting in delivery directly to the cytoplasm of the cell (Lu et al. 2009; McLendon et al. 2010). Studies reporting caveolae-mediated endocytosis as the pathway utilized for active plasmid delivery with polymeric NPs (Gabrielson and Pack 2009; McLendon et al. 2010; Reilly et al. 2012b) question whether

endosome acidification is a requirement for particle release. Upon ruling out endosomal buffering as a means of release to the cytosol for cases of caveolar-dependent mechanisms, it remains unclear how delivery vehicles ultimately escape from various endosomal compartments to reach their final destination. Recently, pDNA-PEI complexes including histone tail peptides were reported to utilize caveolar vesicles for retrograde trafficking to the Golgi followed by the endoplasmic reticulum, presumably en route to the nucleus (Reilly et al. 2012b). However, it remains to be shown if the pathways required for active plasmid delivery mimic the pathways required for active delivery of siRNA when using the same type of delivery vehicle. Advancing beyond cellular delivery, an early study involving translocation of delivery vehicles across epithelial cells (Yacobi et al. 2010) supports the idea that vehicle design must account for intracellular and extracellular trafficking differences to ensure maximal activity of the delivered cargo.

Early attempts at systematic studies of internalization based upon single variables such as particle size (Rejman et al. 2004), shape (Gratton et al. 2008), or surface charge (Dausend et al. 2008) are difficult to compare given variations in other characteristics of the vehicles that were not characterized. Further systematic studies of all variables to determine the best structural and chemical complex characteristics for each cellular entry pathway in concert with the determination of the most efficient trafficking pathway for each type of cargo will be necessary in order to piece together the results of current studies and provide insight towards future design of improved vehicles. It is reasonable to believe that the best vehicle choice may continue to vary depending on the disease and cellular target. Nevertheless, improvements in research identifying the exact mechanism(s) required for the transport of delivery vehicles across the cell membrane, leading to cytoplasmic release of accessible siRNA cargo, will benefit the design of higher-

efficiency vehicles. Upon these developments, future investigations for improving delivery will need to expand toward improving mechanisms within *in vivo*-like environments.

1.6 Clinical Challenges and Successes

Current clinical trials use siRNAs based largely on early design rules and experimental validation of a limited number of candidates. While siRNA sequence selection and design has proven more complex than initially anticipated, improved understanding of the RNAi mechanism has led to development of siRNAs with improved functionality. Moving forward, the advancement of siRNA therapeutics will require a better understanding of the RNAi pathway in regards to the proteins involved and how they recognize siRNAs, leading to the rational inclusion of modifications to the canonical siRNA design.

While improving the function of siRNA itself is important, the majority of ongoing siRNA clinical trials focus on accessible, localized targets (lungs, eyes, solid tumors) or targets that are natural filtering organs (liver, kidneys) (Table 1-2) indicating that the key barrier to successful siRNA therapies is delivery. Targeted delivery agents and increased knowledge into how siRNAs traverse complex tissues are important areas of continued study.

Despite the multitude of candidates, there is no single delivery vehicle that can guarantee reliable, consistent siRNA delivery to all cell types. This is attributable both to a need to optimize the vehicles and to the lack of good model systems for evaluating *in vivo* vectors. The best vehicle choice may also depend on the disease and cellular targets, as generalized toxicity can be an acceptable response if confined to, for instance, cancer cells. The risk of immune complications often hinders viral vector development even though they can show highly efficient

delivery. Lipid vehicles provide simple and efficient transfection and are the standard for cell culture as well as large-scale bioreactors where toxicity isn't a concern. Solid-core particles can be highly modified without altering their structure. While often non-cytotoxic at low concentrations, accumulation of these typically non-degradable particles is a potential concern for long-term or repeated use. Polymer vehicles provide the greatest variety of constructs but currently lack the efficiency attainable with viral vectors. However, their potential for extensive modification, combined with their potential biodegradability, seem to make them the likeliest candidates for future siRNA delivery applications. Additionally, further research into the exact mechanism required for the transport of delivery vehicles across the cell membrane which leads to the cytoplasmic release of accessible siRNA cargo will benefit the design of higher-efficiency vehicles.

Future challenges for therapeutic development include techniques for the reliable large scale processing of both siRNAs as well as complex delivery vehicles. Nonetheless, continued research and optimization of design guidelines related to siRNA sequences, nanoparticle construction, and complex delivery provide a strong starting point for the continued development of RNAi therapeutics.

1.7 Approach and specific aims

The work described here aimed to improve siRNA delivery with the ultimate goal toward developing improved therapeutics. This research investigated characteristics of the siRNA as well as the delivery vehicle required for achieving optimal silencing efficiency and then applied this knowledge toward the development of a novel delivery vehicle. The approach was to experimentally study RNAi interference on a cellular level with the idea that future work can be

expanded in both directions to provide additional detail on molecular level as well as more complex delivery challenges in three dimensional models.

The specific aims of the present study were to:

1. ***Predict highly active siRNAs from an asymmetry-based selection algorithm***

Algorithms used for predicting highly active siRNAs currently involve a variety of techniques (Huesken et al. 2005; Lu and Mathews 2008; Shabalina et al. 2006; Yuan et al. 2004; Takasaki 2009; Ladunga 2006) and can include numerous parameters (Ladunga 2006). In this study, we developed an algorithm for predicting highly active siRNA sequences against desired proteins using only two asymmetric related features – terminal sequence and hybridization stability. The algorithm was tested against 11 EGFP-targeting and 11 PKR-targeting siRNA sequences and found to provide improved predictive ability when using both features. Furthermore, between the two features, end sequence showed greater correlation to activity when compared to thermodynamic stability alone. In addition to algorithm refinement, future work focuses on developing better experimental tools for establishing the asymmetry of a sequence and correlating that with its activity.

2. ***Identify key characteristics of effective delivery vehicles***

Despite the development of hundreds of siRNA delivery vehicles of varying compositions, it is still not clear what physical or chemical properties are needed to ensure the vehicles will form active siRNA complexes that result in efficient silencing. Here, we utilized fluorescent confocal microscopy to analyze the cellular uptake of siRNAs delivered by a variety of active and inactive lipid and polymer-based vehicles as a function of time. Our results showed that effective vehicles

displayed large quantities of siRNA delivered rapidly. In contrast, although ineffective vehicles showed comparable long-term siRNA delivery, they lacked intense concentrations of siRNA initially. It was presumed that these initial concentrated bursts of siRNA internalization are required to overwhelm the basal levels of mRNA to initiate silencing. This knowledge can be employed in the design and optimization of future delivery vehicles.

3. ***Characterize and optimize active siRNA delivery through the use of novel dextran functionalized silica nanoparticles***

The use of solid-core delivery vehicles provides the opportunity for functionalized variety while at the same time conserving core characteristics such as size and shape. To address the final aim, we developed silica-based nanoparticles with varied amine and dextran content to create a novel delivery vehicle with the ability to achieve silencing at levels comparable to commercially available products at minimal siRNA concentrations, and significantly lower toxicity. This study evaluated the effect of varied amine content as well as the presence of dextran on the silencing ability of the siRNA-NP complexes. Through the use of various endocytotic inhibitors, it was shown that these particles utilize multiple uptake pathways with the key mechanism involving an energy dependent process. The relationships between structure, content, and function can be used when transitioning from solid-core particles to biodegradable polymers, a favorable vehicle for future *in vivo* development.

1.8 Chapter 1 Tables and Figures

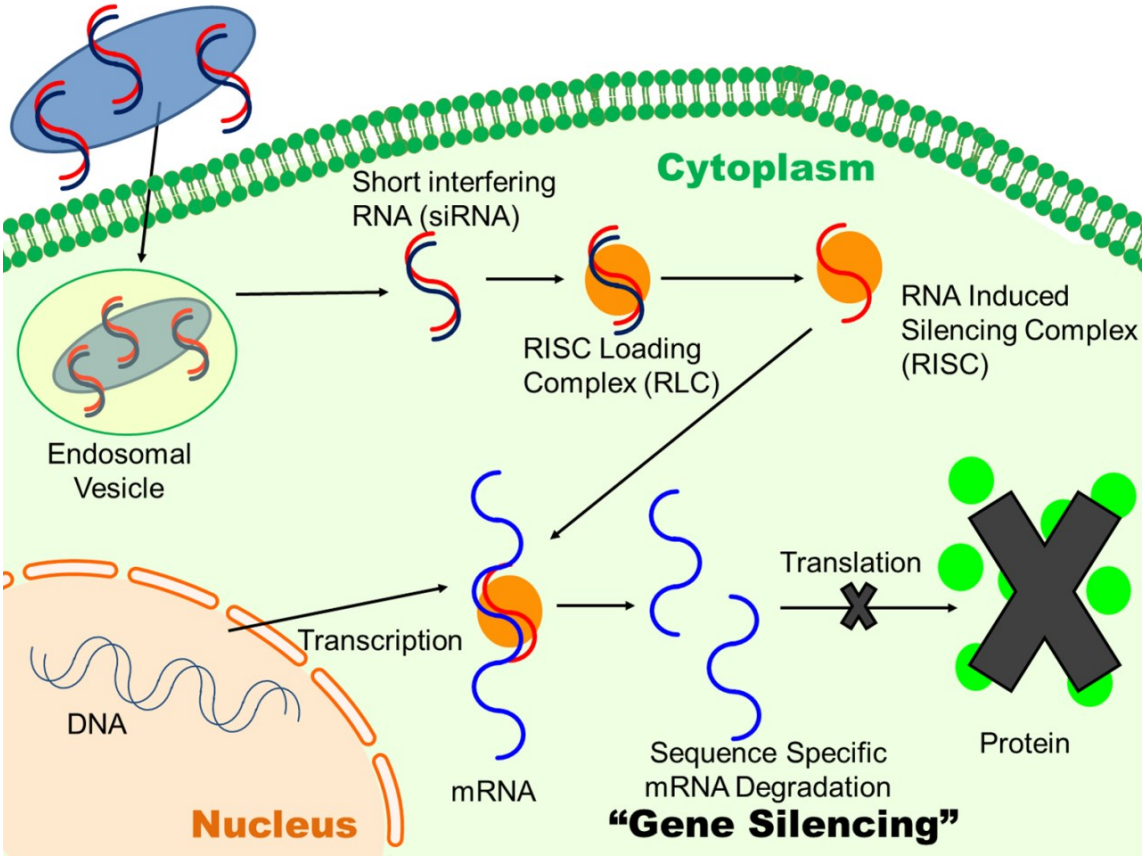

Figure 1-1 Mechanism of RNAi
RNA interference is initiated upon successful delivery of an siRNA into the cell cytoplasm. Lipid-based transfection reagents and most currently used polymeric vehicles enter cells through some type of endosomal pathway. Upon release from the delivery agent, the siRNA must also escape the endosomal vesicle so that the duplex can be bound by a complex of proteins (Dicer, TAR RNA Binding Protein (TRBP) and Argonaute 2 (Ago2)), known collectively as the RNA Induced Silencing Complex (RISC). RISC then utilizes one strand of the siRNA, the guide strand, to bind the target mRNA by complementarity, leading to sequence specific degradation of the mRNA and a subsequent reduction in protein expression. For interpretation of the references to color in this and all other figures, the reader is referred to the electronic version of this dissertation.

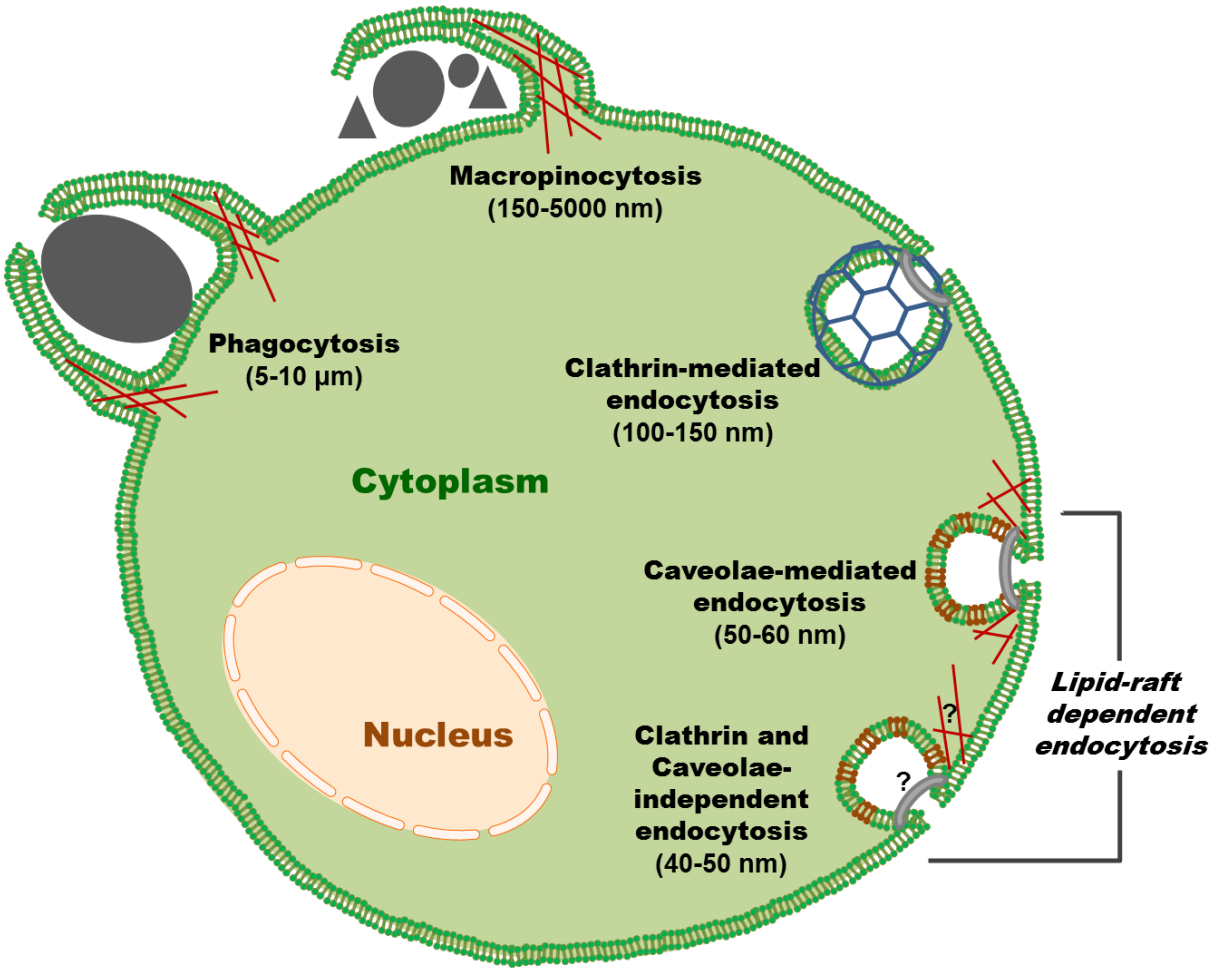

Figure 1-2 Entry pathways for mammalian cells
Routes of cellular internalization vary by cell type but can include phagocytosis (macrophage specific), macropinocytosis (actin dependent), clathrin-mediated (dynamin and clathrin dependent), caveolae-mediated (actin-, dynamin-, and caveolae-dependent) or clathrin- and caveolae-independent routes (some dynamin and actin dependency). In addition to variations in size, these pathways vary by receptor localization as well as internal processing pathways.

Table 1-1 Summary of results from reported mechanism of entry studies for polymer, lipid, and peptide-based delivery vehicles

Basis	Vehicle	Nucleic Acid	Formulation	Complex Characteristics	
				Charge	Size (diameter)
Polymer	Polystyrene NPs	none	75 μg/ml	+59mV and - 60mV	Positive – 113 nm Negative – 121 nm
	PEG cubes and cylinders	None	1 mg/ml	+35mV and -34mV	100 – 5000 nm
	Latex beads	none	Concentration not specified	n/a	50, 100, 200, 500, 1000 nm
	LPEI, folate and transferrin targeting	pDNA	polymer:DNA 0.5 (wt), 1 μg plasmid	n/a	n/a
	LPEI, pDMAEMA	pDNA	PEI - N:P 6, pDMAEMA N:P 5, 1 μg plasmid	Cationic	n/a
	LPEI, BPEI	pDNA	LPEI - N:P 6, BPEI - N:P 6 and 10, 1.25 μg/ml plasmid	Cationic	100 – 1000 nm, depending on buffer
	histidylated-PLL	pDNA	polymer:DNA 3 (wt)	+18mV	110 nm

Table 1-1 (cont'd)

Basis	Vehicle	General Uptake Mechanism(s)	Prominent Mechanism for active delivery	Ref.
Polymer	Polystyrene NPs	Both utilize energy, dynamin and actin dependent pathways. Positive particles utilize macropinocytosis more significantly	n/a	(Dausend et al. 2008)
	PEG cubes and cylinders	Low internalization for μ-sized, and negative particles. Cylindrical particles internalized faster. Multiple pathways utilized.	n/a	(Gratton et al. 2008)
	Latex beads	<200nm – clathrin, 200-500nm – caveolar, >500nm – none	n/a	(Rejman et al. 2004)
	LPEI, folate and transferrin targeting	Folate – primarily caveolar, Transferrin – primarily clathrin	Caveolar	(Gabrielson and Pack 2009)
	LPEI, pDMAEMA	Caveolar and Clathrin pathways	Caveolar	(van der Aa et al. 2007)
	LPEI, BPEI	n/a	COS-7 – clathrin (LPEI & BPEI), HUH-7 – clathrin (LPEI) clathrin&caveolar (BPEI), HeLa – clathrin & caveolar (LPEI & BPEI)	(von Gersdorff et al. 2006)

Table 1-1 (cont'd)

Basis	Vehicle	Nucleic Acid	Formulation	Complex Characteristics	
				Charge	Size (diameter)
Polymer	histone H3 peptide-PEI	pDNA	N:P 10, 20 μg/mL plasmid	+20mV	110 nm
	PEI coated iron oxide	pDNA	polymer:DNA 2 (wt), 0.5 μg plasmid	n/a	>200 nm
Polymer/ Lipid	Poly(glycoamidoamine), JetPEI	pDNA	PGAA - N:P 20, JetPEI - N:P 5, 20 μg/ml plasmid	n/a	PGAA - 75-150 nm in water
	DOTAP, LPEI	pDNA	lipid:DNA 6 (wt), polymer:DNA 30mM/ μg plasmid	n/a	n/a
Lipid	SAINT-2/DOPE (synthetic amphiphile)	pDNA	lipid:DNA 2.5 (wt)	n/a	~200 nm
	DharmaFECT1	siRNA	4uL lipid, 100nM siRNA	n/a	n/a
Peptide	RGD ligand	antisense	100nM	Anionic	MW ~8-9 kDa

Table 1-1 (cont'd)

Basis	Vehicle	General Uptake Mechanism(s)	Prominent Mechanism for active delivery	Ref.
Polymer	histidylated-PLL	Clathrin and Macropinocytosis	Clathrin	(Goncalves et al. 2004)
	histone H3 peptide-PEI	Caveolar and Clathrin pathways	Caveolar	(Reilly et al. 2012b, a)
	PEI coated iron oxide	Multiple pathways	Cell-line dependent	(Huth et al. 2004)
Polymer/ Lipid	Poly(glycoamidoamine), JetPEI	Mostly caveolar and clathrin, macropinocytosis minorly	PGAA – Caveolar, JetPEI – independent of specific mechanism	(McLendon et al. 2010; Liu and Reineke 2006)
	DOTAP, LPEI	DOTAP – clathrin, LPEI – caveolae and clathrin	DOTAP – clathrin, LPEI – caveolae	(Rejman et al. 2005)
Lipid	SAINT-2/DOPE (synthetic amphiphile)	Clathrin	Clathrin	(Zuhorn et al. 2002)
	DharmaFECT1	Multiple endosomal pathways	Independent of endocytosis, membrane fusion event	(Lu et al. 2009)
Peptide	RGD ligand	Caveolar (actin dependent, dynamin dependent)	Not clathrin or macropinocytosis (caveolar not measured)	(Alam et al. 2008; Alam et al. 2010)

Table 1-2 Status of current clinical trials for RNAi therapy

Class	Disease	Name	Target	Sponsor	Status
Skin disorders	Pachyonychia congenital	TD101	Keratin 6A N171K mutant	Pachyonychia Congenita Project	Completed Phase I
Ocular and retinal disorders	Non-arteritic anterior ischaemic optic neuropathy	QPI-1007	Caspase 2	Quark Pharm Inc.	Active, Phase I
	Age-related macular degeneration; choroidal neovascularization	AGN211745	VEGFR1	siRNA Therapeutics Inc	Completed, Phase I, II
	Glaucoma	SYL040012	β2 adrenergic receptor	Sylentis	Active, Phase I, II
	Diabetic macular oedema	Bevasiranib	VEGF	Opko Health, Inc.	Completed, Phase II
	Macular degeneration	Bevasiranib	VEGF	Opko Health, Inc.	Completed, Phase II
Cancer	Solid tumours	FANG	Furin	Gradalis, Inc.	Active, Phase II
	Solid tumours	CALAA-01	RRM2	Calando Pharm.	Active, Phase I
	Chronic myeloid leukemia	SPC2996	BCL-2	Santaris Pharm.	Ongoing, Phase I, II

Table 1-2 (cont'd)

Class	Disease	Name	Administration	Delivery	Unique Features	References
Skin disorders	Pachyonychia congenital	TD101	Intradermal injection	none specified	Specific targeting of dominant-negative mRNA	Leachman et al. 2008, Hickerson et al. 2008
Ocular and retinal disorders	Non-arteritic anterior ischaemic optic neuropathy	QPI-1007	Intravitreal injection	none specified		
	Age-related macular degeneration; choroidal neovascularization	AGN211745	Intravitreal injection	none specified	siRNA modifications: deoxythymidine overhangs, phosphorothioate linkage, inverted 2'-deoxy abasic nucleotides	Shen et al. 2006
	Glaucoma	SYL040012	Topical, eye drops	none specified		Jiminez et al. 2011
	Diabetic macular oedema	Bevasiranib	Intravitreal injection	none specified		
	Macular degeneration	Bevasiranib	Intravitreal injection	none specified		
Cancer	Solid tumours	FANG	Injection of treated cells	ex vivo electroporation	Treated cells express plasmid and shRNA	
	Solid tumours	CALAA-01	Intravenous injection	cyclodextrin polymer with transferrin receptor target	siRNA pool	Davis 2009
	Chronic myeloid leukemia	SPC2996	Systemic administration	none specified	16-mer oligonucleotide	Hansen et al. 2006

Table 1-2 (cont'd)

Class	Disease	Name	Target	Sponsor	Status
Cancer	Solid tumours	ALN-VSP02	VEGF, kinesin spindle protein	Alnylam Pharm.	Active, Phase I
	Pancreas adenocarcinoma	siG12D LODER	KRASG12D	Silenseed Ltd.	Active, Phase I
	Metastatic melanoma	NCT00672542	LMP2, LMP7, and MECL1	Duke University	Active, Phase I
	Advanced, recurrent or metastatic solid malignancies	Atu027	PKN3	Silence Therapeutics	Active, Phase I
Kidney disorders	Delayed graft function kidney transplant	QPI-1002/I5NP	p53	Quark Pharm., Inc.	Active, Phase I, II
	Kidney injury acute renal failure	QPI-1002/I5NP	p53	Quark Pharm., Inc.	Completed, Phase I
Antiviral	Hepatitis C virus	SPC3649/ miravirsen	miR-122	Santaris Pharm	Active, Phase II
	RSV in volunteers	ALN-RSV01	RSV nucleocapsid	Alnylam Pharm.	Completed, Phase II
	RSV in lung transplant patients	ALN-RSV01	RSV nucleocapsid	Alnylam Pharm.	Completed, Phase I
	RSV in lung transplant patients	ALN-RSV01	RSV nucleocapsid	Alnylam Pharm.	Active, Phase II

Table 1-2 (cont'd)

Class	Disease	Name	Administration	Delivery	Unique Features	References
Cancer	Solid tumours	ALN-VSP02	Intravenous injection	none specified		
	Pancreas adenocarcinoma	siG12D LODER	Localized injection of siRNA releasing capsule	miniature biodegradable polymeric matrix		
	Metastatic melanoma	NCT00672542	Intradermal injection of in vitro treated monocytes	ex vivo electroporation	siRNA pool targeting iP subunits LMP2, LMP7, MECL-1	Dannull et al. 2007
	Advanced, recurrent or metastatic solid malignancies	Atu027	Intravenous injection	liposomal siRNA formulation	Methylated siRNA sequences	Aleku et al. 2008
Kidney disorders	Delayed graft function kidney transplant	QPI-1002/I5NP	Intravenous injection	none specified	Methylated siRNA sequences	Feinstein 2011
	Kidney injury acute renal failure	QPI-1002/I5NP	Intravenous injection	none specified		
Antiviral	Hepatitis C virus	SPC3649/ miravirsen	Subcutaneous injection	none specified	miRNA antagonist	
	RSV in volunteers	ALN-RSV01	Inhalent	none specified		Zhang et al. 2002b; Johnson et al. 2007; Alvarez et al. 2009; Meyers 2011
	RSV in lung transplant patients	ALN-RSV01	Inhalent	none specified		
	RSV in lung transplant patients	ALN-RSV01	Inhalent	none specified		

CHAPTER 2: IMPROVED ASYMMETRY PREDICTION FOR SIRNAS

2.1 Abstract

In the development of RNA interference (RNAi) therapeutics, merely selecting short, interfering RNA (siRNA) sequences that are complementary to the messenger RNA (mRNA) target does not guarantee target silencing. Current algorithms for selecting siRNAs rely on many parameters, one of which is asymmetry, often predicted through calculation of the relative thermodynamic stability of the two ends of the siRNA. However, we have previously shown that highly-active siRNA sequences are likely to have particular nucleotides at each 5'-end, independent of their thermodynamic asymmetry. Here, we describe an algorithm for predicting highly active siRNA sequences based only on these two asymmetry parameters. The algorithm uses end sequence nucleotide preferences and predicted thermodynamic stabilities, each weighted based on training data from the literature, to rank the probability that an siRNA sequence will have high or low activity. The algorithm successfully predicts weakly- and highly-active sequences for enhanced green fluorescent protein (EGFP) and protein kinase R (PKR). Use of these two parameters in combination improves the prediction of siRNA activity over current approaches for predicting asymmetry. Going forward, we anticipate that this approach to siRNA asymmetry prediction will be incorporated into the next generation of siRNA selection algorithms.

2.2 Introduction

Therapeutic applications of RNA interference (RNAi) leverage a conserved pathway for gene expression regulation that possesses the potential for exquisite sequence specificity through the complementarity of short interfering RNAs (siRNAs) for their target (Fire et al. 1998; Matranga et al. 2005; Elbashir et al. 2001). Though the technology has yet to demonstrate its full potential in clinical applications (Pollack 2011; Krieg 2011), there remains major interest in developing siRNA-based therapeutics (Gitig 2012). Because RNAi represents a therapeutic approach that can be applied to nearly any disease (Davidson and McCray 2011), improvements in the design and development of siRNA therapeutics have the potential for a significant impact on clinical practice.

A number of intermolecular interactions are critical to the activity of siRNAs, including those with the delivery vehicle (Portis et al. 2010; Lu et al. 2009; Siegwart et al. 2011), the target mRNA (Ameres et al. 2007; Brown et al. 2005; Gredell et al. 2008; Kiryu et al. 2011), and the pathway proteins (MacRae et al. 2007; Maniataki and Mourelatos 2005; Gredell et al. 2010; Kini and Walton 2009). While a single RNA guide strand and Argonaute 2 (Ago2) are the minimal components required for active silencing *in vitro* (Rivas et al. 2005), the proteins Dicer and TAR RNA Binding Protein (TRBP) are important for RLC/RISC activity *in vivo* (Chendrimada et al. 2005; Haase et al. 2005; Lima et al. 2009). Other proteins, such as the protein activator of PKR (PACT) (Kok et al. 2007; Lee et al. 2006) and component 3 promoter of RISC (C3PO) (Ye et al. 2011), may also have important but as yet undefined functional roles in the RNAi process. One essential process executed by the pathway proteins is the identification and loading of the siRNA guide strand into the RLC/RISC and the concomitant destruction of the passenger strand (Tomari et al. 2004; Matranga et al. 2005; Leuschner et al. 2006). The likelihood of one siRNA strand

becoming the guide strand relative to the other strand is termed asymmetry (Schwarz et al. 2003; Tomari et al. 2004).

There are currently multiple proteins thought to participate in sensing the asymmetry of siRNA duplexes (Gredell et al. 2010; Frank et al. 2010; Noland et al. 2011; Betancur and Tomari 2012). When the existence of siRNA asymmetry was first identified, it was proposed that the relative hybridization stability of the two ends of the siRNA sequence was the principal means by which asymmetry was sensed by the pathway proteins (Schwarz et al. 2003). Since that time, nearly all algorithms for selecting highly-active siRNAs have used a thermodynamic calculation for asymmetry, among other parameters (Reynolds et al. 2004; Amarzguioui and Prydz 2004; Ui-Tei et al. 2004; Schwarz et al. 2003; Lu and Mathews 2008; Ichihara et al. 2007). More recently, evidence has begun to accumulate that the terminal nucleotides on each 5'-end of the siRNA may be valuable for predicting the activity of an siRNA (Gredell et al. 2010; Frank et al. 2010; Walton et al. 2010), in particular when classified according to the sixteen possible combinations of nucleotides. When terminal nucleotide classification is combined with relative hybridization stability, the accuracy of predicting siRNA activity improves markedly (Walton et al. 2010).

In this work, we wanted to predict siRNA activities based only on the two asymmetry characteristics, terminal nucleotide classification and relative thermodynamic stability, and establish experimentally their relative importance in determining the activity of an siRNA (Figure 2-1). Using a logistic regression model, we successfully predicted active and inactive sequences for the exogenous protein, enhanced green fluorescent protein (EGFP), as well as the endogenous protein, protein kinase R (PKR). In addition, the combination of both end sequence

and thermodynamic stability features provided improved correlation to siRNA activity when compared to either feature individually. These results demonstrate further that asymmetry may be determined by more factors than just relative stability and algorithms for prediction of siRNA activity should also account for terminal nucleotide sequence classification in asymmetry calculations.

2.3 Results

2.3.1 Ranking and Selection of EGFP-targeting siRNAs

Our ranking algorithm was initially tested on siRNAs to target the EGFP mRNA. From the cDNA sequence (see Supporting Information), there were 824 possible siRNA sequences, which were ranked based on the difference between the algorithm's predicted likelihood of high and low activity. For comparison, commercial algorithms (Dharmacon and Ambion) were also used. These selection algorithms were chosen, because their predictions are based solely on the characteristics of the siRNA and not on other factors used in some selection algorithms, such as target mRNA structure, which would make it difficult to directly compare the accuracy of our asymmetry-based predictions with predictions from more detailed selection approaches. The commercial rankings only included sequences predicted to have high activity as opposed to the entire range of possible siRNA sequences. While this is adequate for those needing effective siRNA sequences, it does not provide sufficient data to compare the characteristics of high activity and low activity siRNAs. The Dharmacon algorithm ranked the recommended siRNAs, whereas for Ambion there were no distinctions among the top 35 candidate sequences. Interestingly, there was no overlap between the lists of recommended sequences provided by the commercial algorithms. Aggregating the commercial recommendations with our predictions, we

chose 11 sequences to test experimentally that would allow us to preliminarily compare the relative utility of the three prediction approaches (Table 2-2).

Transfection experiments were performed using H1299-EGFP cells at various siRNA concentrations (Figure 2-2). Surprisingly, 81% of the sequences had some silencing effect compared to control treatments, with 73% of sequences showing greater than 75% reduction in protein levels at a 50 and 100 nM siRNA concentration. One sequence (EGFP 783) showed intermediate silencing (difference from other sequences indicated by double stars), suggesting a gradient, rather than a step change, in silencing ability between active and inactive sequences. In general, sequences predicted by our algorithm to have higher activity showed increased inhibition of EGFP fluorescence. The rank order of activities was maintained at lower (5 nM) and saturating (50 and 100 nM) siRNA concentrations. The two sequences chosen based on their opposing rankings between the two features in our approach, EGFP 757 (favorable terminal sequence, unfavorable $\Delta\Delta G$) and EGFP 783 (unfavorable terminal sequence, favorable $\Delta\Delta G$), ultimately displayed an activity correlated with their terminal nucleotide classification rather than their thermodynamic stability.

To further investigate the hypothesis that terminal sequence classification was more important than thermodynamic stability in predicting siRNA activity, silencing efficiencies were compared against algorithm rank, terminal nucleotide rank, and $\Delta\Delta G$ values individually (Figure 2-3). The correlation between activity and terminal nucleotide rank was better than for thermodynamic stability alone, with the correlation with full algorithm rank better than either alone. This agrees with our prior work showing that terminal nucleotide classification is generally a more informative predictor of siRNA activity but that inclusion of the

thermodynamic calculation provides some additional complementary information (Walton et al. 2010).

2.3.2 Ranking and Selection of PKR-targeting siRNAs

Although our algorithm successfully predicted active and inactive sequences for EGFP, we wanted to confirm similar results for an endogenous protein, the signaling pathway mediator, PKR. In addition, through systematic selection of siRNAs of high, medium, and low nucleotide ranking and siRNAs having high, medium, and low relative thermodynamic stabilities (Table 2-3), we aimed to further explore the relative importance of each of these characteristics in predicting silencing activity.

Transfection experiments were performed using HepG2 cells at 100 nM siRNA concentrations (Figure 2-4). In this case, 55% of sequences showed greater than 50% reduction in PKR protein levels when compared to control cells. Again, sequences predicted to have higher activity showed increased reduction in PKR protein levels. When sorted by end nucleotide classification, sequences in the UG class showed the best silencing efficiency, on average, regardless of their thermodynamic stability. Conversely, sequences in the low-ranking terminal nucleotide class, CU, do not show significant silencing, even when having highly positive $\Delta\Delta G$ values. In the intermediate category of end sequence (AA), silencing activity correlated strongly with the calculated thermodynamic stability, with a favorable value resulting in significant silencing and an unfavorable value not. Taken together with our results from the GFP experiments, these results support the argument that terminal sequence classification is a stronger predictor of siRNA activity that relative hybridization stability.

Our algorithm achieved improved correlation between rank and siRNA activity than achieved by either terminal nucleotide or thermodynamic stability independently (Figure 2-5). While the PKR terminal nucleotide correlation is less than that achieved from the EGFP data, the thermodynamic stability and overall algorithm rank correlation coefficients remain similar, even with a larger range of possible siRNA sequences (2352 for PKR vs. 824 for EGFP), showing the algorithm's fidelity for various sized targets. It is noteworthy that for both sequences, the top-ranked sequence, i.e., the one that would have been chosen for predicting an siRNA against a new target, was highly-active in silencing the target, further supporting our hypothesis that using only two parameters was sufficient for identifying active siRNAs against novel targets.

2.4 Discussion

The use of asymmetry is well-established as useful and important for selecting active siRNA sequences. Multi-step work flow protocols for selecting effective siRNAs have been developed (Birmingham et al. 2007; Mysara et al. 2011). However the selection algorithms themselves are based in part on using relative thermodynamic stability as the sole factor in determining sequence asymmetry. Other reported algorithms lack a consensus on the best way to calculate thermodynamic asymmetry for siRNA activity prediction (Huesken et al. 2005; Lu and Mathews 2008; Shabalina et al. 2006; Yuan et al. 2004; Takasaki 2009; Ladunga 2006). When utilizing the commercially available algorithms for comparison in this study, there were no overlaps between the sequences predicted to be highly active by Dharmacon and those predicted by Ambion, further illustrating the need for a consensus approach to selecting highly active siRNAs, including which parameters are most important/useful for such predictions.

The results described here further illustrate that accounting only for thermodynamic asymmetry ignores a more important feature in asymmetry, terminal nucleotide classification.

Our selection technique achieves correlation coefficient values > 0.8 whereas previously reported algorithms typically achieve correlation coefficients of 0.5-0.7 between algorithm predictions and experimental results (Birmingham et al. 2007; Matveeva et al. 2007). As our approach is focused on the contribution of asymmetry in the siRNA to its ultimate activity, it was important to compare our approach with others means of determining asymmetry. In calculating thermodynamic asymmetry, it is common to use one, three, or four nearest neighbors at each end of the siRNA as the basis for calculation (Lu and Mathews 2008; Matveeva et al. 2007; Schwarz et al. 2003; Khvorova et al. 2003). In our prior work (Walton et al. 2010), we showed that in concert with terminal nucleotide classification, calculating thermodynamic asymmetry with three nearest neighbor parameters provided the most information while one nearest neighbor provided the most information in the absence of terminal nucleotide classification. Based on this context, we compared the correlation of our data with thermodynamic calculations performed using 1, 3, and 4 nearest neighbor parameters (Figure 2-6). In all cases, the correlation of our experimental data was best with rankings including terminal nucleotide classification (Table 2-4). This strongly supports our contention that all siRNA selection algorithms would be improved by inclusion of our asymmetry approach in place of their current asymmetry calculation.

While our approach is useful for predicting active (and inactive) siRNAs, we have not yet established the causal relationship between the terminal nucleotide classification and siRNA processing and activity. Indeed, it is well-established that the properties of the siRNA alone only provide partial information as to the likely activity of the siRNA (Gredell et al. 2008; Kiryu et al. 2011; Overhoff et al. 2005; Shao et al. 2007). However, studies are increasingly reporting that more active siRNAs and miRNAs tend to contain specific nucleotides at the 5' position of the guide strand (Reynolds et al. 2004; Gredell et al. 2010; Seitz et al. 2011), possibly a result of

Ago2 binding specificity (Frank et al. 2010). We expect that going forward, our ongoing work and that of others, will more firmly tie the presence of particular 5'-end nucleotides on both the guide and passenger strands with important siRNA-protein interactions that occur in the pathway to ensure proper siRNA processing.

2.5 Chapter 2 Tables and Figures

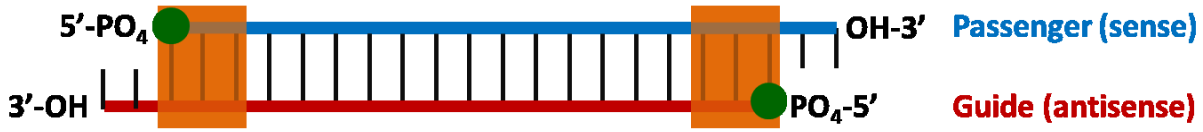

Figure 2-1 Algorithm features for designing highly active siRNAs. From the selected mRNA target, all potential siRNAs were classified according to their terminal sequence and thermodynamic stability. Terminal sequence (circles) uses the 5' terminal nucleotides, antisense:sense strand and thermodynamic stability (shaded rectangles) was calculated based on ΔΔG values using the 3 terminal nearest neighbors. All sequences we synthesized to contain UU overhangs on the 3' ends.

Table 2-1 Values of the coefficients used as weighting factors for predicting the probability of siRNAs at high (top third), medium (middle third), and low (bottom third) activity

Variable	High	Low
ΔΔG	0.2973	-0.1661
U:G	1.8767	-0.9852
A:G	0.3737	-0.0193
U:C	1.8744	-1.3088
U:A	1.7387	-1.0301
A:C	0.4764	-0.406
U:U	1.5084	-1.0877
C:G	-0.2463	0.4025
G:C	-0.6404	0.3337
A:A	0.2381	0.0810
G:G	-0.7873	0.2945
A:U	-0.5707	0.3471
C:C	-0.3552	-0.0987
G:A	-1.1939	0.6077
G:U	-2.2329	1.3262
C:A	-1.1755	0.9055
C:U	-2.2846	1.2957
Intercept	-0.0498	-0.2145

Table 2-2 EGFP-targeting siRNA sequences selected for this study, sorted by algorithm rank

5' Target Position	siRNA Sequence	End 5' Nucleotides Anti:Sense	Rank	Thermodynamic ΔΔG (kcal/mol)	Algorithm Rank	Testing Rationale
415	UGUACUCCAGCUUGUGCCC	U:G	1	4.2	1	Highest algorithm ranking
416	UUGUACUCCAGCUUGUGCC	U:G	1	2.1	17	Highest Dharmacon rank (91)
274	UGCGCUCCUGGACGUAGCC	U:G	1	0.8	38	On Ambion list
757	UGGGCAGCGUGCCAUCAUC	U:G	1	-2.6	177	High end, low ΔΔG
306	CUUGUAGUUGCCGUCGUCC	C:G	7	2.9	239	On Ambion list
396	CAGGAUGUUGCCGUCCUCC	C:G	7	0.5	389	On Ambion list
126	GAUGAACUUCAGGGUCAGC	G:G	10	1.9	418	On Ambion list
711	AUGGCUAAGCUUCUUGUAC	A:G	2	-3.7	551	Low rank, high Dharm. (73)
783	CAUCCCGCUCUCCUGGGCA	C:U	16	3.1	695	Low end, high ΔΔG
159	GGGCCAGGGCACGGGCAGC	G:G	10	-2.3	700	On Ambion list
253	CGGGCAUGGCGGACUUGAA	C:U	16	-5.2	824	Lowest algorithm rank

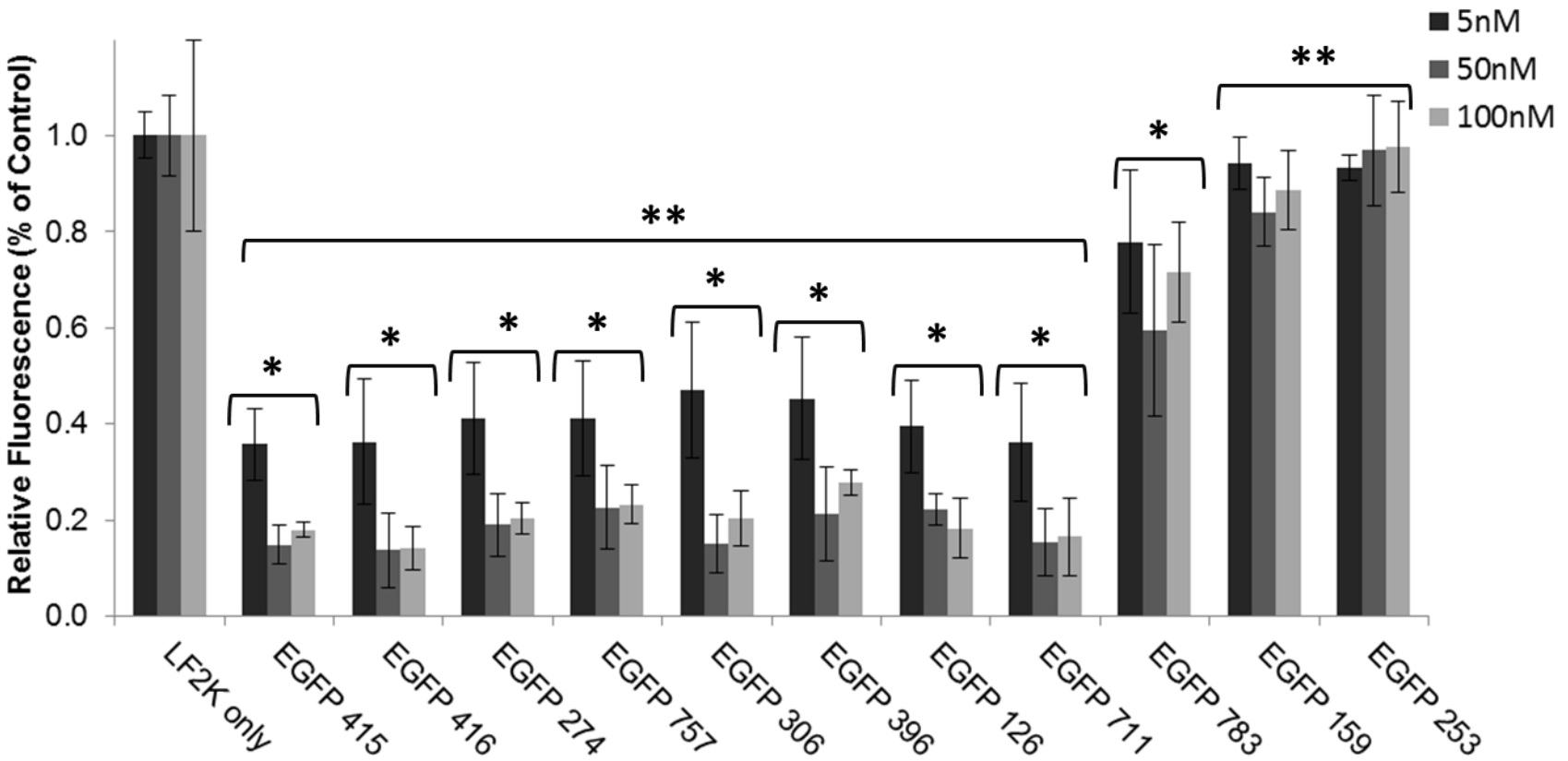

Figure 2-2 Silencing of EGFP by selected siRNAs. H1299 cells expressing EGFP were treated with 5, 50, and 100 nM of siRNA for 24 h using Lipofectamine 2000 (LF2K). Results are normalized EGFP fluorescence of LF2K-only treated control cells. siRNA treatments are ordered based on algorithm predictions (415 = highest predicted activity, 253 = lowest predicted activity). Error bars = +/- 1 standard deviation, n =4 (5 nM), 5 (50 nM), and 3 (100nM). Single stars indicate a significant difference ($p < 0.05$) compared to LF2K only treatments. Double stars indicate a significant difference ($p < 0.05$) compared to EGFP 783.

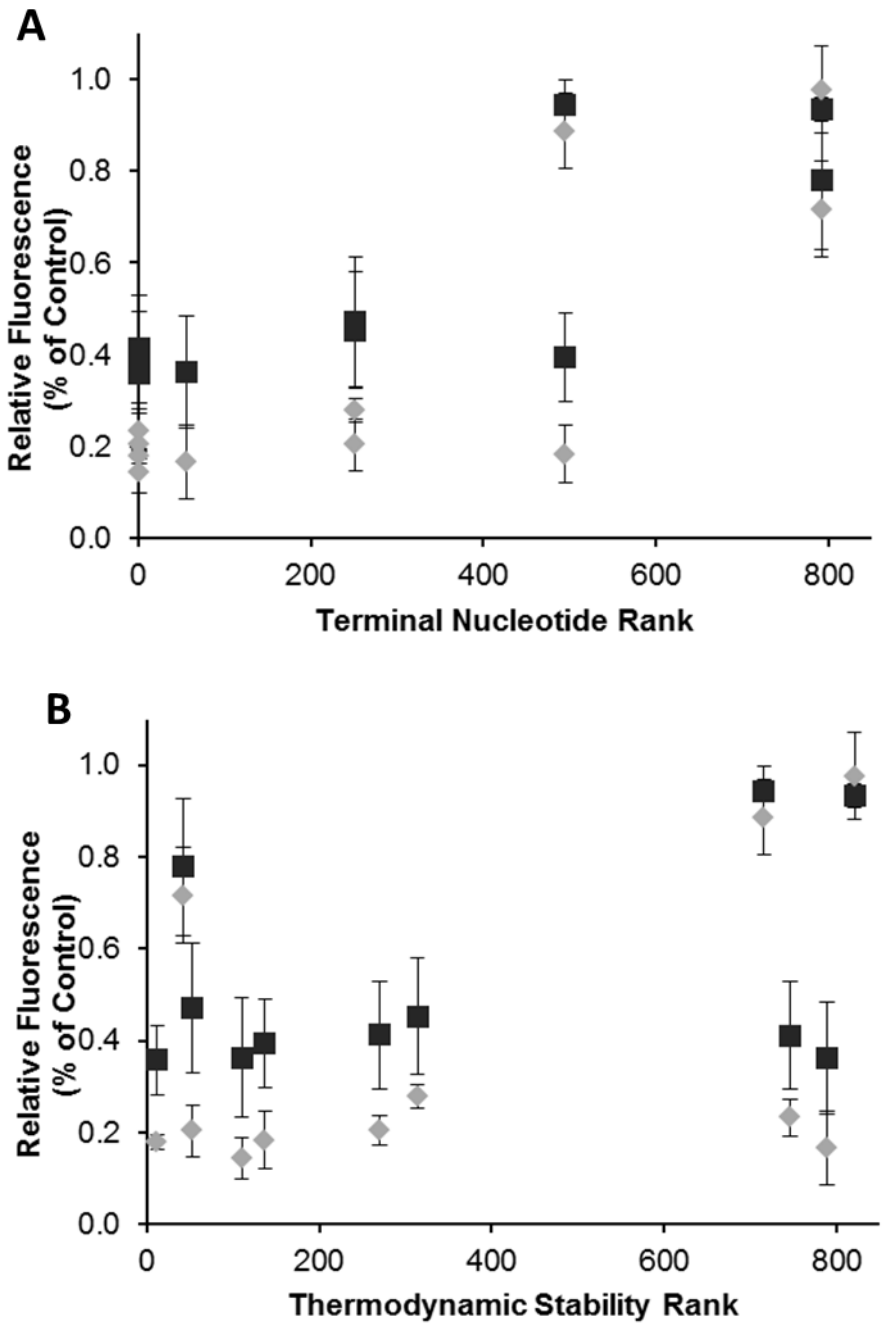

Figure 2-3 Correlation of exogenous gene silencing with each feature of the algorithm.

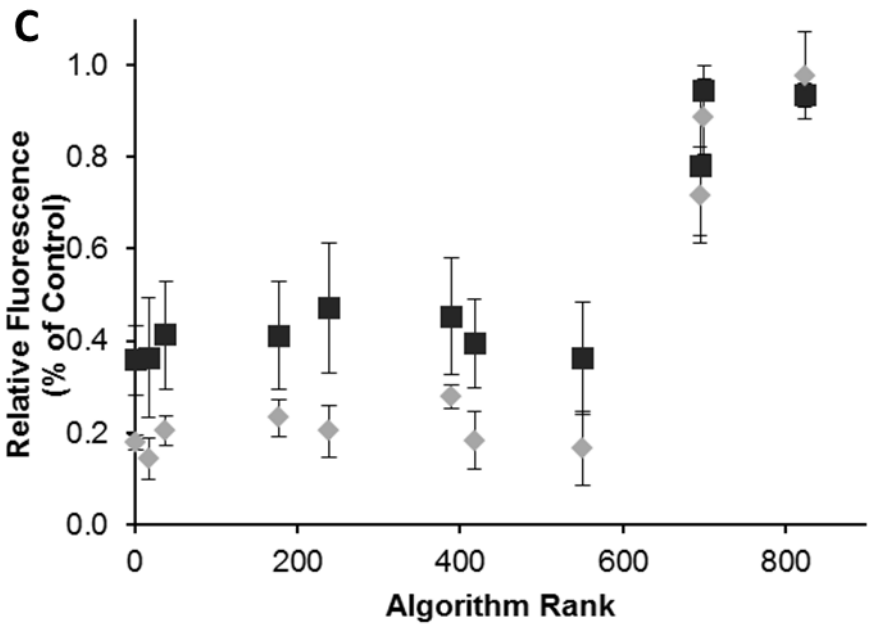

D

Correlation (r)	5nM	50nM	100nM
Algorithm	0.807	0.810	0.814
Terminal Nucleotide	0.822	0.808	0.821
Thermodynamic Stability	0.389	0.478	0.424

Figure 2-3 (cont'd) EGFP silencing results graphed against terminal nucleotide rank only (A), ΔΔG values only (B) or algorithm rank (C). The squares represent 5 nM siRNA while the diamonds are 100 nM siRNA treatments. For visual clarity, the 50 nM data points were not included in the plots but follow the same trend in silencing activity. The correlation coefficients for each dataset are tabulated (D).

Table 2-3 PKR-targeting siRNA sequences selected for this study, sorted by end sequence ranking, followed by relative thermodynamic stability

5' Target Position	siRNA Sequence	5'-End Nucleotides Anti:Sense	Rank	Thermodynamic ΔΔG (kcal/mol)	Algorithm Rank	Testing Rationale
410	UAAUGAAAUCCUUCUGGCC	U:G	1	6.3	1	High end, high ΔΔG
193	UCUUUGAUCUACCUUCACC	U:G	1	1.9	61	Previously validated
816	UUUAAAAUCCAUGCCAAAC	U:G	1	0	230	High. end, med. ΔΔG
952	UUGCCAAUGCUUUUACUUC	U:G	1	-4.2	948	High end, low ΔΔG
336	AAUUCUAUUGAUAAGGCCU	A:A	9	5.3	205	Med. end, high ΔΔG
645	AUCUGCUGAGAAGUCACCU	A:A	9	0	1154	Med. end, med. ΔΔG
379	AUGCACACUGUUCAUAAUU	A:A	9	-5.2	1926	Med end, low ΔΔG
1198	CAAAGAGUUCCAAAGCCAA	C:U	16	5.5	1606	Low end, high ΔΔG
640	CUGAGAAGUCACCUUCAGA	C:U	16	0	2206	Low end, med. ΔΔG
928	CCGCCUUCUCGUUAUUAUA	C:U	16	-5.2	2352	Low end, low ΔΔG

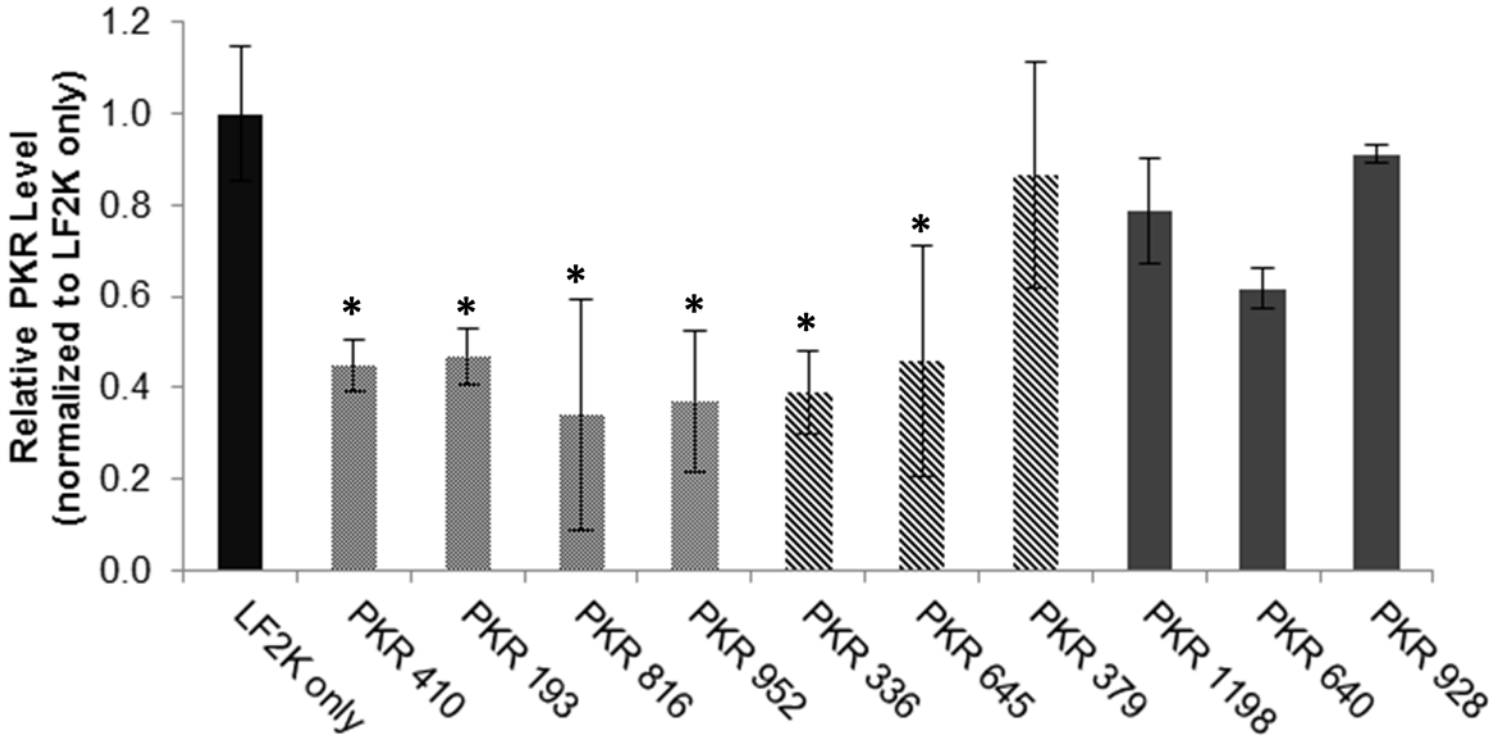

Figure 2-4 Silencing of PKR by selected siRNAs. HepG2 cells were reverse-transfected with 100 nM of siRNA for 48 h using Lipofectamine 2000 (LF2K). Results are normalized to both total protein level and PKR level of LF2K-only treated control cells (black). siRNAs were grouped by end sequence rank, UG (light grey), AA (striped), and CU (med grey). Error bars = +/- 1 standard deviation, n =3. Stars indicate a significant difference ($p < 0.05$) when compared to LF2K only treatment.

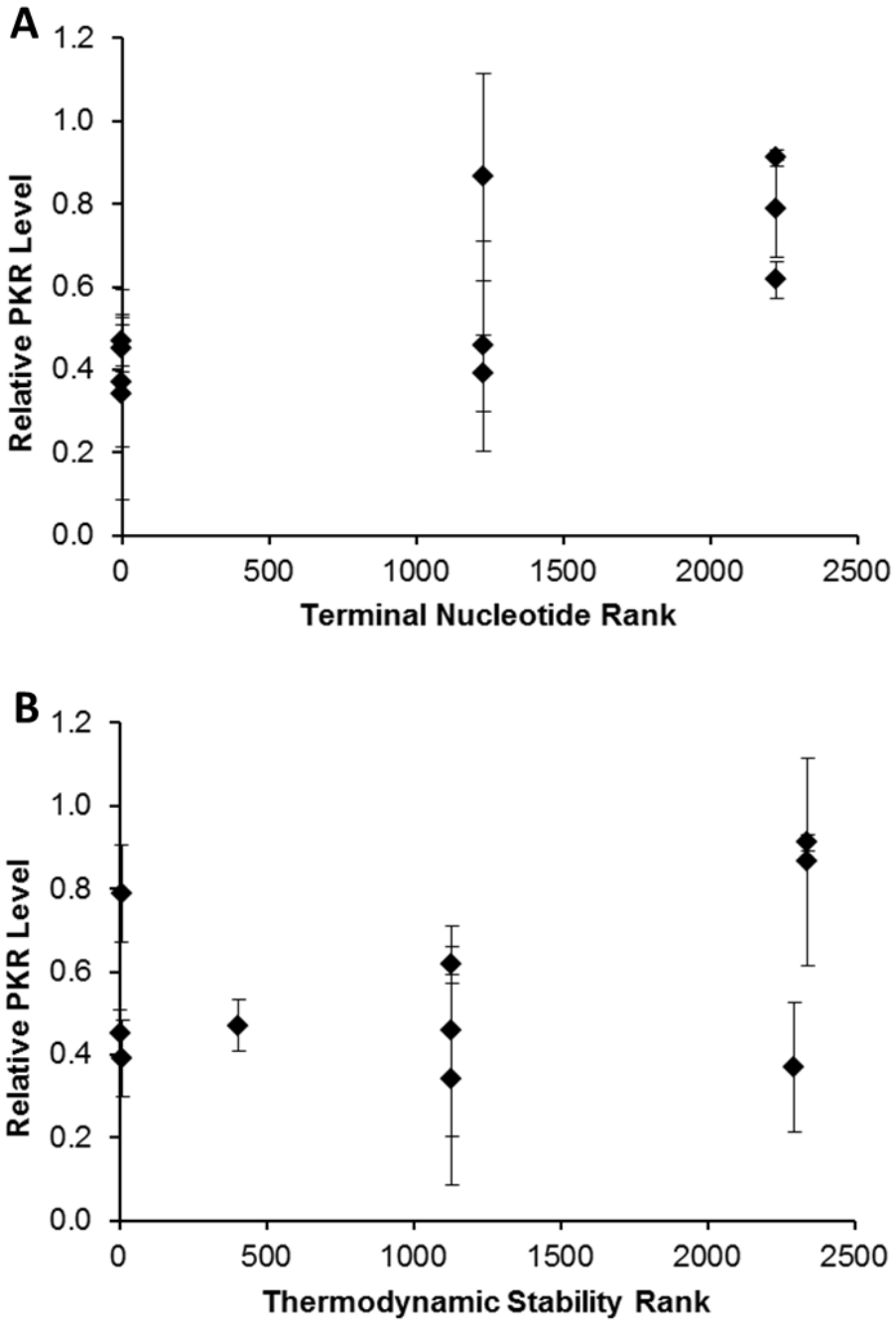

Figure 2-5 Correlation of endogenous gene silencing with each feature of the algorithm.

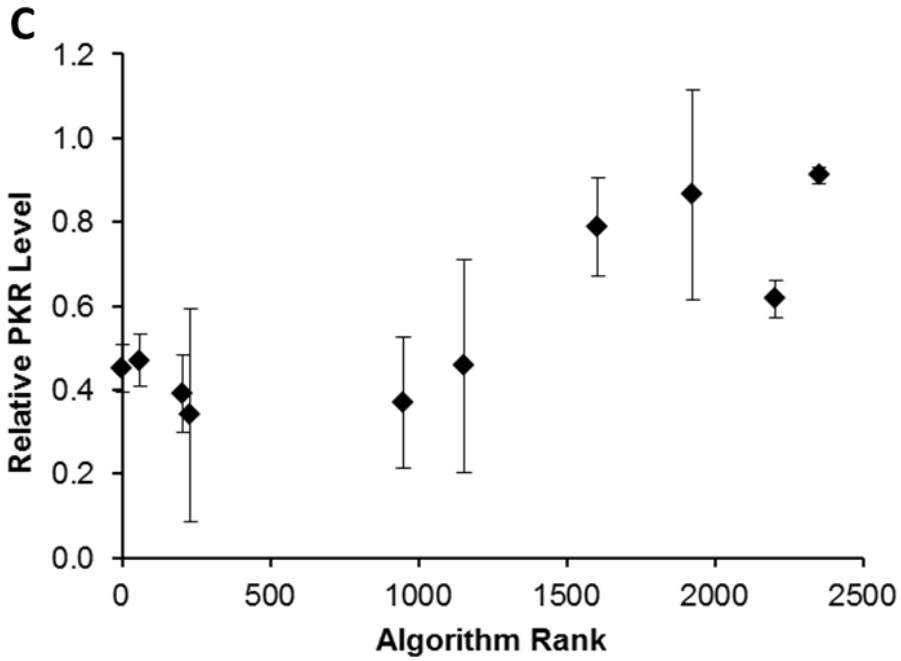

D

Correlation (r)	100nM
Algorithm	0.819
Terminal Nucleotide	0.737
Thermodynamic Stability	0.370

Figure 2-5 (cont'd) PKR silencing results graphed against terminal nucleotide rank only (A), ΔΔG values only (B), or algorithm rank (C). The correlation coefficients for each dataset are tabulated (D).

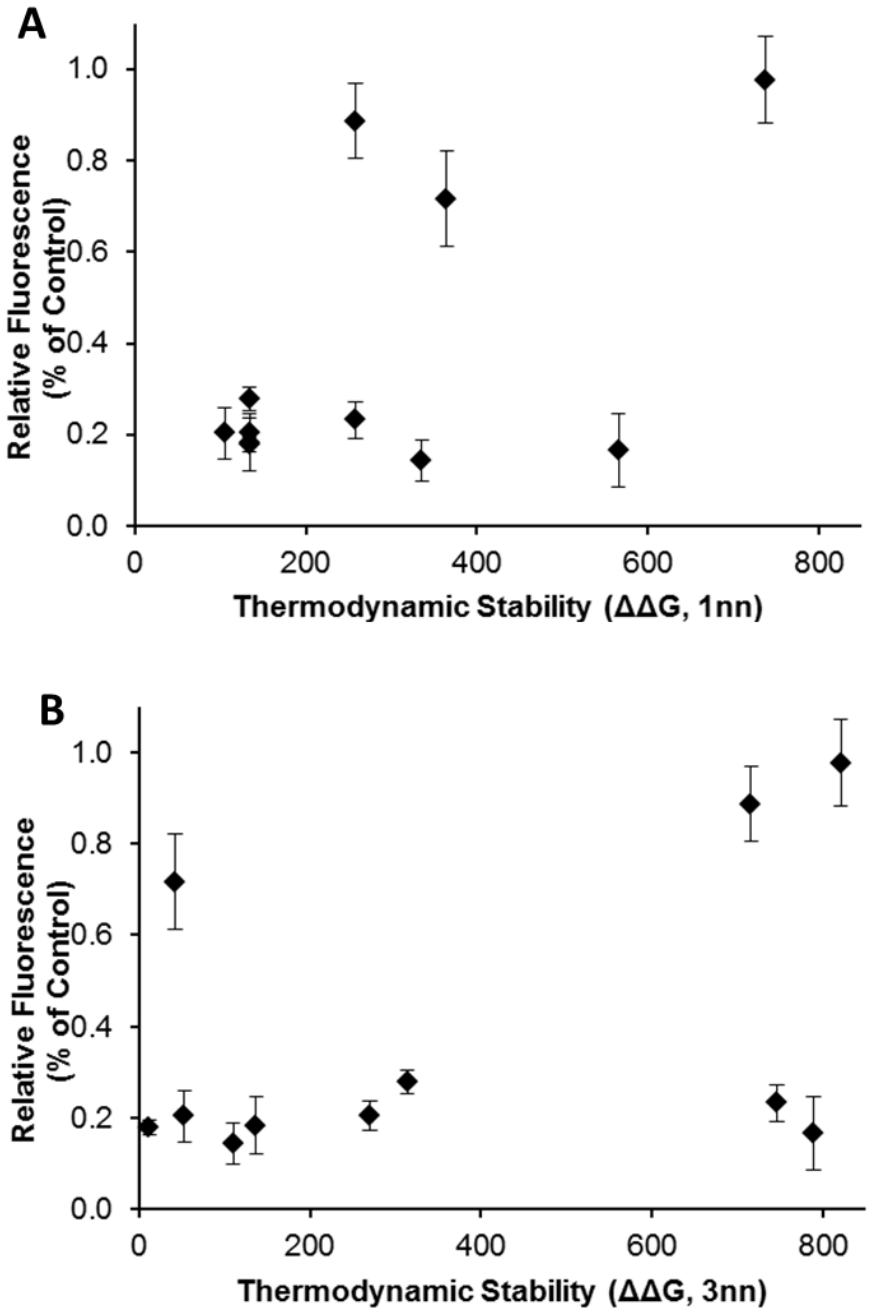

Figure 2-6 Correlation of asymmetry calculations with experimental data.

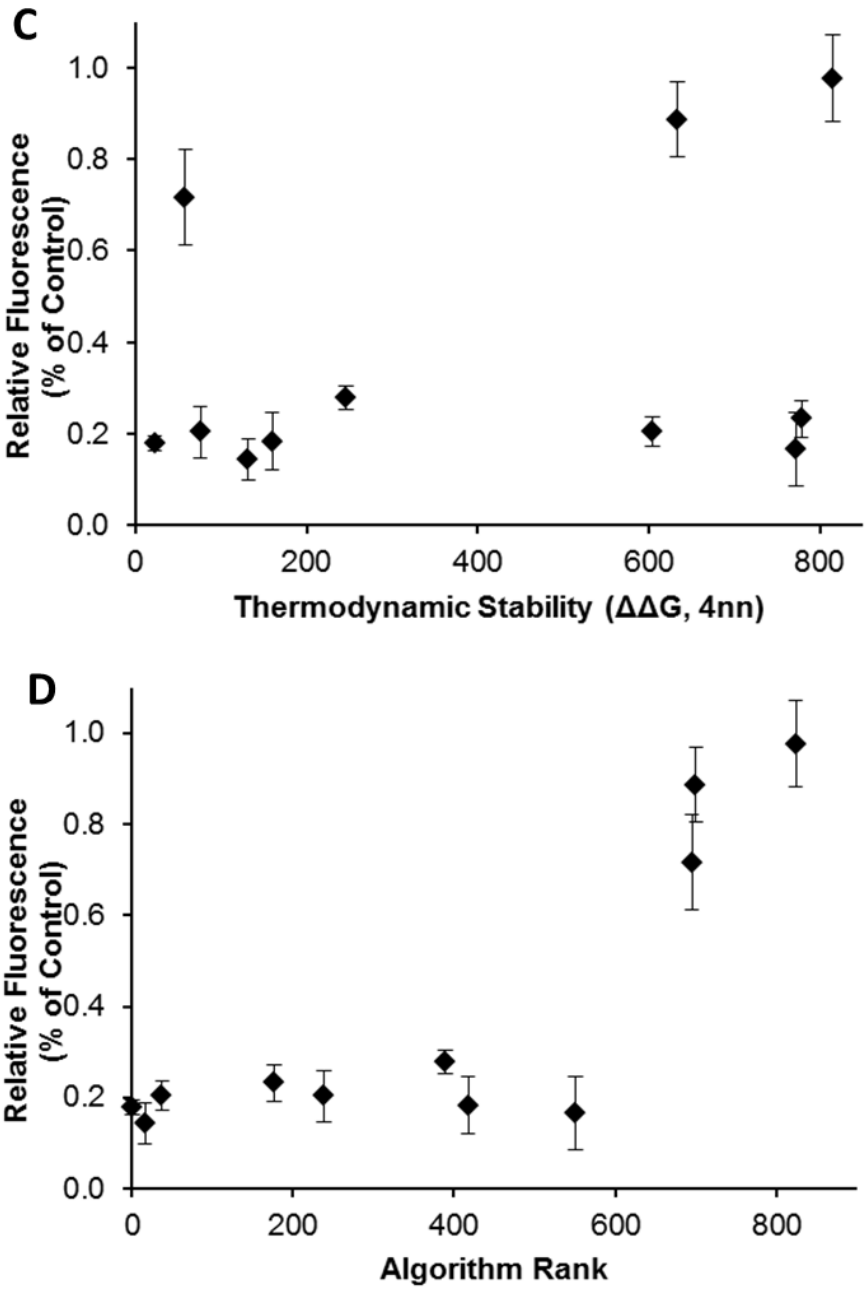

Figure 2-6 (cont'd) 100 nM EGFP silencing results graphed against rankings among all possible siRNA sequences using ΔΔG calculated using 1 nearest neighbor (A), 3 nearest neighbors (B), 4 nearest neighbors (C), or our algorithm (3 nearest neighbors and terminal nucleotide classification (D).

Table 2-4 Correlation coefficients between EGFP silencing at 100nM and the four different ranking methods in Figure 2-6

Correlation Coefficient (r)	100nM
Algorithm	0.814
ΔΔG (1nn)	0.539
ΔΔG (3nn)	0.424
ΔΔG (4nn)	0.327

CHAPTER 3: CONFOCAL MICROSCOPY FOR THE ANALYSIS OF SIRNA DELIVERY BY POLYMERIC NANOPARTICLES

Note: This chapter is published in (Portis et al. 2010)

3.1 Abstract

Clinical applications of genetic therapies, including delivery of short, interfering RNAs (siRNAs) for RNA interference (RNAi), are limited due to the difficulty of delivering nucleic acids to specific cells of interest while at the same time minimizing toxicity and immunogenicity. The use of cationic polymers to deliver nucleic acid therapeutics has the potential to address these complex issues but is currently limited by low delivery efficiencies. While cell culture studies have shown that some polymers can be used to deliver siRNAs and achieve silencing, it is still not clear what physical or chemical properties are needed to ensure that the polymers form active polymer-siRNA complexes. In this study, we used multicolor fluorescence confocal microscopy to analyze the cellular uptake of siRNAs delivered by novel propargyl glycolide polymeric nanoparticles (NPs). Delivery by these vehicles was compared to delivery by linear polyethyleneimine (LPEI) and Lipofectamine 2000 (LF2K), which are both known as effective delivery vehicles for siRNAs. Our results showed that when LF2K and LPEI were used, large quantities of siRNA were delivered rapidly, presumably overwhelming the basal levels of mRNA to initiate silencing. In contrast, our novel polymeric NPs showed delivery of siRNAs but at concentrations that were initially too low to achieve silencing. Nonetheless, the exceptionally low cytotoxicity of our NPs, and the simplicity with which they can be modified, makes them good candidates for further study to optimize their delivery profiles and, in turn, achieve efficient silencing.

3.2 Introduction

Gene therapy has the potential to treat a wide variety of genetic and acquired diseases in which traditional molecular drugs have proven ineffective. The potential to design a highly specific nucleic acid therapy from the coding sequence of the disease protein is appealing over small molecule drugs which are more difficult to develop. These small molecules can have side effects through interactions with untargeted proteins and biomolecules. With the discovery and subsequent explosion of work in RNA interference (RNAi), the realm of nucleic acid therapies has expanded from the traditional focus of delivering genes to add functionality to cells, to include the delivery of a variety of nucleic acids for both upregulation and downregulation of specific proteins.

Clinical applications for nucleic acid delivery have been limited due to the lack of vehicles that survive the challenging in vivo environment. The vehicle must be able to protect the nucleic acid cargo as it is being transported, target only the cells of interest, efficiently deliver the cargo in its active form, and be non-toxic at the concentrations required for delivery. Delivery approaches are generally divided between viral and non-viral methods. Viral delivery methods, such as adenoviruses (Ghosh et al. 2006), retroviruses (Mori et al. 2005), and adeno-associated viruses (Peng et al. 2000), have an advantage of delivery efficiency but often result in safety concerns due to immunogenicity and resistance to repeated infection (Ghosh et al. 2006; Kaiser 2007). Therefore, developing non-viral delivery methods for siRNAs has been and will continue to be a focus of significant research effort (recently reviewed in (Nel et al. 2009)).

Among non-viral approaches, the majority of delivery vehicles are based on cationic lipids (Cardoso et al. 2007; Hong et al. 1997) or cationic polymers (Pack et al. 2005). These cationic species allow electrostatic complex formation with anionic nucleic acids. A variety of

commercial cationic lipid reagents, such as Lipofectamine 2000 (LF2K), are used for nucleic acid delivery to cultured cells. Unfortunately, these reagents are typically cytotoxic at concentrations only slightly higher than that required for effective delivery (Zhang et al. 2007), thus presenting a challenge for their use in vivo. Therefore, for eventual in vivo applications, the development of polymeric delivery vehicles has been an area of considerable study.

Polymeric delivery methods are most often used for the delivery of plasmid DNA (pDNA) (Farrell et al. 2007) and short interfering RNA (siRNA) (Whitehead et al. 2009), with antisense oligonucleotides (Chen et al. 2006) and aptamers (Que-Gewirth and Sullenger 2007) also being studied. The challenges in delivering pDNA and siRNA are unique due to the differences between DNA and RNA and the dramatic difference in size. While pDNA has the ability to provide increased complex condensation (Spagnou et al. 2004) and extended transgene expression (Thierry et al. 1995), delivery is hampered by its large size and the need for the pDNA to reach the nucleus to be active (Gary et al. 2007). siRNAs are more susceptible to degradation by serum nucleases and require repeated delivery for sustained inhibition (Bartlett and Davis 2006). However, they are considerably smaller than pDNA (~5 nm vs. > 30 nm), and therefore require smaller quantities of vehicle and need only to reach the cytoplasm to be active (Gary et al. 2007). Thus, delivery vehicles with the appropriate physical and chemical properties should be able to overcome the challenges presented by siRNA delivery.

Linear and branched polyethylenimine (LPEI, BPEI) have traditionally been the standard cationic polymers of choice (Mehrotra et al. 2009) even though they have been shown to be significantly toxic (Burke and Pun 2008). Modifications of PEI with the addition of poly(ethylene glycol) (PEG) (Mao et al. 2006), ethyl acrylate (Zintchenko et al. 2008), or cross-linking (Hu et al. 2009) have been able to increase delivery efficiency while decreasing toxicity.

Other single polymer systems include poly (β-amino esters) (PBAE) (Lynn and Langer 2000) or poly(amidoamine) (PAMAM) dendrimers (Tang et al. 1996). Combinations of polymers to create di- or tri-block polymers such as polyvinyl alcohol with poly(D,L-lactide-co-glycolide) (PVA-b-PLGA) (Nguyen et al. 2008) or poly(ethylene oxide) (PEO) with poly(ε-caprolactone) (PEO-b-PCL) (Xiong et al. 2009) are also promising methods of improving nucleic acid delivery.

Unfortunately, polymers synthesized with similar characteristics can have widely varying silencing efficiency, as seen in one study where only 46 of the 2350 PBAE derivatives demonstrated transfection efficacies better than that of PEI (Green et al. 2008). In most cases, the presence of amine groups is a common motif among all successful delivery vehicles, with secondary and tertiary amines showing the best nucleic acid binding and endosomal release (Green et al. 2008; Liu and Reineke 2005). Other studies have shown that the presence of disulfide bonds can also aid in the intracellular release of the complex (Rozema et al. 2007; Breunig et al. 2008; Ou et al. 2008). Its reduction by cytoplasmic glutathione and thioredoxin can cause the breakdown of the polymer itself to release the siRNA from a non-covalent complex or sever the bond between the polymer and siRNA for a covalently-linked siRNA. However, no general rules exist for designing siRNA delivery vehicles.

It is believed that polymer-siRNA complexes enter cells through the endosomal pathway, eventually escaping into the cytoplasm, allowing for the release of the siRNA, and eventual silencing of a target gene. To date, siRNA studies have included microscopy images for delivery by LF2K (Berezhna et al. 2006) and at the point of silencing (Xiong et al. 2009). However, the delivery mechanism of polymeric siRNA complexes intracellularly over time, from the

membrane, through endocytosis, to the entry of the siRNA into the cytosol, and silencing of the target mRNA remains unknown.

In our study, we used a poly(propargyl glycolide) (PPGL) polymeric backbone that allows for the addition of a variety of chemical functional groups through an alkyne-azide cycloaddition known as "click chemistry" (Jiang et al. 2008). For the polymers used in this study, we added combinations of primary amines, secondary amines, disulfide linkages, and cholesterol groups to create our delivery vehicles (Figure 3-1). Using confocal laser scanning microscopy, we imaged enhanced green fluorescent protein (EGFP) expressing cells at various time points after transfection of siRNAs by LF2K (a model lipid), LPEI (a model cationic polymer), and two of our PPGL nanoparticles (NPs). By using a fluorescently tagged siRNA and a 7-dimethylaminocoumarin acetic acid (DMACA) tagged particle, we are able to see cellular uptake of both the siRNA and polymer with respect to time. Our results showed that LF2K and LPEI bound more tightly to the siRNA and delivered siRNA to the target cells more quickly and in apparently larger complexes. We conclude that our NPs, which have similar chemical functionality to LPEI, do not result in silencing due to their inability to form the higher order complexes required to deliver a sufficiently high initial dose of siRNA to achieve measurable silencing.

3.3 Results

3.3.1 Polymer Binding Gels

It was first important to understand the association of our polymeric NPs with the siRNAs. To do this, we performed in vitro binding experiments using electrophoresis as the readout (Figure 3-2). For our binding experiments, a 21 base pair dsDNA of analogous structure to the GFP-targeting siRNA was used to help minimize cost.

Both LPEI and LF2K showed markedly stronger binding to the dsDNA than either the Cholesterol NP or the disulfide NP (Figure 3-2, Table 3-1). Only in the case of LPEI did the equation suggest possible binding cooperativity (n = 1.8). The strength of the binding interaction is important to the overall efficacy of the siRNA. Vehicles that form less-stable complexes will have to be used in greater excess concentration to ensure complete encapsulation of the siRNA cargo. Thus, based on our results, when performing cellular uptake experiments, we chose to use 10μg/mL LPEI and 100μg/mL polymer concentrations to maximize siRNA encapsulation while minimizing excess polymer concentration.

3.3.2 Cellular Uptake

We monitored the delivery of polymer/siRNA complexes into GFP expressing H1299 cells over time using confocal microscopy (Figure 3-3). As early as 4h, both LF2K and LPEI begin to show intracellular accumulation. The disulfide NP and siRNA only cell populations do not show any intracellular siRNA signal, while the cholesterol NP shows minimal intracellular signal with significant extracellular accumulation around the cell membrane, perhaps due to increased aggregation and sedimentation of the hydrophobic cholesterol NP as compared to the other polymers. It should be noted that at this early time point, the siRNA signal from the LF2K- and LPEI-treated cells arises primarily from points of concentrated fluorescence (Figure 3-4), suggesting that these vehicles form structures that deliver multiple siRNAs simultaneously to a single cell.

By 8h, siRNA uptake can be seen for all 4 delivery vehicles and the siRNA only treatments (Figure 3-3). For LF2K and LPEI, the intracellular siRNA signal is still primarily concentrated in distinct intracellular locations. In contrast, the cholesterol and disulfide NPs show a more even siRNA distribution throughout the cell. This further suggests the LPEI and LF2K complexes that

enter the cell are more densely packaged than those formed by the cholesterol and disulfide NPs. It is notable that the uptake and distribution pattern after delivery by the cholesterol and disulfide NPs more closely resembles that of the siRNA only treatment than those of the LF2K and LPEI.

After 16h, the LF2K-treated cells begin to show silencing of the GFP. Additionally, the siRNA has spread more uniformly throughout the cells. In the case of the LPEI treatment, changes in the cell morphology can be seen, indicative of the cytotoxicity of LPEI. As with the LF2K, the intracellular siRNA distribution has become more uniform throughout the cell. The cholesterol and disulfide particles, along with the siRNA only treatment, show widespread delivery of the siRNA throughout the cells but, in none of the cases, do the siRNAs significantly silence GFP. However, unlike the LPEI, our NPs show no effect on cell morphology, indicating far less cytotoxicity despite their higher concentration relative to LPEI (100 μg/mL vs. 10 μg/mL). Interestingly, the siRNAs delivered by the cholesterol NP appear to accumulate preferentially around the nuclei of the cells. This could be attributed to the hydrophobicity of the cholesterol causing it to associate with the nuclear membrane. For the disulfide particle, blue areas can also be seen inside the cells apart from the overlapping red siRNA signal. Due to the low binding affinity of this particle, it is likely that uncomplexed particles can also be taken up by the cell, potentially resulting in competition for uptake with complexed particles.

By 24h, it appears that two populations of cells have been generated by LF2K treatment, those cells that received siRNA and have had GFP nearly completely silenced and those cells that did not receive siRNA and have basal GFP expression. For the LPEI, a more graded silencing can be seen where more cells have intermediate fluorescence intensity. Additionally, the changes in morphology are more pronounced, with cells appearing more spindly and less regular in shape. For the cholesterol and disulfide NPs, despite the continuing accumulation of

siRNA, there is no significant silencing. The same can be seen for the siRNA only images, where widespread uptake is seen without silencing. In some cells, the disulfide particle colocalizes with the siRNA, but this does not occur consistently across the cell population.

3.3.3 Intensity Analysis

To confirm the siRNA packaging found in LF2K and LPEI transfected cells are more highly concentrated as compared to the cholesterol NPs at the 4h time point, line intensity graphs were constructed across selected cells from the 160x magnification images (Figure 3-4). The lines were drawn lengthwise across regions of single cells where the siRNA-polymer complexes are present. In both the LF2K and LPEI graphs, there are highly localized regions of strong fluorescence from the siRNA. These fluorescence peaks are suggestive of the presence of multiple siRNAs at these points, likely still complexed with the vehicles. In contrast, the maximal siRNA signal when delivered using the cholesterol NPs, the only other polymeric delivery technique with any intracellular signal at this time point, is three- to six-fold lower than the signal from the LF2K and LPEI. The cholesterol complexes also show multiple siRNA peaks but at a much lower intensity. Because eventual silencing occurs for both the LF2K and LPEI, this suggests that the higher initial concentration of siRNA is necessary to initiate silencing.

3.4 Discussion

Confocal microscopy is a valuable tool for analyzing the delivery and function of siRNAs to cultured cells at the resolution of a single cell. As we found, the uptake of siRNAs delivered by different vehicles can vary by rate, fraction of cells loaded, and the apparent structure of the complexes taken up. Moreover, we were able to identify, particularly for delivery using LF2K, that multiple cell populations could arise within a treatment group and that the distribution of the siRNAs within a cell changed markedly over time. Bulk measurements like western blotting or

average fluorescence would have masked these important details of the delivery process. Additionally, we were able to visualize changes in cell morphology as a result of LPEI exposure, changes that did not occur upon exposure to our polymers. Combining this information improved our understanding of the siRNA delivery process and will greatly enhance our future ability to design more efficient vehicles for siRNA delivery based on our polymer system.

Many studies have reported on key compositional elements that are common among effective vehicles (Breunig et al. 2008; Green et al. 2008; Liu and Reineke 2005; Ou et al. 2008; Rozema et al. 2007). Our binding data support that chemical composition is critical in forming complexes that can achieve silencing, with the more tightly bound complexes resulting in more active silencing (Figures 3-2 and 3-3). However, vehicles containing the key compositional features are not guaranteed to result in silencing when used for siRNA delivery (Green et al. 2008). Our data support that a fundamental aspect to achieving silencing may be in the physical structures of the vehicle-siRNA complexes that form, not just their chemical compositions.

These structures result from both the interaction of the vehicle with the siRNA but also from the aggregation of the complexes into higher order structures. In this way, the cooperativity of the interaction may also be a defining characteristic for the eventual function of the siRNAs. Elucidating the structure of the siRNA-vehicle complexes can be difficult. Modeling approaches could be used to predict the structures of polymer-siRNA complexes, in a similar manner to models used for predicting protein/peptide aggregation (Tjernberg et al. 1999). Several experimental techniques have proven useful for measuring the changes in the polymer complexes with time, concentration, and altered vehicle chemistry. These include dynamic light scattering (DLS) (Breunig et al. 2008; Ou et al. 2008), transmission electron microscopy (TEM) (Cohen et

al. 2000), scanning electron microscopy (SEM) (Mehrotra et al. 2009), and atomic force microscopy (AFM) (Shifrina et al. 2009).

While siRNA delivery by our polymeric NPs did not result in silencing, we were encouraged that our polymers did not show any apparent toxicity, even at concentrations far in excess of that required for LPEI delivery. As we go forward in designing vehicles for siRNA delivery, we will place additional emphasis on understanding the structures formed from the vehicle-siRNA complexes. Moreover, we are investigating strategies for modifying our polymers to improve their binding with the siRNA cargo. Possible means to achieve this include covalent coupling of multiple siRNA to a single polymer and adding side-chains with greater positive charge density to improve the electrostatic attraction between the polymer and the siRNA. In all cases, confocal microscopy will serve as an essential tool for determining the siRNA uptake profiles for our various polymers.

3.5 Chapter 3 Tables and Figures

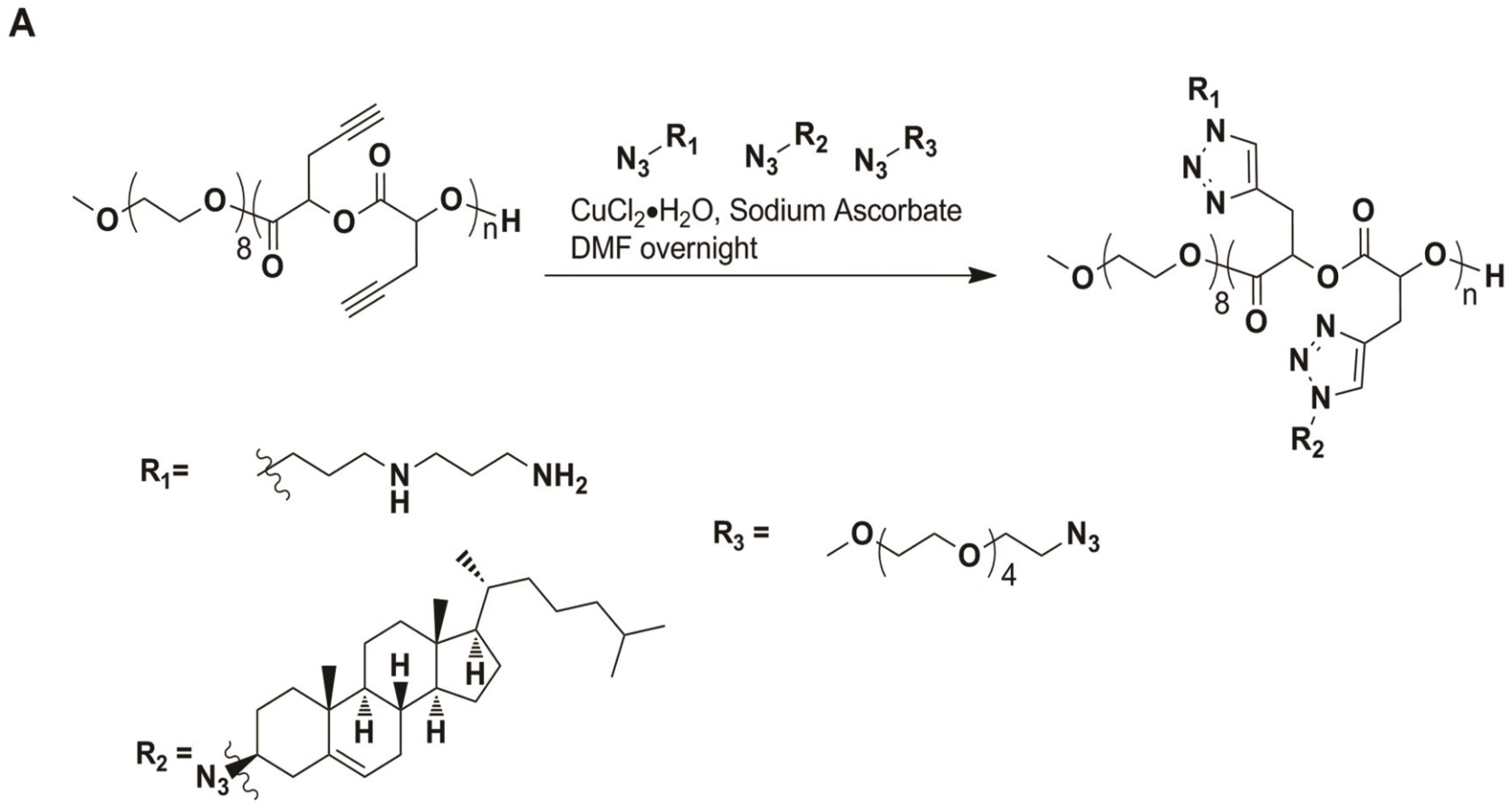

Figure 3-1 Click chemistry schematic

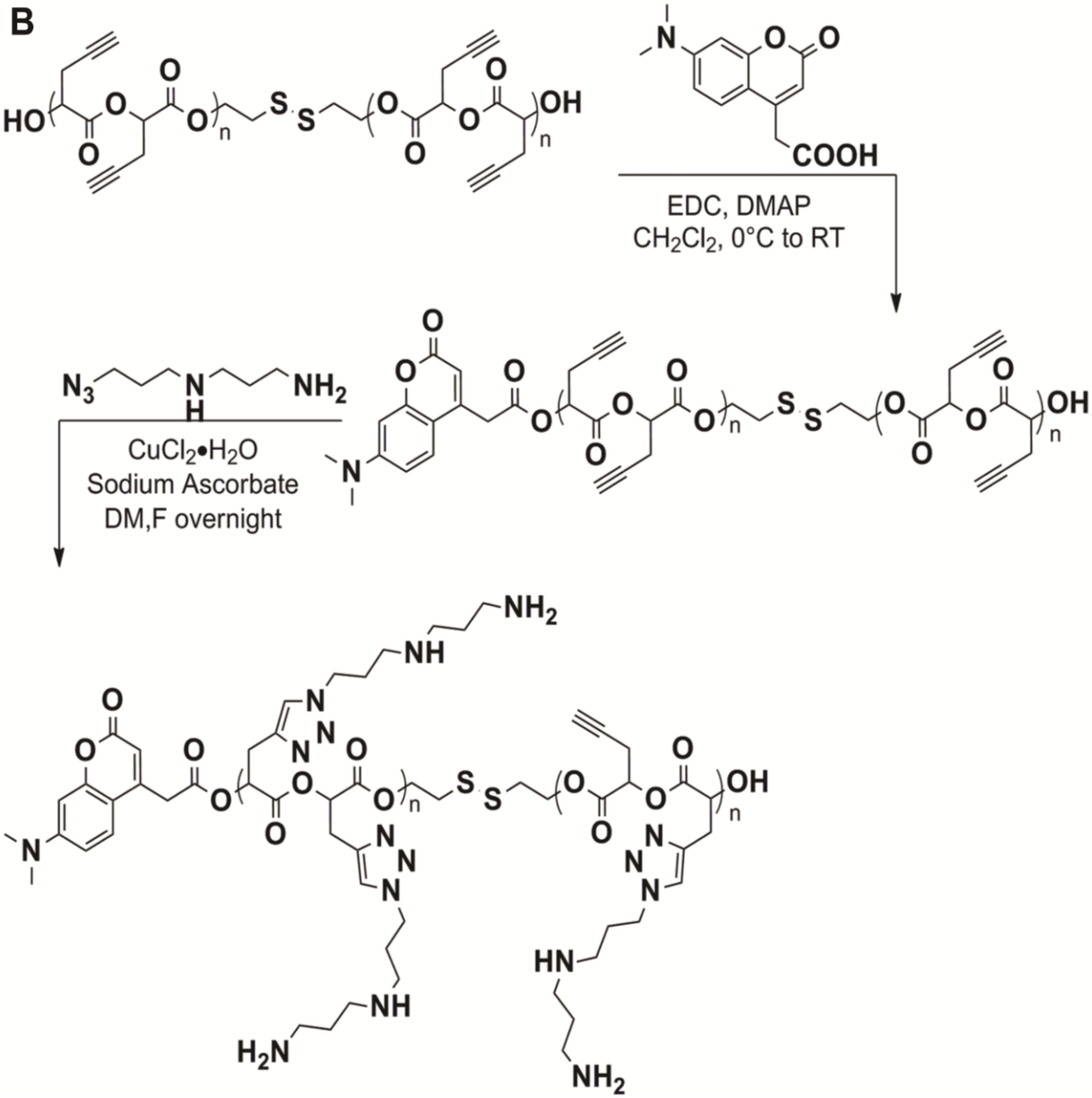

Figure 3-1 (cont'd) The cholesterol particle was made using a long, continuous propargyl glycolide (n=45) backbone with PEG endgroups. The azide-alkene click reaction was used to add the primary amine, secondary amine, and cholesterol ligands. B. The DMACA tagged disulfide particle is synthesized by first adding the fluorescent end group onto two shorter propargyl glycolide backbones (n=5) linked by a disulfide bond. The amine ligand was added to 80% of the available alkynes.

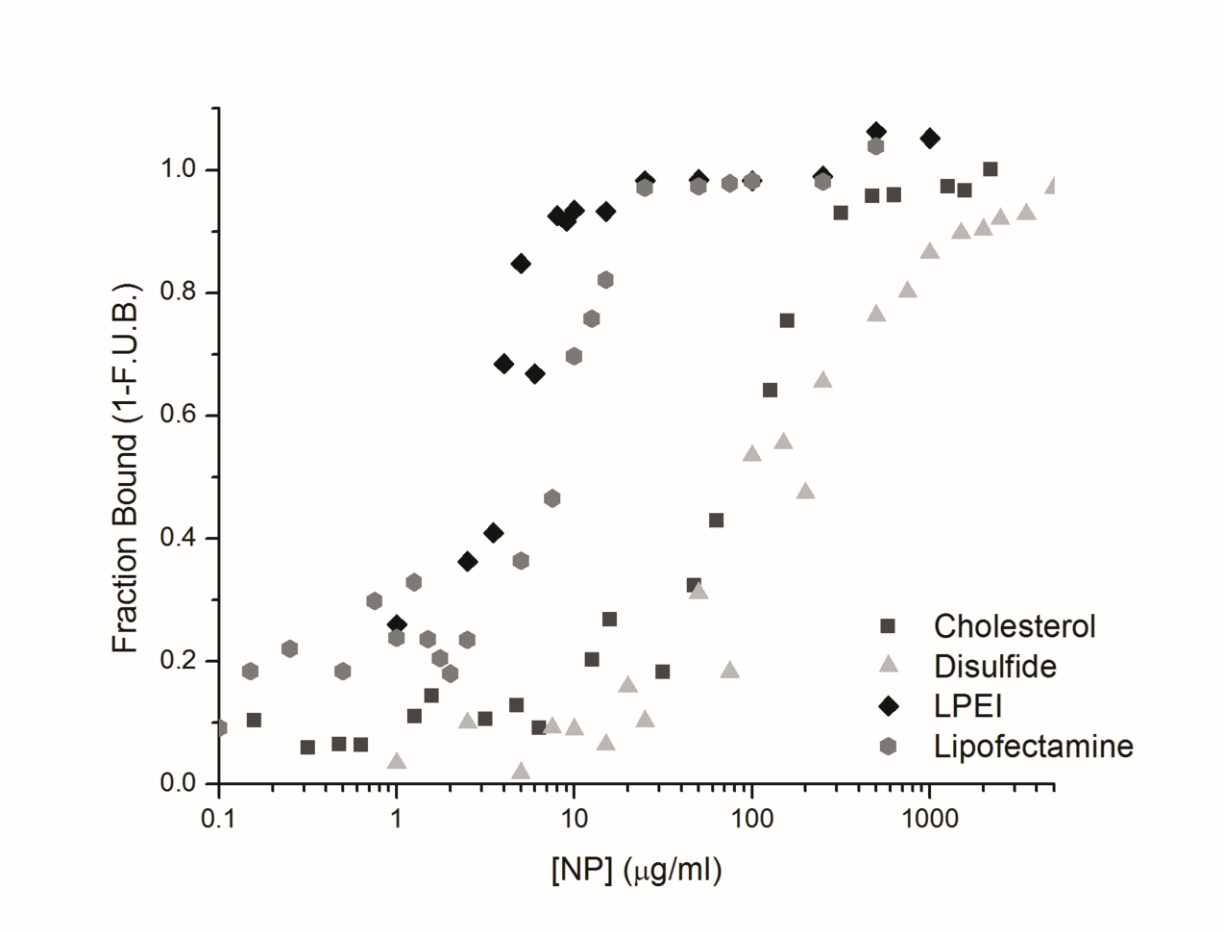

Figure 3-2 Polymer/nucleic acid binding
A graph of the fraction of dsDNA bound at varying polymer concentrations. The dsDNA concentration was maintained at 200nM, and the fraction bound to each particle was calculated as a mass balance from the amount of free dsDNA resolved on the gel.

Table 3-1 Hill equation parameters

Hill Equation Parameters	LF2K	LPEI	Cholesterol NP	Disulfide NP
K (μg/mL)	4.9	3.0	68	151
error (μg/mL)	0.7	0.4	8	14
n (cooperativity)	0.9	1.8	1.1	0.9
error	0.1	0.4	0.1	0.1

Fractional dsDNA binding was fit to a modified form of the Hill equation. The binding constant (K) reflects binding achieved at 15min. An exponential (n) greater than 1 is indicative of cooperative binding. The K values were compared using a two-tailed Student's t-test for unequal variances and all four values were statistically significantly different at $\alpha=0.01$.

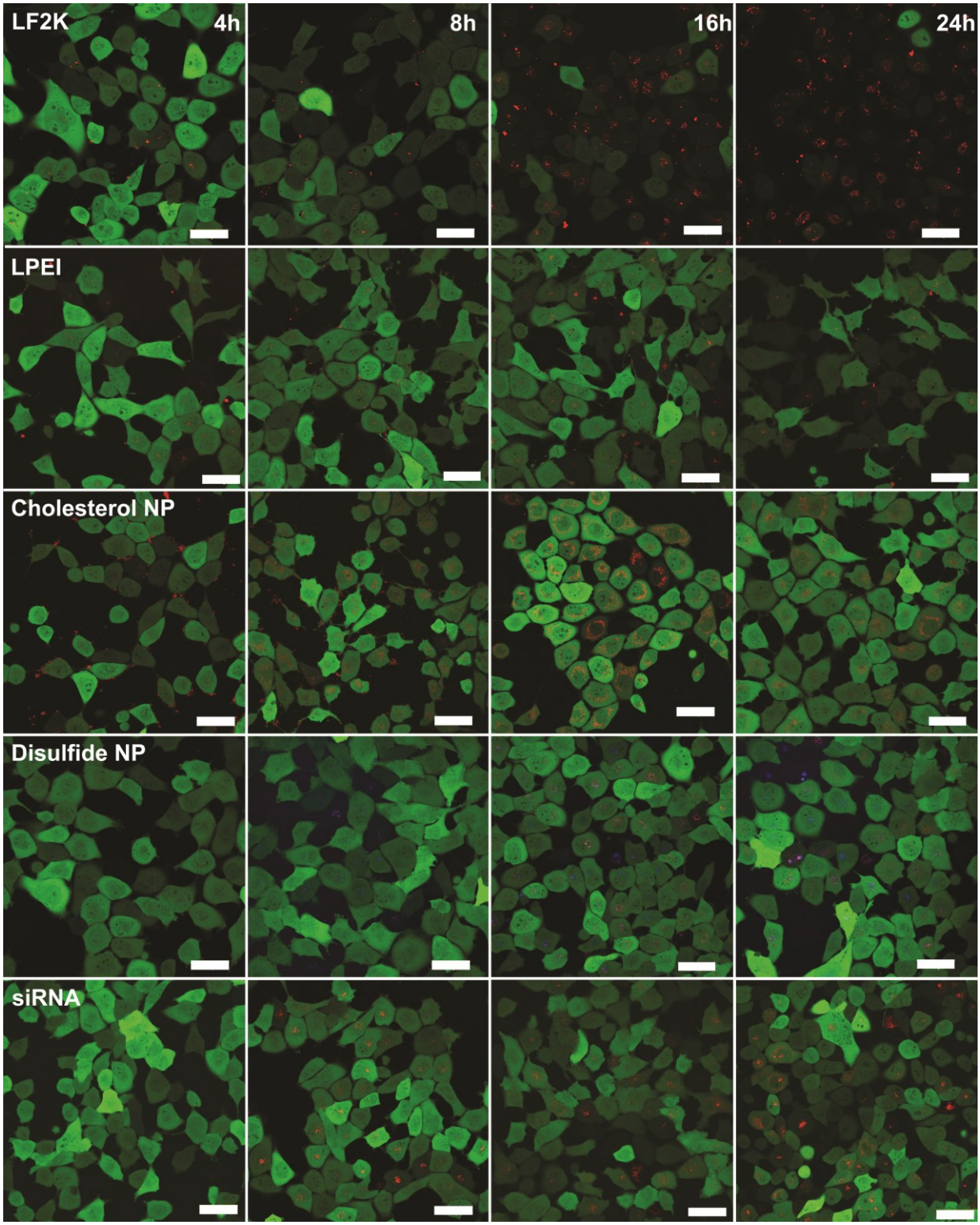

Figure 3-3 Time series microscopy pictures

Figure 3-3 (cont'd)
Confocal images of the uptake of various polymer/EGFPsiRNA complexes into GFP expressing H1299 cells. Pictures were taken at 4, 8, 16, and 24h time points. The green fluorescence represents the GFP expressing cells and the red fluorescence is of the Dy547-tagged siRNA. In the case of the disulfide particle, blue fluorescence indicates the presence of the particle. The scale bars are 50μm.

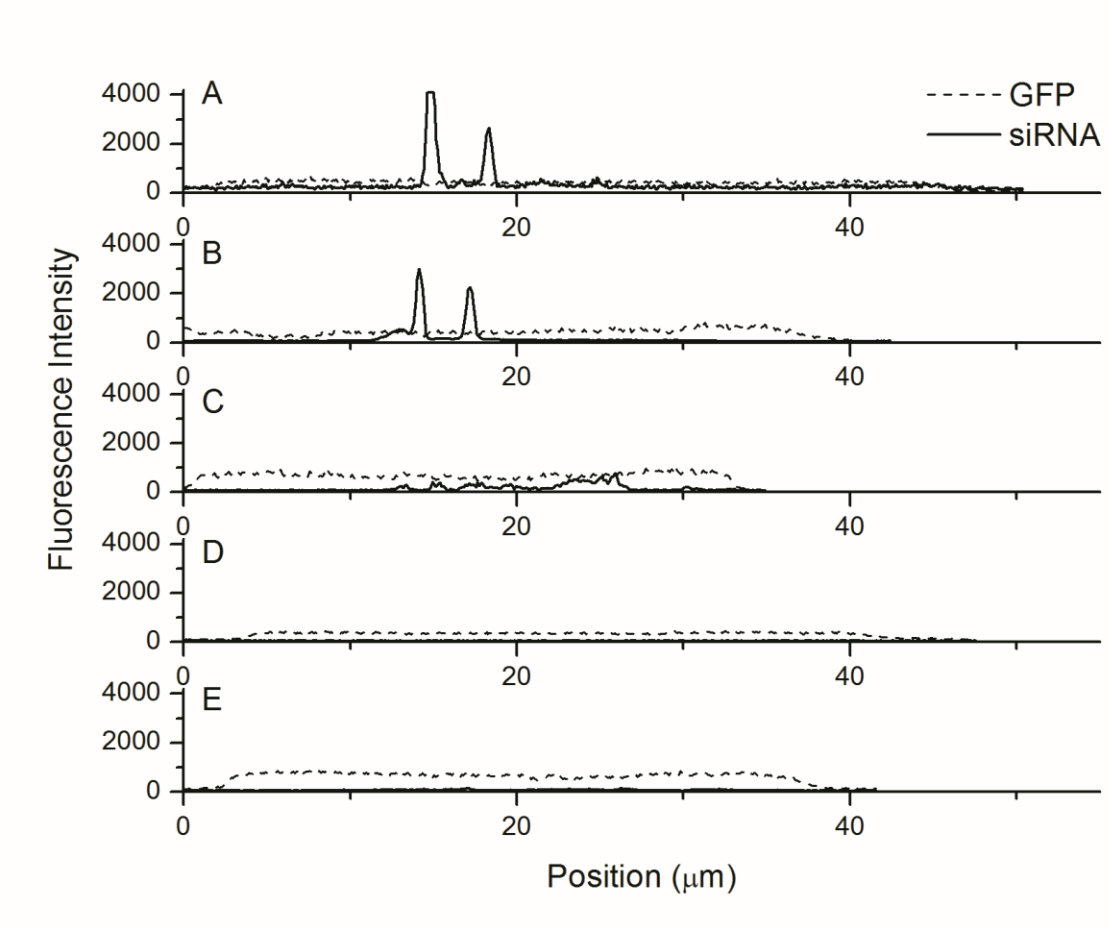

Figure 3-4 4h line intensity graphs
Fluorescence intensity graphs measured across individual cells at 4h after addition of LPEI (A), LF2K(B), Cholesterol NP (C), and Disulfide NP (D) complexes, as well as siRNA alone (E). For each image, the line was constructed by drawing across the longer diameter that intersected the areas of highest intensity red fluorescence. The GFP signal is indicative of the cell area. There was no visible siRNA uptake for the disulfide NPs or siRNA alone at the 4h time point.

CHAPTER 4: DEXTRAN FUNCTIONALIZED SILICA NANOPARTICLES FOR ACTIVE SIRNA DELIVERY

4.1 Abstract

To continue improvements in siRNA therapeutic delivery there is a need to distinguish between physical, chemical, structural, and mechanistic characteristics which are amenable to silencing. For many lipid and polymer-based delivery vehicles these features are interdependent, making it difficult to isolate one variable from another. The use of solid-core nanoparticles provides the ability to modify the external chemical composition while at the same time controlling shape and size. Here, we report the use of a novel dextran containing, amine functionalized silica solid-core nanoparticle with the ability to actively deliver siRNA to cells using an energy-dependent internalization process. Future synthesis variations of this particle can aid in the isolation of key characteristics of effective delivery vehicles, further utilizing this information to synthesize new carriers with increased efficacy and biocompatibility.

4.2 Introduction

Delivery has been recognized as one of the key hurdles in the development of new and effective short interfering RNA (siRNA) therapeutics. Among non-viral approaches, the choices between lipid (Ren et al. 2000; Akinc et al. 2008; Whitehead et al. 2011), polymeric (Burke and Pun 2008; Lynn and Langer 2000; Xiong et al. 2009; Rozema et al. 2007), and solid-core (Hom et al. 2010; Rosi et al. 2006; Veiseh et al. 2011) (NPs) nanoparticles are numerous. However, despite their ability to activate the RNA interference (RNAi) pathway in cell culture, and in some cases animal models (Shim and Kwon 2010), none of these potential delivery vehicles have transitioned into approved treatments.

One reason for the slow development could be attributed to the lack in knowledge on what exactly are the design requirements for effective delivery vehicles, in terms of both composition as well as cellular trafficking. Vehicles synthesized to contain similar chemical characteristics can have widely differing silencing efficiencies (Green et al. 2008; Whitehead et al. 2011; Siegwart et al. 2011), indicating that modifications to chemical composition alone are not sufficient for creating optimized vehicles. Although some generalized design features have been reported (Green et al. 2008; Portis et al. 2010; Siegwart et al. 2011), it is becoming increasingly important to consider how variations in physical and chemical composition affect cellular internalization characteristics when optimizing future vehicles as opposed to solely basing results on silencing ability.

The three major mechanisms for the internalization of extracellular molecules can be subdivided into phagocytosis, macropinocytosis and endocytosis. Clathrin-dependent, caveolae-dependent, and clathrin- and caveolae-independent routes being subsets of endocytosis (Malefyt et al. 2012). The majority of internalization and intracellular trafficking studies for genetic therapies have been performed using vehicle only (Dausend et al. 2008; Gratton et al. 2008; Rejman et al. 2004) or plasmid DNA (pDNA) delivery (Gabrielson and Pack 2009; McLendon et al. 2010; Reilly et al. 2012), with a single study reported for siRNA delivery using a lipid-based delivery vehicle (Lu et al. 2009). Due to differences in their final destinations, it is likely that the preferred internalization pathway will vary between pDNA and siRNA treatments. However, the results of these studies demonstrate that preferred cellular uptake pathways also vary by complex composition, surface charge, and particle size. The major challenge when comparing between studies is the difficulty in associating between vehicles of varied characteristics. To become

conclusive, further systematic studies which include controlled variations in structural and chemical complex characteristics are needed.

One advantage to the use of solid-core NPs is the ability for high modification while still controlling shape and size. Previous work has demonstrated that the most effective delivery vehicles require the ability to deliver large initial quantities of siRNA rapidly to cells (Portis et al. 2010). Through the use of solid-core particles, the ability for siRNA binding to NPs of similar composition can presumably be accounted for by size. In this study, we begin to examine siRNA delivery using functionalized silica nanoparticles (NPs) (Figure 4-1). In addition to amine groups for electrostatic binding, additional functionalization included the presence of dextran, which has shown some success in recent studies (Davis 2009; Kamat et al. 2010). Current results have demonstrated an improved silencing ability (>70% reduction in EGFP) dependent on both amine content and the presence of dextran. The internalization mechanism required for active silencing may be an energy dependent process. We hope to utilize future synthesis variations of this particle to expand our knowledge on the key characteristics of effective delivery vehicles, further utilizing this information to synthesize new carriers with increased efficacy and biocompatibility.

4.3 Results and Discussion

4.3.1 Characterization

The silica solid-core NPs were characterized based on composition, size, ζ potential, and nucleic acid binding ability (Table 4-1) and compared to Lipofectamine 2000 (LF2K, a cationic lipid) and Linear poly(ethyleneimine) (LPEI, a cationic polymer), both commercially available transfection reagents. Dynamic light scattering (DLS) was used to determine particle size without the presence of siRNA. With the exception of the 20% amine with dextran (+D) NP, all

of the silica particles were 2-6 times larger than LPEI, with no noticeable trends between amine content and size. DLS measurements for LF2K were inconclusive due to the concentration of LF2K required and the lack of cationic lipid aggregation in the absence of the anionic siRNA. For similar amine content (10%) the particle containing 1% dextran was roughly twice the size of the particle without dextran. This is expected since the 1% dextran particle is roughly 50% (wt) dextran.

To determine the surface charge of each particle as a function of complex concentration, 100nM solutions of siRNA were titrated with NPs and the ζ potential measured after each addition. The silica NPs all required greater particle concentrations to neutralize the siRNA than either LF2K or LPEI. For the +D NPs, as particle size increased, the amount of particle required to reach a neutral ζ potential also increased. It was hypothesized that as the amine content increase, the amount of particle required for neutralization would decrease. However, there didn't appear to be any correlation between amine content and neutralization point. In fact, the 40% amine +D particle required the largest particle concentration for a neutral ζ potential.

As a third characterization technique, we performed in vitro binding gel shift assays to determine the ability of the particles to electrostatically bind with nucleic acids. For these experiments, a 21 base pair dsDNA of analogous structure to the EGFP-targeting siRNA was used to minimize cost. Both LF2K and LPEI displayed over 20-fold better binding ability than any of the silica NPs. In most cases, the relative binding constant corresponded with the ζ potential neutralization value, the exception being the 10 and 20% amine +D particles which showed different ζ potential profiles but similar binding ability.

In most cases, the particle size appeared to be the influential factor in ζ potential and nucleic acid binding over the amine content of the particle. It is important to note that although the 40%

amine +D NP contains the most amines, this does not take into account the amount of amines present on the particle surface which likely accounted for in ζ potential as well as nucleic acid binding measurements.

4.3.2 Silencing and Optimization

Among the different characterization techniques previously discussed, the composition characteristics of amine content and the presence of dextran where the only two components which showed conclusive trends toward silencing. As amine content increases, silencing in EGFP-expressing cells also increases, with 20-50% amine content showing significantly more silencing than the 10% amine content (Figure 4-2). Additionally, 40% and 50% amine content particles were significantly lower than 20% amine particles, showing a step-wise increase in silencing, although the improved silencing does appear to level off at higher amine concentrations.

To observe the effect of dextran on silencing, two different pairs of particles, one containing dextran and one synthesized in the absence of dextran were tested for their ability to silence (Figure 4-3). In both cases, the silica particles containing dextran silenced better than their non-dextran counterparts, with greater differences occurring at the higher amine content. Both of these composition characteristics, amine and dextran content, appear to be independent of the ability of the particles to bind with the nucleic acid (Table 4-1).

A second synthesis of the 40% amine +D particle was performed to verify the reproducibility of size and binding characteristics (Table 4-1) in addition to silencing ability (Figure 4-4) and compared to LF2K. As a secondary negative control, poorly functional EGFP siRNA was used to verify there were no interactions between the siRNA and particle which could influence EGFP expression or cell count. At 24h, both LF2K (positive control) as well as the 40% amine +D

particle showed significant reductions in EGFP fluorescence when compared to particle only control cells. There were no statistically significant differences between control cells and cells treated with poor EGFP siRNA complexes. Additionally, there was no significant difference between the silencing ability of LF2K and that of the 40% amine +D particles when using 200 nM of siRNA.

When comparing between the two batches of the 40% amine +D particles, the second synthesis resulted in slightly larger particles with a small improvement in binding efficiency. In terms of silencing, they yielded statistically similar profiles, both comparable to similar results using LF2K. It is interesting to note that the strong silencing activity is not correlated to improved nucleic acid binding or smaller particle sizes as originally predicted. One possibility is that the DLS measurements are actually a result of particle aggregates that can be broken apart and internalized by the cell as smaller particles. This does not explain the poor binding quality of the particles. It is possible that the poor binding allows for easier release and improved silencing once inside the cell.

To visually confirm silencing, EGFP expressing cells (green) were treated using fluorescently tagged siRNA (red) complexed with the 40% amine +D NP and imaged using confocal microscopy at various time points (Figure 4-5). The siRNA and NP concentrations were reduced to 100nM and 100μg/mL, respectively. At 4h, there are already large quantities of siRNA internalized by multiple cells, a previously reported characteristic necessary for effective delivery vehicles (Portis et al. 2010). At 24h, there is visible silencing in approximately 30% of the cells with an additional portion of cells showing reductions in EGFP fluorescence, although not complete silencing. The morphology is consistent with that observed at the 4h time point, indicating relatively little toxicity.

4.3.3 Cellular Uptake and Internalization Mechanisms

In an attempt to determine the exact endocytosis mechanisms utilized by the particles and those necessary for active silencing, various endocytotic inhibitors were employed to isolate specific pathways. A reduction in temperature has been used to inhibit energy dependent processes occurring within the cell (Dausend et al. 2008; Khalil et al. 2006; Lu et al. 2009). Cytochalasin D inhibits actin dependent pathways by depolymerizing actin and disrupting filament formation (Alam et al. 2008; Alam et al. 2010; Dausend et al. 2008; Goncalves et al. 2004; Ivanov 2008; Khalil et al. 2006; Lamaze and Schmid 1995; Lu et al. 2009; McLendon et al. 2010; Parton et al. 1994; Yacobi et al. 2010; Zuhorn et al. 2002). This includes caveolin and macropinocytosis pathways. Chlorpromazine inhibits formation of coated pits, a requirement for clathrin mediated endocytosis (Wang et al. 1993; Dausend et al. 2008; Gabrielson and Pack 2009; Goncalves et al. 2004; Ivanov 2008; Khalil et al. 2006; Lamaze and Schmid 1995; Lu et al. 2009; McLendon et al. 2010; Medina-Kauwe et al. 2005; Rejman et al. 2005; Rejman et al. 2004; van der Aa et al. 2007; von Gersdorff et al. 2006; Yacobi et al. 2010). Finally, Filipin complex III binds and sequesters cholesterol to inhibit caveolin and lipid raft based endocytosis (Dausend et al. 2008; Goncalves et al. 2004; Ivanov 2008; Khalil et al. 2006; Lamaze and Schmid 1995; Lu et al. 2009; McLendon et al. 2010; Rejman et al. 2005; Rejman et al. 2004; von Gersdorff et al. 2006; Zuhorn et al. 2002).

Cells were pretreated with the selected inhibitors at times and concentrations representative of previous studies and optimized to minimize toxicity. Following pretreatment cells were treated with LF2K, LPEI, and 40% amine +D complexed with fluorescently tagged siRNA for 4h and then collected at 4, 24, and 48h for analysis by flow cytometry. Intracellular levels of siRNA

were measured as a function of particle type as well as inhibitor and blanked to particle only treatments (Figure 4-6). In the absence of inhibitor, at the 4h time point, LF2K and LPEI had a 10 fold increase in intracellular siRNA when compared to cells treated with siRNA only (Control). The 40% amine +D particles displayed almost 100 times the concentration when compared to siRNA only. At longer timepoints, for identical conditions, siRNA content does not increase but does remain inside the cell for periods longer than 48h. In most cases there was no significant change in siRNA uptake between inhibitors. The only exception was for cells exposed to $4^{O}C$ during the transfection process, which showed a significant decrease in siRNA accumulation at all time points.

To observe how changes in uptake affect changes in the expression, EGFP fluorescence was also analyzed and normalized to particle only treatments (Figure 4-7). As expected, there were no significant changes in EGFP expression at the 4h time point. The siRNA only treated cells showed no protein reduction at all time points for all inhibitor treatments. At 48h, differences between inhibitors were more pronounced for all three types of delivery vehicles.

For LF2K, temperature was the only inhibitor which displayed change in silencing compared to the no inhibitor treatment. These results are consistent with previous reports using other lipid-based vehicles for delivering siRNA (Lu et al. 2009), hypothesizing lipid-based transfection reagents utilize some type of energy dependent, membrane fusion event. For LPEI, at 48h, the reduction in temperature decreases silencing most significantly, with chlorpromazine, cytochalasin, and the inhibitor combination of chlorpromazine and filipin also displaying slight decreases in silencing when compared to the treatment without inhibitors. This suggests that LPEI requires a clathrin-dependent means of endocytosis for active siRNA delivery. Previous studies using PEI-based polymers have only looked at pDNA delivery with mixed results,

reporting both clathrin (von Gersdorff et al. 2006) as well as caveolar (Gabrielson and Pack 2009; Reilly et al. 2012). For the 40% amine +D complexes, the decrease in temperature is the only inhibitor which conclusively displays a decrease in silencing activity. Cytochalasin treatment also results in decreases in silencing but is not significant. This could mean that actin is a requirement for the internalization pathway but is difficult to conclude at this point. Future work will require the use of additional inhibitors which inhibit similar pathways to confirm these results are pathway-based as opposed to solely inhibitor based.

4.4 Conclusion

Silica core shell nanoparticles (NPs) functionalized with amines and dextran have shown successful silencing in cell culture at concentrations comparable to other commercially available reagents. Additionally, these NPs display similar uptake profiles to previously reported effective delivery vehicles and have been shown to be repeatable in synthesis. Currently, the role of dextran in the process is unknown, however particles of similar amine content show improved silencing in the presence of dextran.

These particles are currently internalized to the cell by a variety of routes, however the primary route required for silencing appears to be energy dependent and may require actin. Current and future work focuses on identifying the exact mechanisms involved for internalization, such as preferred endocytosis pathways and cellular trafficking of active complexes, to further explain the role of dextran in the silencing process. Continued optimization of silica particle composition, size, and amine content to increase silencing activity is also in progress.

4.5 Chapter 4 Tables and Figures

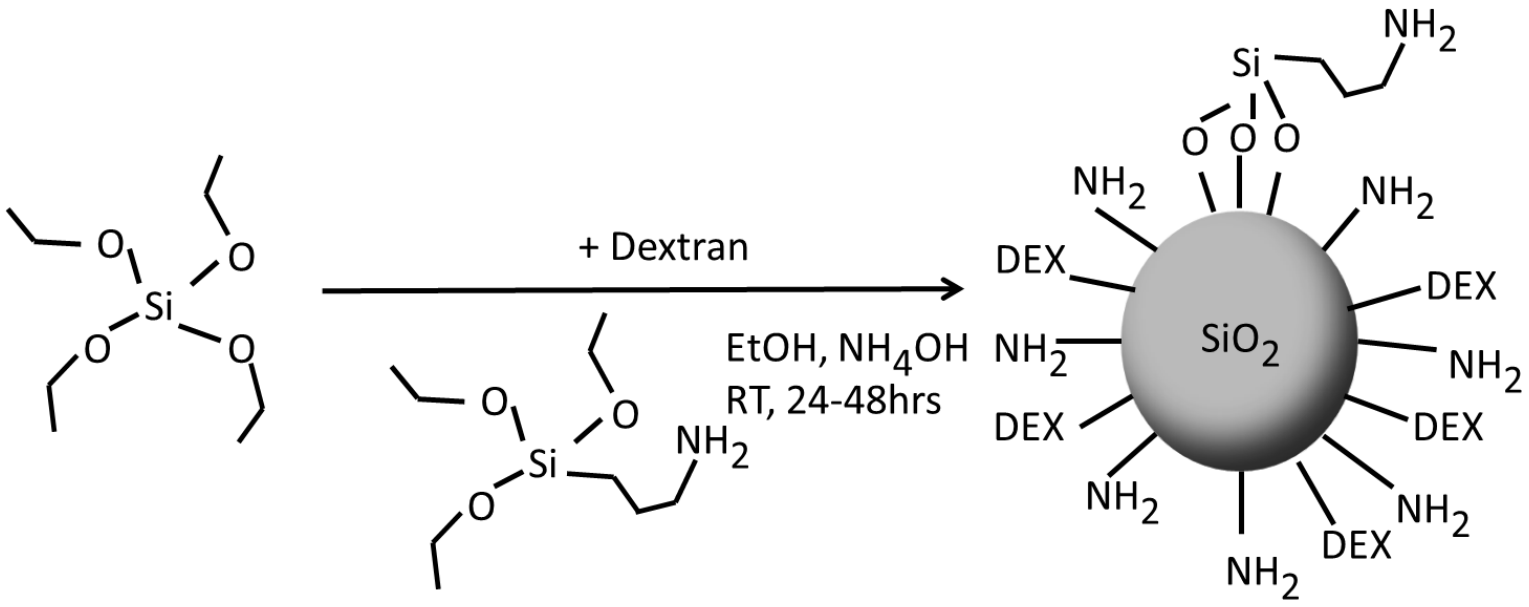

Figure 4-1 Synthesis schematic for silica core-shell nanoparticles
Silicon oxide NPs were formed through the condensation of tetraethoxysilane (TEOS) and 3-(triethoxysilyl)-propylamine (APTES) and synthesized to contain varied amounts of surface amino groups and branched dextran (DEX).

Table 4-1 Characterization of silica-amine NPs

NP Notation	Composition	Radius (nm)	Surface Area	Neutral ζ potential (μg/mL)	K (μg/mL)	sd (μg/mL)	n	sd
LF2K		varied	n/a	4.12	4.9	0.7	0.94	0.12
LPEI		42	7389	7.92	3.0	0.4	1.80	0.43
gacv 25	$TEOS_{90}APTES_{10}$	73	22322	150	255.3	16.6	4.66	1.76
gacv 32	$TEOS_{89}APTES_{10}D_1$	134	75214	49.0	90.2	9.5	1.63	0.29
gacv 37	$TEOS_{79}APTES_{20}D_1$	45	8482	27.4	89.6	4.8	2.64	0.39
gacvi 19	$TEOS_{59}APTES_{40}D_1$	221	204585	298	286	19.1	1.60	0.16
gacvi 40	$TEOS_{59}APTES_{40}D_1$	289	349852	n/a	238	18.4	1.82	0.23

Nanoparticles were characterized through DLS size measurements, the neutral surface charge when complexing with 100 nM siRNA, and well as fractional binding to 200 nM dsDNA. The binding was fit to a modified form of the Hill equation. The binding constant (K) reflects binding achieved at 15min. An exponential (n) greater than 1 is indicative of cooperative binding.

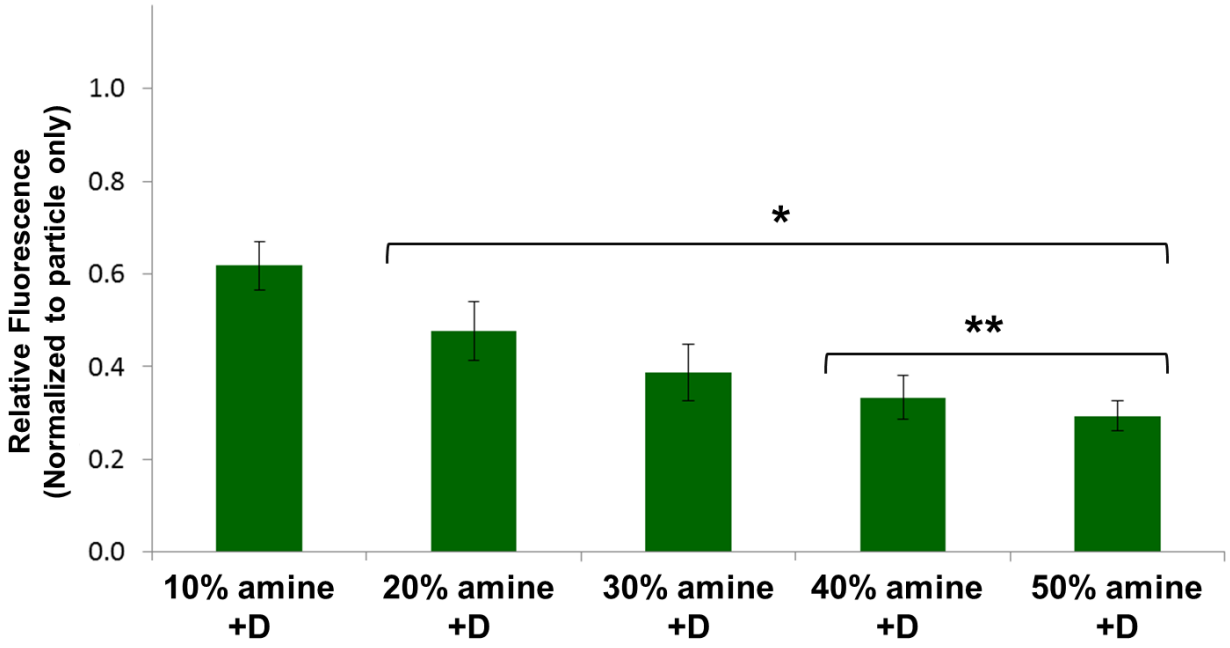

Figure 4-2 Effect of amine content on silencing
The reduction in EGFP fluorescence upon 24h treatment is shown using particles of varied amine content. Statistical analysis was performed using one-way ANOVA, followed by Tukey's HSD post-hoc analysis, n=3, error bars +/- 1sd, * = statistically significant compared to 10%, ** = statistically significant compared to 20% (p-value <0.05)

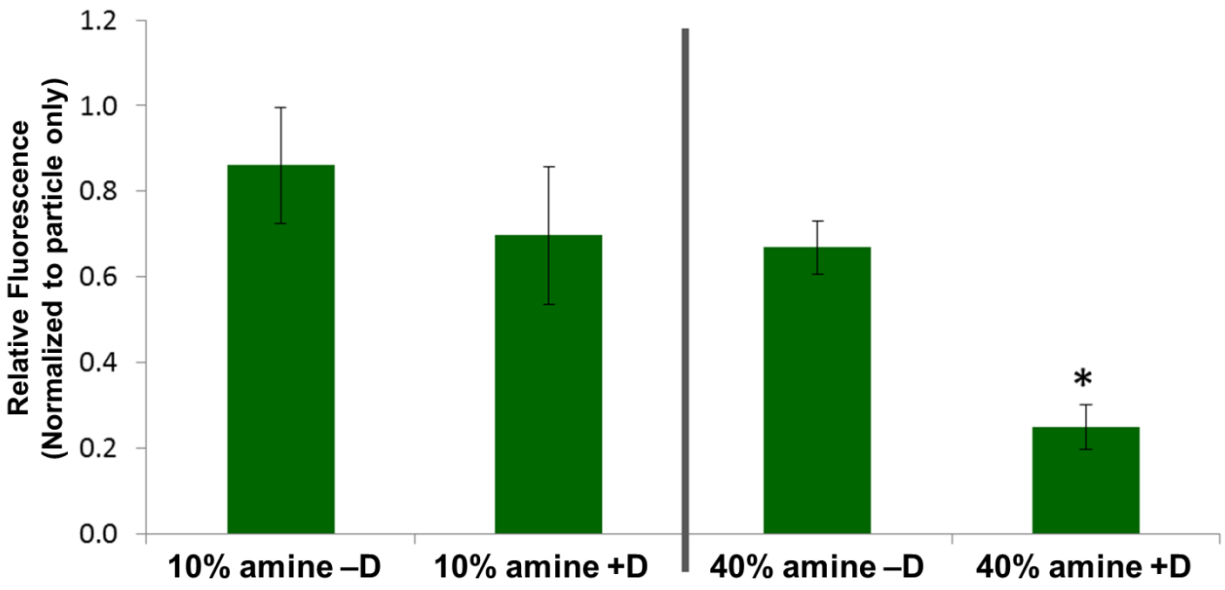

Figure 4-3 Effect of dextran on silencing
The reduction in EGFP fluorescence upon 24h treatment is shown using particles with and without dextran. Statistical analysis was performed using Student's T-test, two-tailed, n=3, error bars +/- 1sd, * = statistically significant compared to –D (p-value = 0.02).

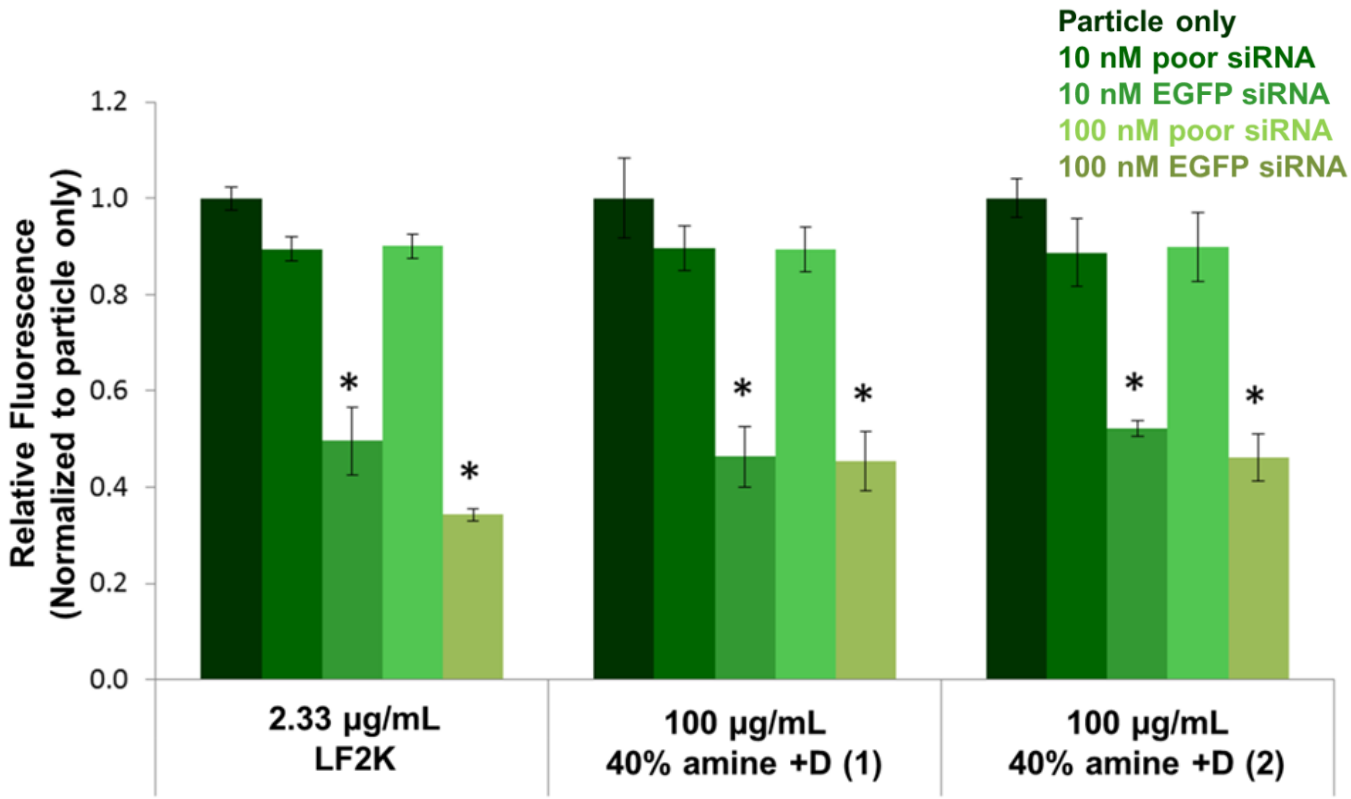

Figure 4-4 Silencing for repeated synthesis of 40% amine +D silica NPs
The reduction in EGFP fluorescence upon 24h treatment is shown with varying one replicate synthesis of the 40% amine +D silica NP. Poorly functional EGFP siRNA was used as a negative control. Statistical analysis was performed using two-way ANOVA, followed by Tukey's HSD post-hoc analysis, n =3, error bars +/- 1sd, * = statistically significant at p-value <0.05 compared to particle only controls. There was no statistically significant difference between treatments of the two separately synthesized particles.

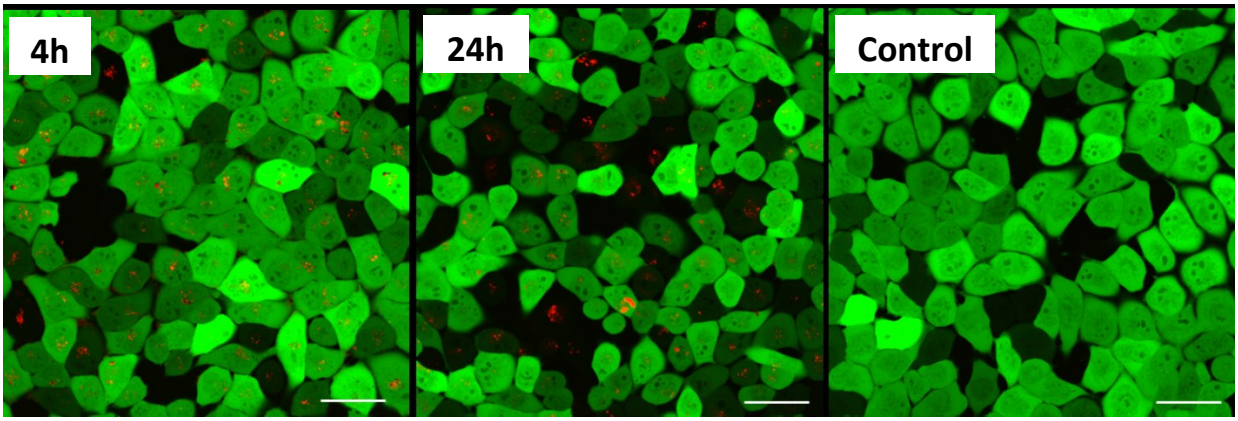

Figure 4-5 Confocal microscopy images of 4h uptake and 24h silencing
Confocal microscopy images of siRNA uptake and silencing using 40% amine +D/siRNA complexes at 100 μg/mL particle and 100 nM fluorescently tagged siRNA (red) into EGFP (green) expressing H1299 cells. Pictures were taken at 4h (left) and 24h (middle) and compared to control cells (right). The scale bars represent 50 μm.

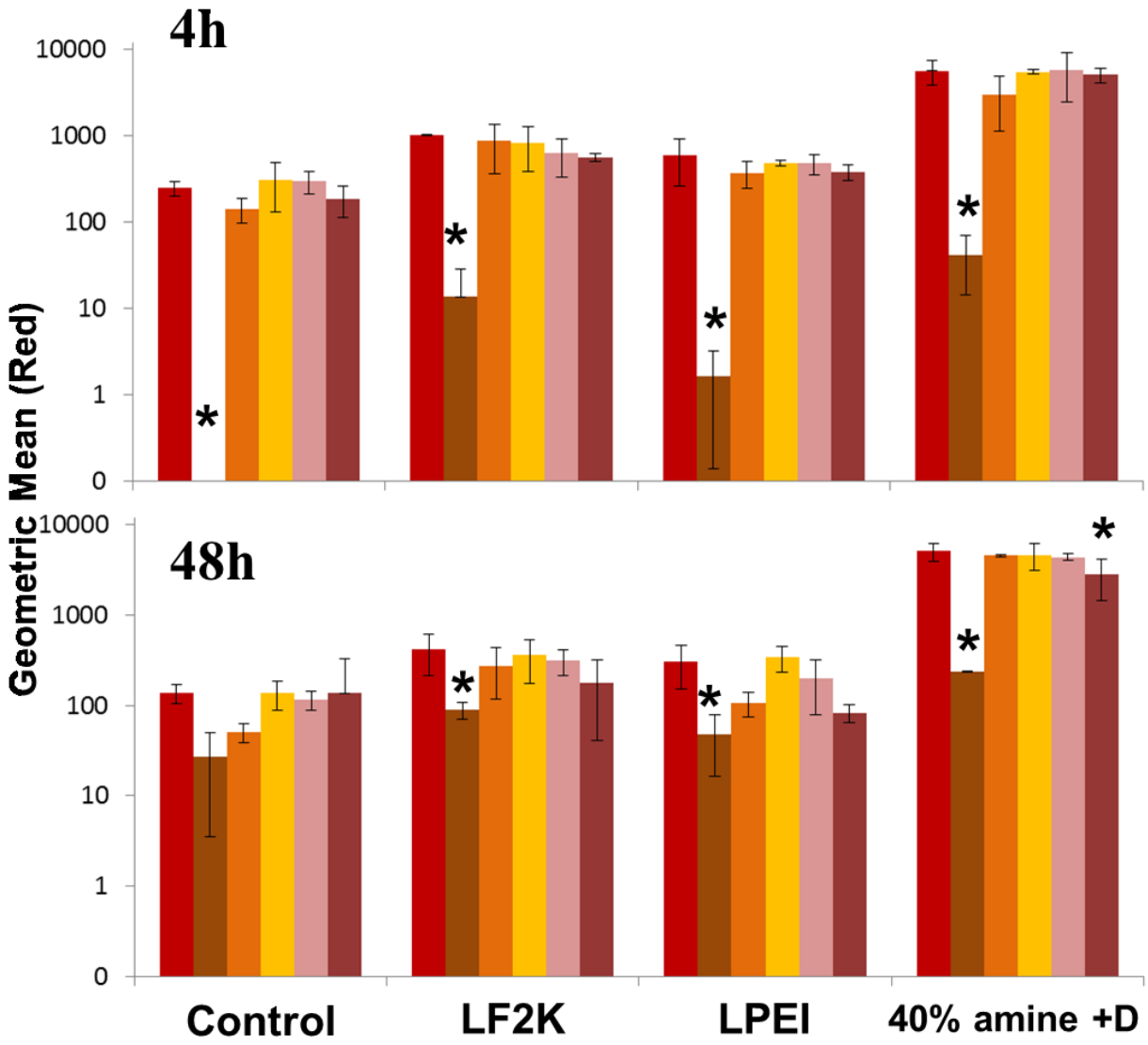

Figure 4-6 Time series uptake of siRNA in the presence of endocytic inhibitors
Cellular uptake efficiency of fluorescently labeled siRNA complexes at 4h and 48h post-transfection. Bars represent no inhibitor, temperature reduction, chloropromazine, filipin, cytochalasin, and a combination of chlorpromazine & filipin pre-treatments, respectively. Data were measured using flow cytometry and uptake results have been blanked to particle only controls. Each data point represents the mean +/- sd for a total of 2-3 separately prepared and analyzed samples. Statistical analysis was performed using one-way ANOVA (per particle type), followed by Tukey's HSD post-hoc analysis. * = statistically significant at p-value <0.05 when compared to no inhibitor controls.

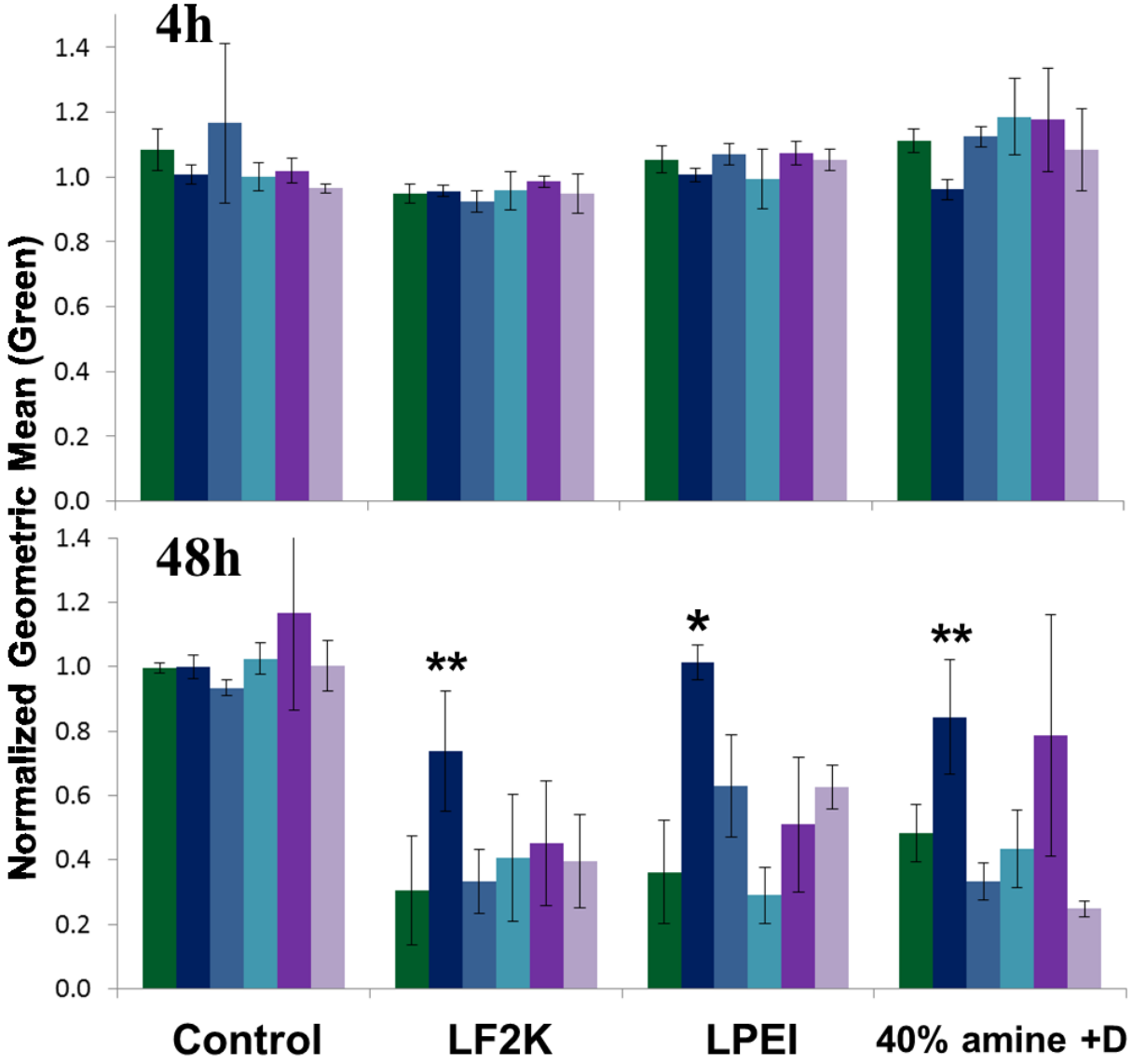

Figure 4-7 Time series EGFP silencing in the presence of endocytic inhibitors
Reduction in EGFP fluorescence of fluorescently labeled siRNA complexes at 4h and 48h post-transfection. Bars represent no inhibitor, temperature reduction, chloropromazine, filipin, cytochalasin, and a combination of chlorpromazine & filipin pre-treatments, respectively. Data were measured using flow cytometry and uptake results have been blanked to particle only controls. Each data point represents the mean +/- sd for a total of 2-3 separately prepared and analyzed samples. Statistical analysis was performed using one-way ANOVA (per particle type), followed by Tukey's HSD post-hoc analysis. * = statistically significant at p-value <0.05 when compared to no inhibitor controls. ** = statistically significant difference when using a t-test between only temperature and no inhibitor controls.

CHAPTER 5: CONCLUSIONS AND FUTURE WORK

5.1 Conclusions

The motivation for the studies described here was for the development of siRNAs as therapeutics. Although the pathway was first characterized in 1998 (Fire et al. 1998), the area still lacks comprehensive knowledge on all of the siRNA-protein-mRNA interactions within the pathway, how these interactions affect siRNA activity, and the refinement of optimal delivery vehicles to overcome the hurdles of systemic delivery. To address these issues, it was shown that both end nucleotide and terminal thermodynamic stability are important for predicting the activity of an siRNA sequence toward its target. Additionally, through the use of these two features alone, the described algorithm is capable of identifying highly active sequences to a correlation >0.8, comparable to other previously reported techniques (Birmingham et al. 2007; Matveeva et al. 2007).

Despite the multitude of candidates able to actively deliver siRNAs into cells, little is known about the characteristics which distinguish them from less efficient vehicles. Here, it was demonstrated that intracellular accumulation of siRNAs alone is not sufficient to guarantee silencing. Effective delivery vehicles require initial concentrated delivery of siRNAs at early time points (4h or earlier) to achieve silencing at longer time points (16h and later). Therefore, the design of future delivery vehicles should consider physical structural characteristics which have the ability for high siRNA loading capacity.

The use of solid-core nanoparticles have the ability to maintain consistent physical structures while at the same time varying chemical compositions. Through the development of novel silica-

based, amine containing, nanoparticles with dextran we were able to achieve silencing profiles similar to those of LF2K, with minimal toxicity. Additionally, in comparison between similar particles, increased amine content as well as the presence of dextran resulted in improved silencing. Reproducibility was achieved through the creation of additional particles using the same synthesis technique which showed statistically identical silencing profiles. Endocytotic analysis revealed this new particle achieves 10-fold higher early siRNA accumulation over LF2K and requires an energy- and actin- dependent internalization process for achieving silencing. Further optimization and characterization of these silica functionalized particles will provide a valuable platform for building active delivery vehicles for siRNA therapeutics.

5.2 Future Work

The results described here are only partial steps toward the ultimate goal of engineering better medicines for personalized siRNA therapeutic treatments. Future initial steps required for continued development, stemming from topics included in this dissertation, are discussed in the sections below.

5.2.1 siRNA-protein interactions on the molecular level

The current algorithm approach is solely based on two features, end nucleotides and terminal thermodynamic stability. Despite the high correlation values achieved, there were multiple sequences displaying high levels of activity, even when their computed probability of having high activity was low. This provides motivation for further algorithm improvement by the addition of other features. When designing the current algorithm approach, and analyzing currently available databases, it was shown that highly active siRNA sequences contained low

frequencies of cytosine at position 7 and guanine at position 14 of the antisense strand. Alternately, sequences of low activity tended to contain high frequencies of these nucleotides at the same positions. These preferences were not as significant as those seen for the terminal nucleotides but nonetheless, may possibly shed light on additional base preferences within siRNA sequences. Previous work in this lab has also identified the importance of local mRNA structure on the silencing activity of individual siRNAs (Gredell et al. 2008) a feature which has been included in other algorithms (Lu and Mathews 2008; Shao et al. 2007; Ladunga 2006). The inclusion of additional nucleotide preferences as well as mRNA structure may be important for further algorithm refinement.

As discussed in chapter 2, the asymmetry features of end sequence and terminal thermodynamic stability were used in the algorithm to predict siRNA activity as measured by reductions in the protein level. These results do not show how each factor related to asymmetry affects siRNA processing within the RNAi mechanism. Additional work related to the development of an *in vitro* assay which can identify the specific preferential incorporation of each strand individually as a function of both asymmetry features would be beneficial for relating algorithm predictions to siRNA-protein interactions on the molecular level.

5.2.2 Dextran nanoparticle optimization

The development of a new delivery vehicle option, such as the dextran containing, amine-silica NP, opens the door toward a multitude of additional optimization and characterization experiments. While some studies have already been performed optimizing the composition of this delivery vehicle, additional optimization of amine and dextran content utilizing identical synthesis techniques would be helpful for the further isolation of key delivery vehicle

characteristics. Current characterization methods such as DLS, zeta potential, and binding affinity can be supplemented with TEM (Cohen et al. 2000) or SEM ((Mehrotra et al. 2009) to further identify the structures of both the delivery vehicle alone as well as the NP-siRNA complexes as well as how these structures change with varied NP compositions.

Following compositional analysis and optimization, the next steps would be to test the ability of these NPs to silence multiple endogenous targets and deliver to various cell types. Additional endocytotic trafficking studies combining flow cytometry and confocal microscopy with a new array of inhibitors including chloroquine (Gabrielson and Pack 2009) and bafilomycin (Gabrielson and Pack 2009; Reilly et al. 2012) can hopefully shed light on the trafficking of these particles after they enter the endosomes as well as confirm the endocytotic results suggested in chapter 4.

When designing solid-core delivery vehicles, their ability for sedimentation has been shown to play a key role in the cell culture delivery process for gold nanoparticles (Cho et al. 2011). Additionally, the magnetofection of iron particles relies on utilizing similar forces to aid in uptake (Lee et al. 2011). One could envision performing similar experiments for the silica particles to determine the importance of gravity on their delivery efficacy.

Despite their ability to effectively deliver siRNA to cells at relatively minimal toxicity, silica based NPs are not biodegradable. The ultimate long term goal for these vehicles would be to take advantage of the important characteristics which have been identified and transition into the creation of amine and dextran containing biodegradable polymers (Jiang et al. 2008). These "clickable" propargyl glycolide polymers would provide the same delivery profiles but allow for

simple modification toward specific cell targeting as well as the ability to degrade into lactic acid derivatives, a biocompatible product.

5.2.3 Three-dimensional transport and delivery of siRNA

As stated throughout the previous chapters, the lack of developed, systemic, siRNA therapeutics demonstrates transport is a significant barrier to delivery and an important issue to be addressed for future development. It is our belief that one of the frequent failures of delivery vehicles to date *in vivo* can be attributed to transport barriers in complex three dimensional environments. *In vivo*, cells are embedded in tissues, with extracellular matrix and cell contacts in all directions. Limited cell culture based models exist for examining the differences in delivery to three-dimensional (3D) cultures versus two-dimensional (2D) cultures, related to siRNA therapeutics.

As shown in chapter 2, one characteristic of effective delivery vehicles is their ability to quickly enter the cell and deliver large initial concentrations of siRNA. In 3D systems, the addition of increased physical and even chemical barriers drastically reduces this delivery ability. Many commercially available transfection reagents can be ineffective when attempting to treat cells embedded within a 3D matrix (Zhang et al. 2010). It has also been shown that cells interact and signal differently in 3D cell cultures (Lai et al. 2009). As cells function differently in 3D, there is the possibility they respond differently to siRNA treatment as well. To address this problem, it would be beneficial to develop an intermediate 3D model of siRNA transport. The idea being, isolation of the differences between 2D and 3D cell cultures will aid in the extended application toward future *in vivo* delivery.

The development of 3D collagen (Ishihara et al. 2010), fibronectin (Zhou et al. 2008), or synthetic PEG (Raeber et al. 2005) hydrogels to study cell morphology and migration has often been used as an intermediate step between cell culture and *in vivo* models. Current 3D studies involving siRNA treatments either resort to pre-treating cells before embedding in the matrix (Ivanov et al. 2008), treatment of cells growing on top of a hydrogel (Lei et al. 2010), or nucleic acid containing hydrogel scaffolds implanted into animal models (Andersen et al. 2010). Previous work in our lab has shown when using collagen or agarose containing gels, delivery vehicles (and most siRNA) remain suspended on the surface of the gel without traversing through the gel. While some siRNA does make it through the gel, it is not enough to achieve silencing. Future work would require the development of some type of porous composite gel which can provide a scaffold for cell proliferation while at the same time reducing the physical transportation barriers. Another research opportunity would be creating smaller, micro gels with the ability to track fluorescently tagged siRNA transport across the gel in a single direction, possibly through the aid of time-series confocal microscopy. By modeling the transport of siRNA across the gel in a one dimensional scale, increased knowledge and characterization of the transportation barriers can be developed.

APPENDICES

Appendix A: Materials and Methods for Chapter 2

Algorithm Design and Parameters

Using information from both terminal nucleotide classification and thermodynamic stability, we developed a 17 parameter logistic regression model based on the 16 possible end sequence combinations as well as the relative thermodynamic stability. The relative stability is calculated by the difference between the hybridization free energy from the 5'-end of the antisense strand and the 5'-end of the sense strand, termed $\Delta\Delta G$, based on the three terminal nearest neighbor pairs (Xia et al. 1998; Walton et al. 2010) (Figure 2-1). This calculation technique, when coupled with terminal sequence information, was shown to have the best predictive accuracy when tested on existing siRNA activity databases (Walton et al. 2010). The weighting factors for each of the 17 parameters were based on fitting the model to the same siRNA databases (Huesken et al. 2005; Shabalina et al. 2006). From a cDNA sequence input, the algorithm predicts the probability the given sequence will have high, medium, or low activity. Using the difference between the high and low probabilities, each siRNA sequence for a given target was ranked from the highest to lowest difference. The cDNA sequences used for EGFP and PKR are included at the end of this section with siRNA target regions highlighted. For comparison with other asymmetry approaches, asymmetry calculations were also performed using one and four nearest neighbor parameters. To ensure the most accurate comparisons across ranking approaches, sequences with equivalent values were all given the best possible ranking.

Logistic Regression Model

The model is a generalized linear model in which we do not directly fit the features (the terminal nucleotide and thermodynamic asymmetry) linearly with the outcomes (silencing efficiency) but attempt to estimate the probability of the siRNA being highly efficient or

inefficient in silencing. The reasons for this are two-fold: (1) we include both continuous (energy) and discrete (terminal nucleotide) features, and (2) the relationship between features and outcomes is not linear (Walton et al. 2010).

Therefore, we apply the logistic regression model, a generalized linear model that assumes the logit (log-odds) of the siRNA being highly efficient are determined by the features:

$$\log\left(\frac{P(high|X)}{P(med|X)}\right) = \beta_0 + \beta^T X$$

in which *P(high|X)* is the probability that the siRNA (given its feature vector X) is highly active, while *P(med|X)* is the average siRNA silencing efficiency, so *P(high|X)/P(med|X)* represents the "Odds" that the siRNA stands out as a "good" siRNA. In a logistic regression model, the odds are associated with an exponential function of the linear combination of the features.

Silencing is a discrete Poisson process, and the frequencies of silencing are subject to an exponential distribution. Therefore, we can relate the odds of good silencing and the sequence features with exponential functions.

Similarly, the log-odds of the siRNA being inefficient are determined as:

$$\log\left(\frac{P(med|X)}{P(low|X)}\right) = \beta_0{}' + \beta'^T X$$

The model predicts the posterior probability of siRNA being highly efficient and inefficient:

$$P(high|X) = \frac{\exp(\beta_0 + \beta^T X)}{1 + \exp(\beta_0 + \beta^T X) + \exp(\beta_0{}' + \beta'^T X)}$$

$$P(med|X) = \frac{\exp(\beta_0{}' + \beta'^T X)}{1 + \exp(\beta_0 + \beta^T X) + \exp(\beta_0{}' + \beta'^T X)}$$

$$P(low|X) = \frac{1}{1 + \exp(\beta_0 + \beta^T X) + \exp(\beta_0{}' + \beta'^T X)}$$

The siRNAs in the datasets are divided into three groups (high/med/low) based on their activity (discretization with equal frequency), and we use Maximum Likelihood Estimation to learn the parameters in the logistic regression model.

Materials

Lipofectamine 2000 (LF2K) was purchased from Invitrogen. All EGFP and PKR siRNA sequences were purchased from Dharmacon. Opti-Mem (GIBCO) was used for preparation of all transfection solutions. Monoclonal anti-PKR (Y117) primary antibody was purchased from Novus Biologicals. Monoclonal anti-β-actin primary antibody was purchased from Sigma. Secondary antibodies (anti-rabbit and anti-mouse) were purchased from ThermoScientific.

Cell Culture

Human lung carcinoma cells (H1299) constitutively expressing a form of EGFP, modified to contain a 2hr half-life, were generously provided by Dr. Jørgen Kjems, University of Aarhus, Denmark. Human hepatocellular carcinoma (HepG2) cells were purchased from American Type Culture Collection (ATCC). Cell culture media was prepared with Dulbecco's Modified Eagle's Medium High Glucose (DMEM, Invitrogen) supplemented with 10% fetal bovine serum (FBS, GIBCO) and 1% penicillin-streptomycin (GIBCO). For the H1299 cells, 1% Geneticin (GIBCO) was added to maintain EGFP expression. Cells were incubated at 37°C, 5% CO_2, 100% relative humidity and subcultured every 4-5 days by trypsinization.

EGFP Silencing and Fluorescence Analysis

H1299-EGFP cells were seeded in 96-well black side, clear bottom plates (Fisher Scientific) at a density of 20,000 cells/well in 0.1 mL of complete media without antibiotics. After 24 h, 50 μL solutions of varied siRNAs and LF2K were prepared in Opti-Mem and allowed to mix for 30 minutes prior to their addition to cells at final concentrations of 5-100 nM siRNA and 2.3 μg/mL

LF2K. Cells were incubated in the transfection solutions at 37°C, 5% CO_2, 100% humidity. After 24h, cells were washed 2 times with DPBS (Gibco), and EGFP fluorescence was quantified using a Gemini EM fluorescent plate reader (Molecular Devices) at 480 nm excitation/525 nm emission. Fluorescence intensity was normalized to control wells that were treated with transfection reagent but no siRNA. Cytotoxicity was assessed by microscopy and was not seen in any of the treatments.

PKR Silencing and Western Blotting

For siRNA transfections targeting human PKR in HepG2 cells, reverse transfection was performed. Briefly, 250 µL solutions of varied siRNAs and LF2K were prepared in Opti-Mem and allowed to mix for 30 minutes prior to their addition to standard six-well tissue culture plates. Freshly trypsinized HepG2 cells suspended in antibiotic-free media were added to the six-well culture plates at a density of 1.5 x 10^6 cells per well to achieve final concentrations of 100 nM siRNA and 2.3 µg/mL LF2K. The cells were then incubated at 37°C, 5% CO_2, 100% humidity for 48 h and collected. PKR levels were measured by western blot analysis. The cells were washed twice with cold PBS and lysed in 200 µl/well of CelLytic M cell lysis buffer (Sigma) supplemented with protease inhibitor cocktail (Sigma). The cell lysate was clarified by centrifugation at 13,000 rpm for 10 min, and the supernatant was collected. Total protein levels were quantified by Quick Start Bradford protein assay (BioRad). Approximately 20 µg of total protein was resolved using 8% resolving, 5% stacking SDS-PAGE gels. Proteins were then transferred to nitrocellulose membranes and probed with primary and secondary antibodies. Biotinylated protein ladders (Cell Signaling Tech.) were loaded to one well of each SDS-PAGE gel, and anti-biotin antibody was used to detect the protein ladders on the western blots. Antibody detection was performed using the SuperSignal West Femto Chemiluminescence

substrate kit (ThermoScientific) and imaged on the Molecular Imager ChemiDoc XRS System (Bio-Rad). Band intensity was normalized to control wells that received transfection reagent but no siRNA. Cytotoxicity was assessed by microscopy and was not seen in any of the treatments.

Statistical Analyses

Multiple comparisons between protein levels across different siRNA treatments conditions were performed using one-way (PKR data) or two-way (EGFP data) ANOVA followed by Tukey's HSD post-hoc analysis with p-value cut-off set at 0.05. Analyses were performed using either Microsoft Excel or Minitab.

EGFP sequence 5' to 3' (targeted regions highlighted; darker highlights indicate overlapping target regions)

atggtgagcaagggcgaggagctgttcaccggggtggtgcccatcctggtcgagctggacggcgacgtaaacggccacaagttcagcgt
gtccggcgagggcgagggcgatgccacctacggcaagctgaccctgaagttcatctgcaccaccggcaagctgcccgtgccctggccc
accctcgtgaccaccctgacctacggcgtgcagtgcttcagccgctaccccgaccacatgaagcagcacgacttcttcaagtccgccatgc
ccgaaggctacgtccaggagcgcaccatcttcttcaaggacgacggcaactacaagacccgcgccgaggtgaagttcgagggcgacac
cctggtgaaccgcatcgagctgaagggcatcgacttcaaggaggacggcaacatcctgggcacaagctggagtacaactacaacagcc
acaacgtctatatcatggccgacaagcagaagaacggcatcaaggtgaacttcaagatccgccacaacatcgaggacggcagcgtgcag
ctcgccgaccactaccagcagaacaccccatcggcgacggccccgtgctgctgcccgacaaccactacctgagcacccagtccgccct
gagcaaagaccccaacgagaagcgcgatcacatggtcctgctggagttcgtgaccgccgccgggatcactctcggcatggacgagctgt
acaagaagcttagccatggcttcccgccggaggtggaggagcaggatgatggcacgctgcccatgtcttgtgcccaggagagcgggatg
gaccgtcaccctgcagcctgtgcttctgctaggatcaatgtgtag

PKR sequence 5' to 3' (targeted regions highlighted; darker highlights indicate overlapping target regions)

aagcttccaaccaggatacgggaagaagaaatggctggtgatctttcagcaggtttcttcatggaggaacttaatacataccgtcagaagca
gggagtagtacttaaatatcaagaactgcctaattcaggacctccacatgataggaggtttacatttcaagttataatagatggaagagaatttc
cagaaggtgaaggtagatcaaagaaggaagcaaaaaatgccgcagccaaattagctgttgagatacttaataaggaaaagaaggcagtta
gtcctttattattgacaacaacgaattcttcagaaggattatccatggggaattacataggccttatcaatagaattgcccagaagaaaagacta
actgtaaattatgaacagtgtgcatcgggggtgcatgggccagaaggatttcattataaatgcaaaatgggacagaaagaatatagtattggt
acaggttctactaaacaggaagcaaaacaattggccgctaaacttgcatatcttcagatattatcagaagaaacctcagtgaaatctgactacc
tgtcctctggttcttttgctactacgtgtgagtcccaaagcaactctttagtgaccagcacactcgcttctgaatcatcatctgaaggtgacttctc
agcagatacatcagagataaattctaacagtgacagtttaaacagttcttcgttgcttatgaatggtctcagaaataatcaaaggaaggcaaaa
agatctttggcacccagatttgaccttcctgacatgaaagaaacaaagtatactgtggacaagaggtttggcatggattttaaagaaatagaat
taattggctcaggtggatttggccaagttttcaaagcaaaacacagaattgacggaaagacttacgttattaaacgtgttaaatataataacgag
aaggcggagcgtgaagtaaaagcattggcaaaacttgatcatgtaaatattgttcactacaatggctgttgggatggatttgattatgatcctga
gaccagtgatgattctcttgagagcagtgattatgatcctgagaacagcaaaaatagttcaaggtcaaagactaagtgccttttcatccaaatg
gaattctgtgataaagggaccttggaacaatggattgaaaaaagaagaggcgagaaactagacaaagtttggctttggaactctttgaacaa
ataacaaaaggggtggattatatacattcaaaaaaattaattcatagagatcttaagccaagtaatatattcttagtagatacaaaacaagtaaa
gattggagactttggacttgtaacatctctgaaaaatgatggaaagcgaacaaggagtaagggaactttgcgatacatgagcccagaacag
atttcttcgcaagactatggaaaggaagtggacctctacgctttggggctaattcttgctgaacttcttcatgtatgtgacactgcttttgaaacat
caaagtttttcacagacctacgggatggcatcatctcagatatatttgataaaaaagaaaaaactcttctacagaaattactctcaaagaaacct
gaggatcgacctaacacatctgaaatactaaggaccttgactgtgtggaagaaaagcccagagaaaaatgaacgacacacatgttagagc
ccttctgaaaaagtatcctgcttctgatatgcagttttccttaaattatctaaaatctgctagggaatatcaatagatatttacctttttatttttaatgtttc
ctttaatttttttactatttttactaatctttctgcagaaacagaaaggttttcttctttttgcttcaaaaacattcttacattttacttttttcctggctcatctct
ttattctttttctttttttttaaagacagagtctcgctctgttgcccaggctggagtgcaatgacacagtcttggctcactgcaacttctgcctcttggg
ttcaagtgattctcctgcctcagcctcctgagtagctggattacaggcatgtgccacccacccaactaatttttgtgtttttaataaagacagggtt
tcaccatgttggccaggctggtctcaaactcctgacctcaagtaatccacctgcctcggcctcccaaagtgctgggattacagggatgagcc
accgcgcccagcctcatctctttgttctaaagatggaaaaaccacccccaaattttctttttatactattaatgaatcaatcaattcatatctatttatt
aaatttctaccgcttttaggccaaaaaaatgtaagatcgttctctgcctcacatagcttacaagccagctggagaaatatggtactcattaaaaa
aaaaaaaaaaaa

Appendix B: Materials and Methods for Chapter 3

Materials

All synthesis reagents were purchased from Aldrich (St. Louis, MO) or Alfa Aesar (Ward Hill, MA), and were ACS reagent grade. Lipofectamine 2000 (LF2K) was purchased from Invitrogen (Carlsbad, CA). Linear poly(ethyleneimine) (LPEI, Mw = 25 kDa) was obtained from Polysciences, Inc (Warrington, PA). A working solution for LPEI was prepared in Milli-Q water at a concentration of 2.5 mg/mL. The solution was acidified using HCl to aid in solubility. Once dissolved, the solution was readjusted to pH 7.0 using NaOH. All polymer solutions were filtered through 0.22 μm Millex-GV PVDF sterile filters (Millipore) prior to being added to cells. The siRNA (Dharmacon; Lafayette, CO) sequence used was: siRNA guide strand - GAU GAA CUU CAG GGU CAG CUU; siRNA passenger strand - GCU GAC CCU GAA GUU CAU CUU. The dsDNA (IDT; Coraville, IA) was constructed to have identical hybridization structure to the siRNA (19 nucleotides hybridized with 2 nucleotide overhangs on each 3' end). The dsDNA sequence used was: dsDNA strand 1 - CCA CTA CCT GAG CAC CCA GTT; dsDNA strand 2 - CAG GGT GCT CAG GTA GTG GTT. For microscopy, the 5'-end of the siRNA passenger strand was labeled with Dy547. For the binding studies, the dsDNA strand 1 5'-end was labeled with 6-carboxyfluorescein (6-FAM). Tris/Boric Acid/EDTA running buffer and nucleic acid sample loading buffer were purchased from Bio-Rad (Hercules, CA).

Poly(propargyl glycolide) polymer synthesis

Prior to use, chloroform was dried over phosphorous pentoxide, dichloromethane was dried over CaH_2, and THF was dried over sodium and benzophenone. 4,4-N,N-dimethylaminopyridine (DMAP) was purified by sublimation at 35-40°C. 2-hydroxyethyldisulfide was distilled under vacuum. All glassware was oven-dried.

Synthesis of poly(propargyl glycolide) with disulfide initiator (PGSSPG)(Hou, 2009): An oven dried Schlenk flask was charged with propargyl glycolide (PGL) and DMAP, the flask was evacuated for at least two hours, then bis-(2-hydroxyethyl)disulfide initiator solution (0.11M in $CHCl_3$) [M]/[I] 10:1 was added, the monomer concentration was adjusted to 0.5 M by adding dry chloroform. The reaction mixture was degassed by 3 freeze-pump-thaw cycles, then backfilled with nitrogen gas. The flask was immersed in an oil bath at 60°C and was stirred for 12hrs. After polymerization, the solvent was removed and the white stringy solid was redissolved in THF and dialyzed against THF/Water 3:1 in a 1000 MWCO cellulose membrane. The polymer was then dried under vacuum. Nuclear Magnetic Resonance (NMR) was performed in 500 MHz or 300 MHz spectrometer. FTIR spectra were taken in a Mattson Galaxy series FTIR 3000. 1H NMR (CDCl3) δ5.47-5.35 (br, 1H) 5.26-5.22 (br,1H) 4.52-4.36 (m, 6H) 3.0-2.66 (br m, 2H) 2.12-2.03 (br, 1H)

Synthesis of poly(propargyl glycolide-b-ethylene oxide monomethyl ether) PEG_8PG: An ampoule was loaded with propargyl glycolide and stir bar. The ampoule was made from 3/8 in. diameter glass tubing was connected via a cajon fitting to a T-shape vacuum adapter with a stopcock and an air free Teflon valve. The apparatus was connected to vacuum and evacuated through the Teflon valve, and then it was backfilled with nitrogen gas. Predetermined amounts of Tin II 2-ethylhexanoate catalyst (51mM) in toluene and PEG 350 initiator (100 mM) in toluene were transferred to the ampoule through the stopcock. The solution was stirred for 30 minutes. The solvent was removed via vacuum and the ampoule was flame-sealed. The polymerization was carried out for 30 minutes at 130°C. The polymerization was quenched in ice water, the ampoule was broken and the residue was dissolved in CH_2Cl_2 to a 10% solution. A small

amount was withdrawn to evaluate conversion via 1H NMR. The rest was precipitated into ice cold methanol and the polymer was filtered and dried under vacuum. 1H NMR ($CDCl_3$) δ: 5.43-5.33 (br, 1H) 3.70-3.66 (q, 2H) 3.64-3.61(dd, 2H) 3.54-3.51 (q, 2H) 3.36 (s, 3H) 3.0-2.82 (m, 2H) 2.14-2.06 (br s, 1H)

Standard Click Chemistry Procedure: A Schlenk flask was loaded with 40-60 mg of polymer, the desired mol % of azide ligand according to moles of alkyne in the polymer, and 24 mol% of sodium ascorbate. The mixture was dissolved in DMF and degassed by 3-4 freeze-pump-thaw cycles and backfilled with nitrogen gas. A 0.1 M solution of $CuCl_2•2H_2O$ in DMF was added after degassing. The reaction mixture was stirred at room temperature overnight (Figure 3-1). Cholesteryl Iodide (R): Modified procedure from (Posner et al. 1976) 1H NMR (CDCl3) 5.31 (t, 1H), 4.02 (m, 1H), 2.91 (t, 1H), 2.69-2.60 (dq, 1H) 2.32-1.03 (m, 24H), 1.02 (s, 3H), 0.97 (m, 2H), 0.89 (d, 3H), 0.84 (dd, 6H), 0.65 (s, 3H).

Cholesteryl Azide (S): Cholesteryl iodide (2mmol, 1.03g) was combined with sodium azide (4mmol, 0.65g) and dissolved in 10 ml DMF. The reaction mixture was stirred at 80°C overnight. The solvent was removed under high vacuum. The solid was redissolved in diethyl ether and washed with water, sodium metabisulfite ($Na_2S_2O_3$) and NaCl. The organic layer was dried over $MgSO_4$. The solid was recrystallized from absolute ethanol (60 % yield) 1H NMR ($CDCl_3$) δ: 5.38 (t, 1H), 3.86 (t, 1H), 2.54-2.45 (m, 1H), 2.21-2.13 (1H), 2.04-2.02 (2H), 1.86-1.02 (24H), 0.99 (s, 3H), 0.90 (d, 3H), 0.85 (dd, 6H), 0.66 (s, 3H)) $_{13}C$ NMR ($CDCl_3$) 138.08, 123.17, 58.28, 56.7, 56.1, 49.9, 42.3, 39.7, 39.5, 37.1, 36.2, 36.0, 35.8, 33.6, 31.82, 31.79, 28.2, 28.0, 26.1, 24.26, 23.8, 22.8, 22.5, 20.7, 18.9, 18.7, 11.8 FTIR 2080 cm-1 N3

Polymer Binding Gels

Solutions were prepared in Milli-Q water using 200nM dsDNA. To each sample, polymer was added and allowed to mix for 15 minutes. Bound complexes were resolved on 0.8% agarose gels. Signal intensities of free dsDNA were quantified from gel images and normalized to dsDNA only control lanes. Example: Fraction Bound = 1 – (intensity of unbound dsDNA from NP-containing lane/intensity of unbound dsDNA from lane without NP). A single plot of fraction bound versus NP concentration (in μg/ml) was constructed from all of the data from two independent experiments (Figure 3-2). The combined data were simultaneously fit by a modified form of the Hill equation (Hill 1910) to obtain values for the binding constant (K) and a value to capture binding cooperativity (n) (Table 3-1).

$$f = \frac{[NP]^n}{K^n + [NP]^n}$$

The K value reflects binding at 15min, which is not necessarily equivalent to the equilibrium dissociation constant since the time required to reach equilibrium varies with the NP composition and can approach up to ~24hrs for some NPs (data not shown). An n value greater than 1 indicates the possibility of cooperative binding. The K values were compared using a two-tailed Student's t-test for unequal variances with α=0.01.

Cell Culture

Human lung carcinoma cells (H1299) constitutively expressing EGFP were generously provided by Dr. Jørgen Kjems, University of Aarhus, Denmark. Cell culture media was prepared with Dulbecco's Modified Eagle's Medium High Glucose (DMEM, #11965, Invitrogen) supplemented with 10% fetal bovine serum (FBS, GIBCO), 1% penicillin-streptomycin (GIBCO), and 1% Geneticin (GIBCO). Cells were maintained in an incubator at 37°C, 5% CO2,

100% relative humidity and subcultured approximately weekly by trypsinization. Leibovitz Medium (L-15, Sigma, St. Louis, MO) was used for cell imaging. All experiments were performed using cells with passages earlier than 20.

Transfection

Opti-Mem (GIBCO) was used for all transfections. H1299-EGFP cells were seeded in 4-well Nunc Lab-Tek chambered coverglasses (Fisher Scientific, Pittsburgh, PA) at a density of 37,500 cells/well in 0.5 mL of complete media without antibiotics. After 24 h, treatments were initiated in a staggered fashion so that all samples would be ready for processing and imaging at the same time. In other words, the 24 h time points were started first, with the 16 h points started 8 hours later, etc. 100 μL solutions of siRNA-NP were prepared in Opti-Mem and allowed to mix for 20 minutes prior to their addition to cells at final concentrations of 100 nM siRNA and 100 μg/mL NP. LPEI polyplexes and LF2K lipoplexes were prepared in a final volume of 600 μL at concentrations of 100 nM siRNA and either 10 μg/mL LPEI or 2.3 μg/mL LF2K (1.4 μL of 1μg/μL stock solution). Cells were incubated in the transfection solutions for 24h, 16h, 8h, and 4h prior to imaging.

Confocal Microscopy

Immediately prior to imaging, the cell media was removed, the cells were rinsed, and 0.5mL of L-15 media were added. Confocal imaging was performed on an Olympus FluoView 1000 Inverted IX81 microscope, using a 40x oil objective. Images were taken sequentially, using a Kalman average of 2x. DMACA tagged particles were excited using a 405 nm diode laser and detected through a BA430-470nm emission filter. EGFP fluorescence was assayed using an excitation of 488 nm with a multi-line Argon laser and detected through a BA505-525nm emission filter. Dy547 fluorescence (siRNA) was excited at 543 nm by a HeNe laser and

detected through a BA560-IFnm emission filter. The focal plane selected for each image was based on the highest intensity of green fluorescence. The line intensity graphs were constructed from the 4h, 160x magnification images. A line was drawn lengthwise across the cell so that it would intersect with the areas of highest intensity red fluorescence.

Appendix C: Materials and Methods for Chapter 4

Materials

All synthesis reagents were purchased from Aldrich and used as received. MQ water was obtained from a Millipore Synergy UV water purification system, RNAase free water was purchased from Fisher Scientific. Lipofectamine 2000 (LF2K) was purchased from Invitrogen. Linear poly(ethyleneimine) (LPEI, Mw = 25 kDa) was obtained from Polysciences, Inc. A working solution for LPEI was prepared in Milli-Q water at a concentration of 2.5 mg/mL. The solution was acidified using HCl to aid in solubility. Once dissolved, the solution was readjusted to pH 7.0 using NaOH. The siRNA (Dharmacon) sequence used was: siRNA guide strand - GAU GAA CUU CAG GGU CAG CUU; siRNA passenger strand - GCU GAC CCU GAA GUU CAU CUU. A poorly active EGFP targeting sequence was used to act as a negative control (siRNA guide strand – CGG GCA UGG CGG ACU UGA AUU; siRNA passenger strand – UUC AAG UCC GCC AUG CCC GUU) and was also purchased from Dharmacon. The dsDNA (IDT) was constructed to have identical hybridization structure to the siRNA (19 nucleotides hybridized with 2 nucleotide overhangs on each 3' end). The dsDNA sequence used was: dsDNA strand 1 - CCA CTA CCT GAG CAC CCA GTT; dsDNA strand 2 - CAG GGT GCT CAG GTA GTG GTT. For microscopy, the 5'-end of the siRNA passenger strand was labeled with Dy547. For the binding studies, the dsDNA strand 1 5'-end was labeled with 6-carboxyfluorescein (6-FAM). Tris/Boric Acid/EDTA running buffer and nucleic acid sample loading buffer were purchased from Bio-Rad. For the inhibition studies, all inhibitors were purchased through Sigma, including the heparin sodium.

Hydrodynamic radius

DLS and ζ potential were measured using a Malvern zetasizer NanoZS. Measurements by dynamic light scattering were performed using disposable UV cuvettes (Brandtech®). The nanoparticle stock sample of 500 μL was measured at the original concentration, and then it was diluted by two-fold and measured again. After every measurement the sample was diluted by two-fold until the concentration is close to 0.05 mg/mL at which time the size will also be stabilized.

siRNA titration using ζ potential

A 100 nM solution of siRNA was added to a disposable cuvette and the dipcell was fixed. The ζ potential and hydrodynamic radius was measured. 5 μL of 1mg/mL polymer solution in milliQ water were added to the cuvette and mixed. After each aliquot addition of polymer solution the ζ potential and hydrodynamic radius were measured. The titration was stopped once the curved seemed to plateau. A plot of polymer concentration vs. ζ potential was generated using Microsoft Excel.

Synthesis of Silicon oxide nanoparticles +/- dextran

Three different synthetic methods were employed for the synthesis of +/- dextran silicon oxide nanoparticles. The methods were denominated α, β and γ. Table A-1 shows the main differences between methods.

Table A-1 Silica solid-core NP synthesis parameters

	Method α	**Method β**	**Method γ**
Ethanol	150 mL	150 mL	150mL
Water	5 mL	60 mL	90 mL
NH_4OH	10 mL	10 mL	10 mL
TEOS concentration	0.06 M	0.01M	0.0096M
APTES addition time (min)	30	10	15
Representative NP	GACV.37	GACVI.19	GACVI.32

Method α

A 500 mL round bottom Schlenk flask was charged with 150 mL of absolute ethanol. Dextran 9-11 KDa ($1.0x10^{-5}$mol, 100 mg) was dissolved in 5mL of MQ water. Tetraethoxysilane (TEOS, 10 mmol, 2.2 mL) and dextran solution were added simultaneously dropwise via syringe. Following the addition of TEOS, 10mL of NH_4OH (~30% as NH_3) were added via syringe. The mixture was stirred at room temperature for 30 minutes under nitrogen. 3-aminopropyltriethoxysilane (APTES, 20% mol, 2mmol, 0.46 mL) was added. The reaction mixture was stirred for 24 hours at room temperature under nitrogen atmosphere. The reaction mixture was purified by pressure filtration using a regenerated cellulose membrane (Millipore, 30 KDa MWCO, 47mm diameter) at 40 PSI rinsing with MQ water three times. The filtered solid were suspended in MQ water and sonicated until well dispersed.

Method β

A 500 mL round bottom Schlenk flask was charged with 150 mL of absolute ethanol and 50 mL of MQ water. Dextran 9-11 KDa (2.4×10^{-6} mol, 24 mg) was dissolved in 10mL of MQ water

and added, followed by 10mL of NH_4OH (~30% as NH_3). TEOS, (2.4 mmol, 0.53 mL) was added dropwise via syringe. The mixture was stirred at room temperature for 10 minutes under nitrogen. APTES (40% mol, 9.6 x 10^{-4} mol, 0.46 mL) was added. The reaction mixture was stirred for 24 hours at room temperature under nitrogen atmosphere. The reaction mixture was purified by pressure filtration using a regenerated cellulose membrane (Millipore, 30 KDa MWCO, 47mm diameter) at 40 PSI rinsing with MQ water three times. The filtered solid were suspended in MQ water and sonicated until well dispersed.

Method γ

A 500 mL round bottom Schlenk flask was charged with 150 mL of absolute ethanol and 80 mL of MQ water. Dextran 9-11 KDa (2.4 x 10^{-6} mol, 24 mg) was dissolved in 10mL of MQ water and added, followed by 10mL of NH_4OH (~30% as NH_3). TEOS, (2.4 mmol, 0.53 mL) was added dropwise via syringe. The mixture was stirred at room temperature for 15 minutes under nitrogen. APTES (40% mol, 9.6 x 10^{-4} mol, 0.46 mL) was added. The reaction mixture was stirred for 24 hours at room temperature under nitrogen atmosphere. The reaction mixture was purified by pressure filtration using a regenerated cellulose membrane (Millipore, 30 KDa MWCO, 47mm diameter) at 40 PSI rinsing with MQ water three times. The filtered solid were suspended in MQ water and sonicated until well dispersed.

Binding Gels

Solutions were prepared in Milli-Q water using 200nM dsDNA. To each sample, polymer was added and allowed to mix for 15 minutes. Bound complexes were resolved on 0.8% agarose gels. Signal intensities of free dsDNA were quantified from gel images and normalized to dsDNA only control lanes. Example: Fraction Bound = 1 – (intensity of unbound dsDNA from

NP-containing lane/intensity of unbound dsDNA from lane without NP). A single plot of fraction bound versus NP concentration (in μg/mL) was constructed from all of the data from two independent experiments (Figure 3-2). The combined data were simultaneously fit by a modified form of the Hill equation (Hill 1910) to obtain values for the binding constant (K) and a value to capture binding cooperativity (n) (Table 3-1).

$$f = \frac{[NP]^n}{K^n + [NP]^n}$$

The K value reflects binding at 15min, which is not necessarily equivalent to the equilibrium dissociation constant since the time required to reach equilibrium varies with the NP composition and can approach up to ~24hrs for some NPs (data not shown). An n value greater than 1 indicates the possibility of cooperative binding.

Cell Culture

Human lung carcinoma cells (H1299) constitutively expressing EGFP were generously provided by Dr. Jørgen Kjems, University of Aarhus, Denmark. Cell culture media was prepared with Dulbecco's Modified Eagle's Medium High Glucose (DMEM, #11965, Invitrogen) supplemented with 10% fetal bovine serum (FBS, GIBCO), 1% penicillin-streptomycin (GIBCO), and 1% Geneticin (GIBCO). Cells were maintained in an incubator at 37°C, 5% CO2, 100% relative humidity and subcultured approximately weekly by trypsinization. Leibovitz Medium (L-15, Sigma, St. Louis, MO) was used for cell imaging. All experiments were performed using cells with passages earlier than 30.

EGFP Transfection and Fluorescence Analysis

H1299-EGFP cells were seeded in 96-well black side, clear bottom plates (Fisher Scientific) at a density of 20,000 cells/well in 0.1 mL of complete media without antibiotics. After 24 h, 50

μL solutions of varied siRNAs and NPs were prepared in Opti-Mem and allowed to mix for 30 minutes prior to their addition to cells at varied concentrations of siRNA and NP. LPEI polyplexes and LF2K lipoplexes were prepared at varied siRNA concentrations and particle concentrations of 10 μg/mL LPEI and 2.3 μg/mL LF2K (1.4 μL of 1μg/μL stock solution). Cells were incubated in the transfection solutions at 37°C, 5% CO_2. After 24h, cells were washed 2 times with DBPS (Gibco) and EGFP fluorescence was quantified using a Gemini EM fluorescent plate reader (Molecular Devices) at 480 excitation/525 emission. Fluorescence intensity was normalized to control wells.

Confocal Microscopy

Opti-Mem (GIBCO) was used for all transfections. H1299-EGFP cells were seeded in 4-well Nunc Lab-Tek chambered coverglasses (Fisher Scientific, Pittsburgh, PA) at a density of 37,500 cells/well in 0.5 mL of complete media without antibiotics. After 24 h, solutions of siRNA-NP were prepared in Opti-Mem as described above. Immediately prior to imaging, the cell media was removed, the cells were rinsed, and 0.5mL of L-15 media were added. Confocal imaging was performed on an Olympus FluoView 1000 Inverted IX81 microscope, using a 40x oil objective. Images were taken sequentially, using a Kalman average of 2x. EGFP fluorescence was assayed using an excitation of 488 nm with a multi-line Argon laser and detected through a BA505-525nm emission filter. Dy547 fluorescence (siRNA) was excited at 543 nm by a HeNe laser and detected through a BA560-IFnm emission filter. The focal plane selected for each image was based on the highest intensity of green fluorescence.

Inhibition experiments/Flow cytometry

For time series inhibition studies, cells were plated onto 12-well plates at a density of 150,000 cells/well and cultured in antibiotic free media. Immediately prior to transfection cells

were washed with media and replaced with media containing various inhibitors for the appropriate pre-treatment time (Table A-2). Following pre-treatment, cells were treated with 100uL of various transfection solutions in Optimem (200nM siRNA, 2.3μg/mL LF2K, 10 μg/mL LPEI, 200 μg/mL NP) and incubated for 4h. After 4h, extracellularly bound complexes were removed with a 20 μg/mL heparin wash for 15 minutes at 37^{O}C. Following the heparin wash, the 4h timepoint samples were collected for FACS analysis. The 24h and 48h timepoint samples were washed and replaced with antibiotic free media.

Table A-2 Inhibitor treatment conditions

Chemical	Inhibition target	Concentration	Pretreatment time (min)
Chlorpromazine	Clathrin	10 μg/mL	30
Filipin	Caveolae	2 μg/mL	60
Cytochalasin D	Actin dependent processes/intracellular trafficking	5 μg/mL	15
Temperature	Energy dependent processes	4^{O}C	60

For FACS analysis, cells were trypsinized and collected by resuspension in 0.5mL PBS and centrifuged at 4^{O}C, 200rcf for 5 minutes. The supernatant was removed and cells were resuspended and collected into 5mL round bottom tubes (Falcon) using 0.25-0.75mL PBS (depending on cell concentration). Immediately prior to analysis, cells were treated with DAPI at a final concentration of 1 μg/mL for live/dead analysis. Cells were analyzed using a Becton Dickinson Influx Flow Cytometer to detect DAPI (355ex, 460/50em), EGFP (488ex, 530/40em), and Dy547 tagged siRNA (561ex, 585/29em) and gated to include 10,000 cells/sample. For comparison between experiments, the instrument was calibrated using Sphero Rainbow

Calibration particles (Spherotech). EGFP fluorescence was normalized to particle only controls and siRNA uptake was measured by blanking the fluorescence to that of particle only controls.

Statistical Analysis

Multiple comparisons between protein levels across different siRNA treatments conditions were performed using one-way or two-way ANOVA followed by Tukey's HSD post-hoc analysis with p-value cut-off set at 0.05 using both Microsoft Excel and Minitab.

REFERENCES

REFERENCES

Akinc A, Thomas M, Klibanov AM, Langer R (2005) Exploring polyethylenimine-mediated DNA transfection and the proton sponge hypothesis. J Gene Med 7 (5):657-663. doi:10.1002/jgm.696

Akinc A, Zumbuehl A, Goldberg M, Leshchiner ES, Busini V, Hossain N, Bacallado SA, Nguyen DN, Fuller J, Alvarez R, Borodovsky A, Borland T, Constien R, de Fougerolles A, Dorkin JR, Jayaprakash KN, Jayaraman M, John M, Koteliansky V, Manoharan M, Nechev L, Qin J, Racie T, Raitcheva D, Rajeev KG, Sah DWY, Soutschek J, Toudjarska I, Vornlocher HP, Zimmermann TS, Langer R, Anderson DG (2008) A combinatorial library of lipid-like materials for delivery of RNAi therapeutics. Nature Biotechnology 26 (5):561-569. doi:10.1038/nbt1402

Alam M, Dixit V, Kang H, Li Z-B, Chen X, Trejo J, Fisher M, Juliano R (2008) Intracellular delivery of an anionic antisense oligonucleotide via receptor-mediated endocytosis. Nucleic Acids Research 36 (8):2764-2776. doi:10.1093/nar/gkn115

Alam M, Ming X, Dixit V, Fisher M, Chen X, Juliano R (2010) The Biological Effect of an Antisense Oligonucleotide Depends on Its Route of Endocytosis and Trafficking. Oligonucleotides 20 (2):103-109. doi:10.1089/oli.2009.0211

Alvarez-Erviti L, Seow YQ, Yin HF, Betts C, Lakhal S, Wood MJA (2011) Delivery of siRNA to the mouse brain by systemic injection of targeted exosomes. Nature Biotechnology 29 (4):341-U179. doi:10.1038/nbt.1807

Amarzguioui M, Prydz H (2004) An algorithm for selection of functional siRNA sequences. Biochemical and Biophysical Research Communications 316:1050-1058. doi:10.1016/j.bbrc.2004.02.157

Ameres SL, Martinez J, Schroeder R (2007) Molecular basis for target RNA recognition and cleavage by human RISC. Cell 130 (1):101-112. doi:10.1016/j.cell.2007.04.037

Andersen MO, Nygaard JV, Burns JS, Raarup MK, Nyengaard JR, Bunger C, Besenbacher F, Howard KA, Kassem M, Kjems J (2010) siRNA Nanoparticle Functionalization of Nanostructured Scaffolds Enables Controlled Multilineage Differentiation of Stem Cells. Molecular Therapy 18 (11):2018-2027. doi:10.1038/mt.2010.166

Bartlett D, Davis ME (2006) Insights into the kinetics of siRNA-mediated gene silencing from live-cell and live-animal bioluminescent imaging. Nucleic Acids Research 34:322-333

Berezhna S, Supekova L, Supek F, Schultz P, Deniz A (2006) siRNA in human cells selectively localizes to target RNA sites. Proceedings of the National Academy of Sciences of the United States of America 103:7682-7687

Betancur JG, Tomari Y (2012) Dicer is dispensable for asymmetric RISC loading in mammals. RNA 18:24-30. doi:10.1261/rna.029785.111

Birmingham A, Anderson E, Sullivan K, Reynolds A, Boese Q, Leake D, Karpilow J, Khvorova A (2007) A protocol for designing siRNAs with high functionality and specificity. Nature Protocols 2 (9):2068-2078. doi:10.1038/nprot.2007.278

Breunig M, Hoza C, Lungwitz U, Watanabe K, Umeda I, Kato H, Goepferich A (2008) Mechanistic investigation of poly(ethylene imine)-based siRNA delivery: disulfide bonds boost intracellular release of the cargo. J Control Release 130:57-63

Brown KM, Chu C-Y, Rana TM (2005) Target accessibility dictates the potency of human RISC. Nature structural & molecular biology 12 (5):469-470. doi:10.1038/nsmb931

Burke RS, Pun SH (2008) Extracellular barriers to in Vivo PEI and PEGylated PEI polyplex-mediated gene delivery to the liver. Bioconjugate Chemistry 19 (3):693-704. doi:10.1021/bc700388u

Buyens K, Lucas B, Raemdonck K, Braeckmans K, Vercammen J, Hendrix J, Engelborghs Y, De Smedt SC, Sanders NN (2008) A fast and sensitive method for measuring the integrity of siRNA-carrier complexes in full human serum. J Control Release 126 (1):67-76. doi:10.1016/j.jconrel.2007.10.024

Cardoso ALC, Simoes S, de Almeida LP, Pelisek J, Culmsee C, Wagner E, de Lima MCP (2007) SiRNA detivery by a transferrin-associated lipid-based vector: a non-viral strategy to mediate gene silencing. J Gene Med 9 (3):170-183. doi:10.1002/jgm.1006

Carthew RW, Sontheimer EJ (2009) Origins and Mechanisms of miRNAs and siRNAs. Cell 136:642-655. doi:10.1016/j.cell.2009.01.035

Champion JA, Mitragotri S (2006) Role of target geometry in phagocytosis. Proceedings of the National Academy of Sciences of the United States of America 103 (13):4930-4934. doi:10.1073/pnas.0600997103

Chang CI, Lee TY, Dua P, Kim S, Li CJ, Lee D-K (2011) Long Double-Stranded RNA-Mediated RNA Interference and Immunostimulation: Long Interfering Double-Stranded RNA as a Potent Anticancer Therapeutics. Oligonucleotides 21 (3):149-155. doi:10.1089/nat.2011.0296

Chen A, Santhakumaran L, Nair S, Amenta P, Thomas T, He H, Thomas T (2006) Oligodeoxynucleotide nanostructure formation in the presence of polypropyleneimine dendrimers and their updake in breask cancer cells. Nanotechnology 17:5449-5460

Chendrimada TP, Gregory RI, Kumaraswamy E, Norman J, Cooch N, Nishikura K, Shiekhattar R (2005) TRBP recruits the Dicer complex to Ago2 for microRNA processing and gene silencing. Nature 436:740-744. doi:10.1038/nature03868

Cho EC, Zhang Q, Xia YN (2011) The effect of sedimentation and diffusion on cellular uptake of gold nanoparticles. Nat Nanotechnol 6 (6):385-391. doi:10.1038/nnano.2011.58

Cho YW, Kim JD, Park K (2003) Polycation gene delivery systems: escape from the endosomes to the cytosol. Journal of Pharmaceutical Pharmacology 55:721-734

Cockrell AS, Kafri T (2007) Gene delivery by lentivirus vectors. Mol Biotechnol 36 (3):184-204. doi:10.1007/s12033-007-0010-8

Cohen H, Levy R, Gao J, Fishbein I, Kousaev V, Sosnowski S, Slomkowsk S, Golomb G (2000) Sustained delivery and expression of DNA encapsulated in polymeric nanoparticles. Gene Ther 7:1896-1905

Conner SD, Schmid SL (2003) Regulated portals of entry into the cell. Nature 422:37-44

Coura RD, Nardi NB (2007) The state of the art of adeno-associated virus-based vectors in gene therapy. Virol J 4:99. doi:10.1186/1743-422x-4-99

Damm E-M, Pelkmans L, Kartenbeck J, Mezzacasa A, Kurzchalia T, Helenius A (2005) Clathrin- and caveolin-1-independent endocytosis: entry of simian virus 40 into cells devoid of caveolae. Journal of Cell Biology 168 (3):477-488. doi:10.1083/jcb.200407113

Dande P, Prakash TP, Sioufi N, Gaus H, Jarres R, Berdeja A, Swayze EE, Griffey RH, Bhat B (2006) Improving RNA interference in mammalian cells by 4 '-thio-modified small interfering RNA (siRNA): Effect on siRNA activity and nuclease stability when used in combination with 2 '-O-alkyl modifications. Journal of Medicinal Chemistry 49 (5):1624-1634. doi:10.1021/jm050822c

Dausend J, Musyanovych A, Dass M, Walther P, Schrezenmeier H, Landfester K, Mailander V (2008) Uptake Mechanism of Oppositely Charged Fluorescent Nanoparticles in HeLa Cells. Macromol Biosci 8 (12):1135-1143. doi:10.1002/mabi.200800123

Davidson BL, McCray PB (2011) Current prospects for RNA interference-based therapies. Nat Rev Genet 12 (5):329-340. doi:10.1038/nrg2968

Davis ME (2009) The First Targeted Delivery of siRNA in Humans via a Self-Assembling, Cyclodextrin Polymer-Based Nanoparticle: From Concept to Clinic. Molecular Pharmaceutics 6 (3):659-668. doi:10.1021/mp900015y

Elbashir SM, Harborth J, Lendeckel W, Yalcin A, Weber K, Tuschl T (2001a) Duplexes of 21-nucleotide RNAs mediate RNA interference in cultured mammalian cells. Nature 411 (6836):494-498. doi:10.1038/35078107

Elbashir SM, Lendeckel W, Tuschl T (2001b) RNA interference is mediated by 21- and 22-nucleotide RNAs. Genes & Development 15 (2):188-200. doi:10.1101/gad.862301

Farrell L-L, Pepin J, Kucharski C, Lin X, Xu Z, Uludag H (2007) A comparison of the effectiveness of cationic polymers poly-L-lysine (PLL) and polyethylenimine (PEI) for non-viral delivery of plasmid DNA to bone marrow stromal cells (BMSC). European journal of pharmaceutics and biopharmaceutics 65:388-397

Fire A, Xu S, Montgomery M, Kostas S, Driver S, Mello C (1998) Potent and specific genetic interference by double-stranded RNA in Caenorhabditis elegans. Nature 391 (6669):806-811. doi:10.1038/35888

Frank F, Sonenberg N, Nagar B (2010) Structural basis for 5'-nucleotide base-specific recognition of guide RNA by human AGO2. Nature 465 (7299):818-822. doi:10.1038/nature09039

Fujimoto T, Kogo H, Nomura R, Une T (2000) Isoforms of caveolin-1 and caveolar structure. J Cell Sci 113:3509-3517

Gabrielson NP, Pack DW (2009) Efficient polyethylenimine-mediated gene delivery proceeds via a caveolar pathway in HeLa cells. J Control Release 136:54-61. doi:10.1016/j.jconrel.2009.02.003

Gary D, Puri N, Won Y-Y (2007) Polymer-based siRNA delivery: Perspectives on the fundamental and phenomenological distinctions from polymer-based DNA delivery. J Control Release 121:64-73

Ghosh SS, Gopinath P, Ramesh A (2006) Adenoviral vectors - A promising tool for gene therapy. Appl Biochem Biotechnol 133 (1):9-29. doi:10.1385/abab:133:1:9

Gitig D (2012) Use of siRNA in Therapeutic Arena on the Upswing. Genetic Engineering & Biotechnology News, vol 32. doi:10.1089/gen.32.8.10

Goncalves C, Mennesson E, Fuchs R, Gorvel J-P, Midoux P, Pichon C (2004) Macropinocytosis of Polyplexes and Recycling of Plasmid via the Clathrin-Dependent Pathway Impair the Transfection Efficiency of Human Hepatocarcinoma Cells. Molecular Therapy 10 (2):373-385. doi:10.1016/j.ymthe.2004.05.023

Gratton SE, Ropp PA, Pohlhaus PD, Luft JC, Madden VJ, Napler ME, De Simone JM (2008) The effect of particle design on cellular internalization pathways. Proceedings of the National

Academy of Sciences of the United States of America 105 (33):11613-11618. doi:10.1073/pnas.0801763105

Gredell JA, Berger AK, Walton SP (2008) Impact of target mRNA structure on siRNA silencing efficiency: A large-scale study. Biotechnology and Bioengineering 100 (4):744-755. doi:10.1002/bit.21798

Gredell JA, Dittmer MJ, Wu M, Chan C, Walton SP (2010) Recognition of siRNA asymmetry by TAR RNA binding protein. Biochemistry 49 (14):3148-3155. doi:10.1021/bi902189s

Green JJ, Langer R, Anderson DG (2008) A combinatorial polymer library approach yields insight into nonviral gene delivery. Accounts of chemical research 41 (6):749-759. doi:10.1021/ar7002336

Grimm D, Streetz KL, Jopling CL, Storm TA, Pandey K, Davis CR, Marion P, Salazar F, Kay MA (2006) Fatality in mice due to oversaturation of cellular microRNA/short hairpin RNA pathways. Nature 441 (7092):537-541. doi:10.1038/nature04791

Guo PX, Coban O, Snead NM, Trebley J, Hoeprich S, Guo SC, Shu Y (2010a) Engineering RNA for Targeted siRNA Delivery and Medical Application. Advanced drug delivery reviews 62 (6):650-666. doi:10.1016/j.addr.2010.03.008

Guo ST, Huang YY, Jiang QA, Sun Y, Deng LD, Liang ZC, Du QA, Xing JF, Zhao YL, Wang PC, Dong AJ, Liang XJ (2010b) Enhanced Gene Delivery and siRNA Silencing by Gold Nanoparticles Coated with Charge-Reversal Polyelectrolyte. ACS Nano 4 (9):5505-5511. doi:10.1021/nn101638u

Gustavsson J, Parpal S, Karlsson M, Ramsing C, Thorn H, Borg M, Lindroth M, Peterson KH, Magnusson K-E, Stralfors P (1999) Localization of the insulin receptor in caveolae of adipocyte plasma membrane. The FASEB Journal 13:1961-1971

Haase AD, Jaskiewicz L, Zhang H, Laine S, Sack R, Gatignol A, Filipowicz W (2005) TRBP, a regulator of cellular PKR and HIV-1 virus expression, interacts with Dicer and functions in RNA silencing. EMBO reports 6 (10):961-967. doi:10.1038/sj.embor.7400509

Hammond SM, Bernstein E, Beach D, Hannon GJ (2000) An RNA-directed nuclease mediates post-transcriptional gene silencing in Drosophila cells. Nature 404 (6775):293-296. doi:10.1038/35005107

Hartman ZC, Appledorn DM, Amalfitano A (2008) Adenovirus vector induced innate immune responses: Impact upon efficacy and toxicity in gene therapy and vaccine applications. Virus Res 132 (1-2):1-14. doi:10.1016/j.virusres.2007.10.005

Hewlett L, Prescott A, Watts C (1994) The Coated Pit and Macropinocytic Pathways Serve Distinct Endosome Populations. The Journal of Cell Biology 124 (5):689-703. doi:0021-9525/94/03/689/15

Hill A (1910) The possible effects of the aggregation of the molecules of haemoglobin on its dissociation curves. Journal of Physiology 40:iv-vii

Hom C, Lu J, Liong M, Luo HZ, Li ZX, Zink JI, Tamanoi F (2010) Mesoporous Silica Nanoparticles Facilitate Delivery of siRNA to Shutdown Signaling Pathways in Mammalian Cells. Small 6 (11):1185-1190. doi:10.1002/smll.200901966

Hong K, Zheng W, Baker A, Papahadjopoulos D (1997) Stabilization of cationic liposome-plasmid DNA complexes by polyamines and poly(ethylene glycol)-phospholipid conjugates for efficient in vivo gene delivery. FEBS letters 400:223-237

Hossbach M, Gruber J, Osborn M, Weber K, Tuschl T (2006) Gene silencing with siRNA duplexes composed of target-mRNA-complementary and partially palindromic or partially complementary single-stranded siRNAs. RNA biology 3 (2):82-89

Hu P, Quick G, Yeo Y (2009) Gene delivery through the use of a hyaluronate-associated intracellulary degradable crosslinked polyethyleneimine. Biomaterials 30:5834-5843

Huesken D, Lange J, Mickanin C, Weiler J, Asselbergs F, Warner J, Meloon B, Engel S, Rosenberg A, Cohen D, Labow M, Reinhardt M, Natt F, Hall J (2005) Design of a genome-wide siRNA library using an artificial neural network. Nature Biotechnology 23 (8):995-1001. doi:10.1038/nbt1118

Huotari J, Helenius A (2011) Focus Review: Endosome Maturation. The EMBO journal 30:4481-3500. doi:10.1038/emboj.2011.286

Huth S, Lausier J, Gersting S, Rudolph C, Plank C, Welsch U, Rosenecker J (2004) Insights into the mechanism of magnetofection using PEI-based magnetofectins for gene transfer. The Journal of Gene Medicine 6:923-936. doi:10.1002/jgm.577

Ichihara M, Murakumo Y, Masuda A, Matsuura T, Asai N, Jijiwa M, Shinmi J, Yatsuya H, Qiao S, Takahashi M, Ohno K (2007) Thermodynamic instability of siRNA duplex is a prerequisite for dependable prediction of siRNA activites. Nucleic Acids Research 35 (18):e123. doi:10.1093/nar/gkm699

Ishihara S, Haga H, Yasuda M, Mizutani T, Kawabata K, Shirato H, Nishioka T (2010) Integrin beta 1-dependent invasive migration of irradiation-tolerant human lung adenocarcinoma cells in 3D collagen matrix. Biochemical and Biophysical Research Communications 396 (3):651-655. doi:10.1016/j.bbrc.2010.04.150

Ivanov AI (2008) Pharmacological Inhibition of Endocytic Pathways: Is It Specific Enough to Be Useful? Methods in Molecular Biology 440 (Exocytosis and Endocytosis):15-33

Ivanov AI, Hopkins AM, Brown GT, Gerner-Smidt K, Babbin BA, Parkos CA, Nusrat A (2008) Myosin II regulates the shape of three-dimensional intestinal epithelial cysts. J Cell Sci 121 (11):1803-1814. doi:10.1242/jcs.015842

Jackson AL, Linsley PS (2010) Recognizing and avoiding siRNA off-target effects for target identification and therapeutic application. Nature Reviews Drug Discovery 9 (1):57-67. doi:10.1038/nrd3010

Jiang X, Vogel EB, Smith III MR, Baker GL (2008) "Clickable" polyglycolides: tunable synthons for thermoresponsive degradable polymers. Macromolecules 41:1937-1944. doi:10.1021/ma7027962

Kaiser J (2007) Clinical research: Death prompts a review of gene therapy vector. Science 317 (5838):580-580. doi:10.1126/science.317.5838.580

Kaksonen M, Toret CP, Drubin DG (2006) Harnessing actin dynamics for clathrin-mediated endocytosis. Nature Reviews Molecular Cell Biology 7:404-415. doi:10.1038/nrm1940

Kamat M, El-Boubbou K, Zhu DC, Lansdell T, Lu X, Li W, Huang X (2010) Hyaluronic acid immobilized magnetic nanoparticles for active targeting and imaging of macrophages. Bioconjugate Chemistry 21:2128-2135. doi:10.1021/bc100354m

Katas H, Alpar HO (2006) Development and characterisation of chitosan nanoparticles for siRNA delivery. J Control Release 115 (2):216-225. doi:10.1016/j.jconrel.2006.07.021

Kerr MC, Teasdale RD (2009) Defining Macropinocytosis. Traffic 10:364-371

Khalil IA, Kogure K, Akita H, Harashima H (2006) Uptake pathways and subsequent intracellular trafficking in nonviral gene delivery. Pharmacological Reviews 58 (1):32-45. doi:10.1124/pr.58.1.8.

Khvorova A, Reynolds A, Jayasena SD (2003) Functional siRNAs and miRNAs Exhibit Strand Bias. Cell 115 (2):209-216. doi:10.1016/S0092-8674(03)00801-8

Kini HK, Walton SP (2009) Effect of siRNA terminal mismatches on TRBP and Dicer binding and silencing efficacy. FEBS Journal 276 (22):6576-6585. doi:10.1111/j.1742-4658.2009.07364.x

Kirkham M, Parton RG (2005) Clathrin-independent endocytosis: New insights into caveolae and non-caveolar lipid raft carriers. Biochimica et Biophysica Acta 1745:273-286. doi:10.1016/j.bbamcr.2005.06.002

Kiryu H, Terai G, Imamura O, Yoneyama H, Suzuki K, Asai K (2011) A detailed investigation of accessibilities around target sites of siRNAs and miRNAs. Bioinformatics 27 (13):1788-1797. doi:10.1093/bioinformatics/btr276

Kok KH, Ng MHJ, Ching YP, Jin DY (2007) Human TRBP and PACT directly interact with each other and associate with dicer to facilitate the production of small interfering RNA. Journal of Biological Chemistry 282 (24):17649-17657. doi:10.1074/jbc.M611768200

Krieg AM (2011) Is RNAi Dead? Molecular Therapy 19 (6):1001-1002. doi:10.1038/mt.2011.94

Kwon EJ, Bergen JM, Pun SH (2008) Application of an HIV gp41-derived peptide for enhanced intracellular trafficking of synthetic gene and siRNA delivery vehicles. Bioconjugate Chemistry 19 (4):920-927. doi:10.1021/bc700448h

Ladunga I (2006) More complete gene silencing by fewer siRNAs: transparent optimized design and biophysical signature. Nucleic Acids Research 35 (2):433-440. doi:10.1093/nar/gkl1065

Lai N, Jayaraman A, Lee K (2009) Enhanced proliferation of human umbilical vein endothelial cells and differentiation of 3T3-L1 adipocytes in coculture. Tissue Engineering 15 (5):1053-1061. doi:10.1089/ten.tea.2008.0101

Lamaze C, Schmid SL (1995) The emergence of clathrin-independent pinocytic pathways. Current Opinion in Cell Biology 7:573-580

Lee JS, Green JJ, Love KT, Sunshine J, Langer R, Anderson DG (2009) Gold, Poly(beta-amino ester) Nanoparticles for Small Interfering RNA Delivery. Nano Lett 9 (6):2402-2406. doi:10.1021/nl9009793

Lee S, Shim G, Kim S, Kim YB, Kim CW, Byun Y, Oh YK (2011) Enhanced Transfection Rates of Small-Interfering RNA Using Dioleylglutamide-Based Magnetic Lipoplexes. Oligonucleotides 21 (3):165-172. doi:10.1089/nat.2010.0274

Lee SH, Bae KH, Kim SH, Lee KR, Park TG (2008) Amine-functionalized gold nanoparticles as non-cytotoxic and efficient intracellular siRNA delivery carriers. Int J Pharm 364 (1):94-101. doi:10.1016/j.ijpharm.2008.07.027

Lee Y, Hur I, Park SY, Kim YK, Suh MR, Kim VN (2006) The role of PACT in the RNA silencing pathway. EMBO journal 25 (3):522-532. doi:10.1038/sj.emboj.7600942

Lei YG, Ng QKT, Segura T (2010) Two and Three-Dimensional Gene Transfer from Enzymatically Degradable Hydrogel Scaffolds. Microsc Res Tech 73 (9):910-917. doi:10.1002/jemt.20840

Leuschner PJF, Ameres SL, Kueng S, Martinez J (2006) Cleavage of the siRNA passenger strand during RISC assembly in human cells. EMBO reports 7 (3):314-320. doi:10.1038/sj.embor.7400637

Lima WF, Murray H, Nichols JG, Wu H, Sun H, Prakash TP, Berdeja AR, Gaus HJ, Crooke ST (2009) Human Dicer binds short single-strand and double-strand RNA with high affinity and interacts with different regions of the nucleic acids. Journal of biological Chemistry 284 (4):2535-2548. doi:10.1074/jbc.M803748200

Liu J, Carmell MA, Rivas FV, Marsden CG, Thomson JM, Song J-J, Hammond SM, Joshua-Tor L, Hannon GJ (2004) Argonaute2 Is the Catalytic Engine of Mammalian RNAi. Science Signaling 305 (5689):1437-1437. doi:10.1126/science.1102513

Liu XD, Howard KA, Dong MD, Andersen MO, Rahbek UL, Johnsen MG, Hansen OC, Besenbacher F, Kjems J (2007) The influence of polymeric properties on chitosan/siRNA nanoparticle formulation and gene silencing. Biomaterials 28 (6):1280-1288. doi:10.1016/j.biomaterials.2006.11.004

Liu Y, Reineke TM (2005) Hydroxyl Stereochemistry and amine number within poly(glycoamidoamine)s affect intracellular DNA delivery. J Am Chem Soc 127:3004-3015

Liu Y, Reineke TM (2006) Poly(glycoamidoamine)s for Gene Delivery: Stability of Polyplexes and Efficacy with Cardiomyoblast Cells. Bioconjugate Chemistry 17:101-108. doi:10.1021/bc050275+

Lu JJ, Langer R, Chen JZ (2009) A Novel Mechanism Is Involved in Cationic Lipid-Mediated Functional siRNA Delivery. Molecular Pharmaceutics 6 (3):763-771. doi:10.1021/mp900023v

Lu W, Zhang GD, Zhang R, Flores LG, Huang Q, Gelovani JG, Li C (2010) Tumor Site-Specific Silencing of NF-kappa B p65 by Targeted Hollow Gold Nanosphere-Mediated Photothermal Transfection. Cancer Res 70 (8):3177-3188. doi:10.1158/0008-5472.can-09-3379

Lu ZJ, Mathews DH (2008) Efficient siRNA selection using hybridization thermodynamics. Nucleic Acids Research 36 (2):640-647. doi:10.1093/nar/gkm920

Lynn DM, Langer R (2000) Degradable poly(beta-amino esters): Synthesis, characterization, and self-assembly with plasmid DNA. J Am Chem Soc 122 (44):10761-10768. doi:10.1021/ja0015388

Macia E, Ehrlich M, Massol R, Boucrot E, Brunner C, Kirchhausen T (2006) Dynasore, a Cell-Permeable Inhibitor of Dynamin. Developmental Cell 10:839-850. doi:10.1016/j.devcel.2006.04.002

MacRae IJ, Ma E, Zhou M, Robinson CV, Doudna JA (2007) In vitro reconstitution of the human RISC-loading complex. Proceedings of the National Academy of Sciences of the United States of America 105 (2):512-517. doi:10.10173/pnas.0710869105

Malefyt AP, Angart PA, Chan C, Walton SP (2012a) siRNA Therapeutic Design: Tools and Challenges. In: Mallick B (ed) Regulatory RNAs. Springer. doi:10.1007/978-3-642-22517-8_19

Malefyt AP, Walton SP, Chan C (2012b) Endocytosis Pathways for Nucleic Acid Therapeutics. Nano LIFE 2 (3):1241005

Malone RW, Felgner PL, Verma IM (1989) CATIONIC LIPOSOME-MEDIATED RNA TRANSFECTION. Proceedings of the National Academy of Sciences of the United States of America 86 (16):6077-6081. doi:10.1073/pnas.86.16.6077

Maniataki E, Mourelatos Z (2005) A human, ATP-independent, RISC assembly machine fueled by pre-miRNA. Genes & Development 19:2979-2990. doi:10.1101/gad.1384005

Mao SR, Neu M, Germershaus O, Merkel O, Sitterberg J, Bakowsky U, Kissel T (2006) Influence of polyethylene glycol chain length on the physicochemical and biological properties of poly(ethylene imine)-graft-poly(ethylene glycol) block copolymer/SiRNA polyplexes. Bioconjugate Chemistry 17 (5):1209-1218. doi:10.1021/bc060129j

Matranga C, Tomari Y, Shin C, Bartel DP, Zamore PD (2005) Passenger-strand cleavage facilitates assembly of siRNA into Ago2-containing RNAi enzyme complexes. Cell 123 (4):607-620. doi:10.1016/j.cell.2005.08.044

Matveeva OV, Nechipurenko YD, Rossi L, Moore B, Saetrom P, Ogurtsov AY, Atkins JF, Shabalina SA (2007) Comparison of approaches for rational siRNA design leading to a new efficient and transparent method. Nucleic Acids Research 35 (8):e63. doi:10.1093/nar/gkm088

McLendon PM, Fichter KM, Reineke TM (2010) Poly(glycoamidoamine) vehicles promote pDNA uptake through multiple routes and efficient gene expression via caveolae-mediated endocytosis. Molecular Pharmaceutics 7 (3):738-750. doi:10.1021/mp900282e

Medina-Kauwe LK, Xie J, Hamm-Alvarez S (2005) Intracellular trafficking of nonviral vectors. Gene Ther 12 (24):1734-1751. doi:10.1038/sj.gt.3302592

Mehrotra S, Lee I, Chan C (2009) Multilayer mediated forward and patterned siRNA transfection using linear-PEI at extended N/P ratios. Acta Biomaterialia 5:1474-1488

Meng HA, Liong M, Xia TA, Li ZX, Ji ZX, Zink JI, Nel AE (2010) Engineered Design of Mesoporous Silica Nanoparticles to Deliver Doxorubicin and P-Glycoprotein siRNA to

Overcome Drug Resistance in a Cancer Cell Line. ACS Nano 4 (8):4539-4550. doi:10.1021/nn100690m

Mori T, Kiyono T, Imabayashi H, Takeda Y, Tsuchiya K, Miyoshi S, Makino H, Matsumoto K, Saito H, Ogawa S, Sakamoto M, Hata J-I, Umezawa A (2005) Combination of hTERT and bmi-1, E6, or E7 induces prolongation of the life span of bone marrow stromal cells from an elderly donor without affecting their neurogenic potential. Molecular and Cellular Biology 25:5183-5195

Mysara M, Garibaldi JM, ElHefnawi M (2011) MysiRNA-Designer: A Workflow for Efficient siRNA Design. Plos One 6 (10):e25642. doi:doi:10.1371/journal.pone.0025642

Nel A, Madler L, Velego D, Xia T, Hoek E, Somasundaran P, Klaessig F, Castranova V, Thompson M (2009) Understanding biophysicochemical interactions at the nano-bio interface. Nature Materials 8:543-557

Nguyen J, Steele TWJ, Merkel O, Reul R, Kissel T (2008) Fast degrading polyesters as siRNA nano-carriers for pulmonary gene therapy. J Control Release 132 (3):243-251. doi:10.1016/j.jconrel.2008.06.010

Noland CL, Ma E, Doudna JA (2011) siRNA Repositioning for Guide Strand Selection by Human Dicer Complexes. Molecular cell 43 (1):110-121. doi:10.1016/j.molcel.2011.05.028

Nykänen A, Haley B, Zamore PD (2001) ATP Requirements and Small Interfering RNA Structure in the RNA Interference Pathway. Cell 107 (3):309-321. doi:10.1016/S0092-8674(01)00547-5

Ou M, Wang X-L, Xu R, Chang C-W, Bull D, Kim S (2008) Novel biodegradable poly(disulfide amine)s for gene delivery with high efficiency and low cytotoxicity. Bioconjugate Chemistry 19:626-633

Overhoff M, Alken M, Far RK-K, Lemaitre M, Lebleu B, Sczakiel G, Robbins I (2005) Local RNA target structure influences siRNA efficacy: a systematic global analysis. Journal of molecular biology 348 (4):871-881. doi:10.1016/j.jmb.2005.03.012

Pack D, Hoffman A, Pun S, Stayton P (2005) Design and development of polymers for gene delivery. Nature Reviews Drug Discovery 4:481-593

Parton RG, Joggerst B, Simons K (1994) Regulated Internalization of Caveolae. The Journal of Cell Biology 127 (5):1199-1215

Patel PCH, L.; Yeung, W.S.A.; Mirkin, C.A. (2011) Duplex end breathing determines serum stability and intracellular potency of siRNA-Au NPs. Molecular Pharmaceutics 8:6

Pelkmans L, Helenius A (2002) Endocytosis Via Caveolae. Traffic 3 (5):311-320

Peng D, Qian C, Sun Y, Barajas M, Prieto J (2000) Transduction of hepatocellular carcinoma (HCC) using recombinant adeno-associated virus (rAAV): in vitro and in vivo effects of genotoxic agents. Journal of Hepatology 32:975-985

Pollack A (2011) Drugmakers' fever for the power of RNA interference has cooled. New York Times, February 8, 2011,

Portis AM, Carballo G, Baker GL, Chan C, Walton SP (2010) Confocal Microscopy for the Analysis of siRNA Delivery by Polymeric Nanoparticles. Microsc Res Tech 73 (9):878-885. doi:10.1002/jemt.20861

Posner G, Ting J, Lentz C (1976) A mechanistic and synthetic study of organocopper substitution reactions with some homoallylic and cyclopropylcarbinyl substrates: Application to isoprenoid synthesis. Tetrahedron 32:2281-2287

Que-Gewirth N, Sullenger B (2007) Gene therapy progress and prospects: RNA aptamers. Gene Ther 14:283-291

Raeber GP, Lutolf MP, Hubbell JA (2005) Molecularly engineered PEG hydrogels: A novel model system for proteolytically mediated cell migration. Biophys J 89 (2):1374-1388. doi:10.1529/biophysj.104.050682

Reilly MJ, Larsen JD, Sullivan MO (2012a) Histone H3 Tail Peptides and Poly(ethylenimine) Have Synergistic Effects for Gene Delivery. Molecular Pharmaceutics 9:1031-1040. doi:10.1021/mp200372s

Reilly MJ, Larsen JD, Sullivan MO (2012b) Polyplexes Traffic through Caveolae to the Golgi and Endoplasmic Reticulum en Route to the Nucleus. Molecular Pharmaceutics 9 (5):1280-1290. doi:10.1021/mp200583d

Rejman J, Bragonzi A, Conese M (2005) Role of Clathrin- and Caveolae-Mediated Endocytosis in Gene Transfer Mediated by Lipo- and Polyplexes. Molecular Therapy 12 (3):468-474. doi:10.1016/j.ymthe.2005.03.038

Rejman J, Oberle V, Zuhorn IS, Hoekstra D (2004) Size-dependent internalization of particles via the pathways of clathrin- and caveolae-mediated endocytosis. Biochemical Journal 377:159-169

Ren T, Song YK, Zhang G, Liu D (2000) Structural basis of DOTMA for its high intravenous transfection activity in mouse. Gene Ther 7 (9):764-768. doi:10.1038/sj.gt.3301153

Reynolds A, Leake D, Boese Q, Scaringe S, Marshall WS, Khvorova A (2004) Rational siRNA design for RNA interference. Nature Biotechnology 22 (3):326-330. doi:10.1038/nbt936

Rivas FV, Tolia NH, Song JJ, Aragon JP, Liu JD, Hannon GJ, Joshua-Tor L (2005) Purified Argonaute2 and an siRNA form recombinant human RISC. Nature Structural & Molecular Biology 12 (4):340-349. doi:10.1038/nsmb918

Robbins M, Judge A, MacLachlan I (2009) siRNA and Innate Immunity. Oligonucleotides 19 (2):89-101. doi:10.1089/oli.2009.0180

Rosi NL, Giljohann DA, Thaxton CS, Lytton-Jean AKR, Han MS, Mirkin CA (2006) Oligonucleotide-modified gold nanoparticles for intracellular gene regulation. Science 312 (5776):1027-1030. doi:10.1126/science.1125559

Rozema DB, Lewis DL, Wakefield DH, Wong SC, Klein JJ, Roesch PL, Bertin SL, Reppen TW, Chu Q, Blokhin AV, Hagstrom JE, Wolff JA (2007) Dynamic PolyConjugates for targeted in vivo delivery of siRNA to hepatocytes. Proceedings of the National Academy of Sciences of the United States of America 104 (32):12982-12987. doi:10.1073/pnas.0703778104

Sakurai K, Amarzguioui M, Kim D-H, Alluin J, Heale B, Song M-s, Gatignol A, Behlke MA, Rossi JJ (2011) A role for human Dicer in pre-RISC loading of siRNAs. Nucleic Acids Research 39 (4):1510-1525. doi:10.1093/nar/gkq846

Samuel-Abraham S, Leonard JN (2010) Staying on message: design principles for controlling nonspecific responses to siRNA. The FEBS journal 277 (23):4828-4836. doi:10.1111/j.1742-4658.2010.07905.x

Schubert S, Grünweller A, Erdmann VA, Kurreck J (2005) Local RNA target structure influences siRNA efficacy: systematic analysis of intentionally designed binding regions. Journal of molecular biology 348 (4):883-893. doi:10.1016/j.jmb.2005.03.011

Schwarz D, Hutvagner G, Du T, Xu Z, Aronin N, Zamore P (2003) Asymmetry in the assembly of the RNAi enzyme complex. Cell 115 (2):199-208

Seitz H, Tushir J, Zamore P (2011) A 5′-uridine amplifies miRNA/miRNA* asymmetry in Drosophila by promoting RNA-induced silencing complex formation. Silence

Seow Y, Wood MJ (2009) Biological Gene Delivery Vehicles: Beyond Viral Vectors. Molecular Therapy 17 (5):767-777. doi:10.1038/mt.2009.41

Shabalina SA, Spiridonov AN, Ogurtsov AY (2006) Computational models with thermodynamic and composition features improve siRNA design. BMC Bioinformatics 7:65. doi:10.1186/1471-2105-7-65

Shao Y, Chan CY, Maliyekkel A, Lawrence CE, Roninson IB, Ding Y (2007) Effect of target secondary structure on RNAi efficiency. RNA 13 (10):1631-1640. doi:10.1261/rna.546207

Shifrina Z, Kuchkina N, Rutkevich P, Vlasik T, Sushko A, Izumrudov V (2009) Water-soluble cationic aromatic dendrimers and their complexation with DNA. Macromolecules 42:9548-9560

Shim MS, Kwon YJ (2010) Efficient and targeted delivery of siRNA in vivo. Febs Journal 277 (23):4814-4827. doi:10.1111/j.1742-4658.2010.07904.x

Siegwart DJ, Whitehead KA, Nuhn L, Sahay G, Cheng H, Jiang S, Ma M, Lytton-Jean A, Vegas A, Fenton P, Levins CG, Love KT, Lee H, Cortez C, Collins SP, Li YF, Jang J, Querbes W, Zurenko C, Novobrantseva T, Langer R, Anderson DG (2011) Combinatorial synthesis of chemically diverse core-shell nanoparticles for intracellular delivery. Proceedings of the National Academy of Sciences of the United States of America 108 (32):12996-13001. doi:10.1073/pnas.1106379108

Sioud M (2007) RNA interference and innate immunity. Advanced drug delivery reviews 59 (2-3):153-163. doi:10.1016/j.addr.2007.03.006

Sonawane ND, Szoka FC, Verkman AS (2003) Chloride accumulation and swelling in endosomes enhances DNA transfer by polyamine-DNA polyplexes. Journal of Biological Chemistry 278 (45):44826-44831. doi:10.1074/jbc.M308643200

Soutschek J, Akinc A, Bramlage B, Charisse K, Constien R, Donoghue M, Elbashir S, Geick A, Hadwiger P, Harborth J, John M, Kesavan V, Lavine G, Pandey RK, Racie T, Rajeev KG, Rohl I, Toudjarska I, Wang G, Wuschko S, Bumcrot D, Koteliansky V, Limmer S, Manoharan M, Vornlocher HP (2004) Therapeutic silencing of an endogenous gene by systemic administration of modified siRNAs. Nature 432 (7014):173-178. doi:10.1038/nature03121

Spagnou S, Miller A, Keller M (2004) Lipidic Carriers of siRNA: Differences in the formulation, cellular uptake and delivery with plasmid DNA. Biochemistry 43:13348-13356

Sun X, Rogoff HA, Li CJ (2008) Asymmetric RNA duplexes mediate RNA interference in mammalian cells. Nature Biotechnology 26 (12):1379-1382. doi:10.1038/nbt.1512

Takasaki S (2009) Selecting effective siRNA target sequences by using Bayes' theorem. Computational Biology and Chemistry 33:368-372. doi:10.1016/j.compbiolchem.2009.07.009

Tang MX, Redemann CT, Szoka FC (1996) In vitro gene delivery by degraded polyamidoamine dendrimers. Bioconjugate Chemistry 7 (6):703-714. doi:10.1021/bc9600630

Thery C (2011) Exosomes: secreted vesicles and intercellular communications. F1000 Biology Reports 3

Thierry A, Lunardi-Iskandar Y, Bryant J, Rabinovich P, Gallo R, Mahan L (1995) Systemic gene therapy:biodistribution and long-term expression of a transgene in mice. Proceedings of the National Academy of Sciences of the United States of America 92:9742-9748

Tjernberg L, Callaway D, Tjernberg A, Hahne S, Lilliehook C, Terenius L, Thyberg J, Nordstedt C (1999) A molecular model of Alzheimer amyloid β-peptide fibril formation. Journal of Biological Chemistry 274:12619-12625

Tomari Y, Matranga C, Haley B, Martinez N, Zamore PD (2004) A protein sensor for siRNA asymmetry. Science 306 (5700):1377-1380. doi:10.1126/science.1102755

Ui-Tei K, Naito Y, Takahashi F, Haraguchi T, Ohki-Hamazaki H, Juni A, Ueda R, Saigo K (2004) Guidelines for the selection of highly effective siRNA sequences for mammalian and chick RNA interference. Nucleic Acids Research 32 (3):936-948. doi:10.1093/nar/gkh247

Valadi H, Ekstrom K, Bossios A, Sjostrand M, Lee JJ, Lotvall JO (2007) Exosome-mediated transfer of mRNAs and microRNAs is a novel mechanism of genetic exchange between cells. Nat Cell Biol 9 (6):654-U672. doi:10.1038/ncb1596

van de Water FM, Boerman OC, Wouterse AC, Peters JGP, Russel FGM, Masereeuw R (2006) Intravenously administered short interfering RNA accumulates in the kidney and selectively suppresses gene function in renal proximal tubules. Drug Metab Dispos 34 (8):1393-1397. doi:10.1124/dmd.106.009555

van der Aa M, Huth U, Hafele S, Schubert R, Oosting R, Mastrobattista E, Hennink W, R P-S, GA K, DJA C (2007) Cellular Uptake of Cationic Polymer-DNA Complexes Via Caveolae Play a Pivotal Role in Gene Transfection in COS-7 Cells. Pharmaceutical Research 24 (8):1590-1598. doi:10.1007/s11095-007-9287-3

Veiseh O, Kievit FM, Mok H, Ayesh J, Clark C, Fang C, Leung M, Arami H, Park JO, Zhang MQ (2011) Cell transcytosing poly-arginine coated magnetic nanovector for safe and effective siRNA delivery. Biomaterials 32 (24):5717-5725. doi:10.1016/j.biomaterials.2011.04.039

Vickers TA, Koo S, Bennett CF, Crooke ST, Dean NM, Baker BF (2003) Efficient reduction of target RNAs by small interfering RNA and RNase H-dependent antisense agents. A comparative analysis. Journal of biological Chemistry 278 (9):7108-7118. doi:10.1074/jbc.M210326200

von Gersdorff K, Sanders NN, Vandenbroucke R, De Smedt SC, Wagner E, Ogris M (2006) The Internalization Route Resulting in Successful Gene Expression Depends on both Cell Line and Polyethylenimine Polyplex Type. Molecular Therapy 14 (5):745-753. doi:10.1016/j.ymthe.2006.07.006

Walton SP, Wu M, Gredell JA, Chan C (2010) Designing highly active siRNAs for therapeutic applications. The FEBS journal 277 (23):4806-4813. doi:10.1111/j.1742-4658.2010.07903.x

Wang HW, Noland C, Siridechadilok B, Taylor DW, Ma EB, Felderer K, Doudna JA, Nogales E (2009) Structural insights into RNA processing by the human RISC-loading complex. Nature Structural & Molecular Biology 16 (11):1148-1153. doi:10.1038/nsmb.1673

Wang L-H, Rothberg KG, Anderson RG (1993) Mis-Assembly of Clathrin Lattices on Endosomes Reveals a Regulatory Switch for Coated Pit Formation. Journal of Cell Biology 123 (5):1107-1117

Watts JK, Deleavey GF, Damha MJ (2008) Chemically modified siRNA: tools and applications. Drug Discovery Today 13 (842-855). doi:10.1016/j.drudis.2008.05.007

Weitzer S, Martinez J (2007) The human RNA kinase hClp1 is active on 3′ transfer RNA exons and short interfering RNAs. Nature 447 (7141):222-227. doi:10.1038/nature05777

Whitehead KA, Langer R, Anderson DG (2009) Knocking down barriers: advances in siRNA delivery. Nature Reviews Drug Discovery 8 (2):129-138. doi:10.1038/nrd2742

Whitehead KA, Sahay G, Li GZ, Love KT, Alabi CA, Ma M, Zurenko C, Querbes W, Langer R, Anderson DG (2011) Synergistic silencing: combinations of lipid-like materials for efficacious siRNA delivery. Molecular Therapy 19 (9):1688-1694. doi:10.1038/mt.2011.141

Xia T, SantaLucia Jr J, Burkard ME, Kierzek R, Schroeder SJ, Jiao X, Cox C, Turner DH (1998) Thermodynamic parameters for an expanded nearest-neighbor model for formation of RNA duplexes with watson-crick base pairs. Biochemistry 37:14719-14735. doi:10.1021/bi9809425

Xiang SL, Fruehauf J, Li CJ (2006) Short hairpin RNA-expressing bacteria elicit RNA interference in mammals. Nature Biotechnology 24 (6):697-702. doi:10.1038/nbt1211

Xiong XB, Uludag H, Lavasanifar A (2009) Biodegradable amphiphilic poly(ethylene oxide)-block-polyesters with grafted polyamines as supramolecular nanocarriers for efficient siRNA delivery. Biomaterials 30 (2):242-253. doi:10.1016/j.biomaterials.2008.09.025

Yacobi N, Malmstadt N, Fazlollahi F, DeMaio L, Marchelletta R, Hamm-Alvarez S, Borok Z, Kim K-J, Crandall E (2010) Mechanisms of Alveolar Epithelial Translocation of Defined Population of Nanoparticles. American Journal of Respiratory Cell and Molecular Biology 42:604-614. doi:10.1165/rcmb.2009-0138OC

Ye X, Huang N, Liu Y, Paroo Z, Huerta C, Li P, Chen S, Liu Q, Zhang H (2011) Structure of C3PO and mechanism of human RISC activation. Nature structural & molecular biology 18 (6):650-657. doi:10.1038/nsmb.2032

York AW, Zhang Y, Holley AC, Guo Y, Huang F, McCormick CL (2009) Facile Synthesis of Multivalent Folate-Block Copolymer Conjugates via Aqueous RAFT Polymerization: Targeted Delivery of siRNA and Subsequent Gene Suppression. Biomacromolecules 10:936-943. doi:10.1021/bm8014768

Yuan B, Latek R, Hossbach M, Tuschl T, Lewitter F (2004) siRNA selection server: an automated siRNA oligonucleotide prediction server. Nucleic Acids Research 32:W130-W134. doi:10.1093/nar/gkh366

Zamore PD, Tuschl T, Sharp PA, Bartel DP (2000) RNAi: double-stranded RNA directs the ATP-dependent cleavage of mRNA at 21 to 23 nucleotide intervals. Cell 101 (1):25-33. doi:10.1016/S0092-8674(00)80620-0

Zhang HY, Lee MY, Hogg MG, Dordick JS, Sharfstein ST (2010) Gene Delivery in Three-Dimensional Cell Cultures by Superparamagnetic Nanoparticles. ACS Nano 4 (8):4733-4743. doi:10.1021/nn9018812

Zhang SB, Zhao B, Jiang HM, Wang B, Ma BC (2007) Cationic lipids and polymers mediated vectors for delivery of siRNA. J Control Release 123 (1):1-10. doi:10.1016/j.jconrel.2007.07.016

Zhou XM, Rowe RG, Hiraoka N, George JP, Wirtz D, Mosher DF, Virtanen I, Chernousov MA, Weiss SJ (2008) Fibronectin fibrillogenesis regulates three-dimensional neovessel formation. Genes & Development 22 (9):1231-1243. doi:10.1101/gad.1643308

Zintchenko A, Philipp A, Dehshahri A, Wagner E (2008) Simple modifications of branched PEI lead to highly efficient siRNA carriers with low toxicity. Bioconjugate Chemistry 19 (7):1448-1455. doi:10.1021/bc800065f

Zuhorn IS, Kalicharan R, Hoekstra D (2002) Lipoplex-mediated Transfection of Mammalian Cells Occurs through Cholesterol-dependent Clathrin-mediated Pathway of Endocytosis. The Journal of Biological Chemistry 277 (20):18021-18028